Mid-Ocean Ridges and Their Geomorphological Features

J. Escartín, J.-A. Olive

Mid-Ocean Ridges
Mid-Ocean Ridges and their geomorphological features

J. Escartín & J.-A. Olive

Laboratoire de Géologie, UMR 8538, Département de Géosciences, Ecole Normale Supérieure de Paris, PSL Research University, Paris, France

Emails:
escartin@geologie.ens.fr
olive@geologie.ens.fr

Glossary

Abyssal hill

Elevated seafloor that is elongated in the direction or the ridge axis, and often showing regular spacing in the direction of spreading. Abyssal hills form along the axis of mid-ocean ridges, from ultra-slow ones to ultra-fast ones, and thus are present throughout most of the seafloor. Their length varies from a few km to a few tens of km, and their height over surrounding seafloor from a few tens of m to a few km. These structures are bound by normal fault scarps.

Axial magma chamber (AMC)

Magma chamber underlying the axis of mid-ocean ridges, that is the source of dikes reaching the seafloor and feedin volcanic eruptions. AMCs are ubiquitous at fast-spreading mid-ocean ridges, where they are often continuous over several tens of km along-axis. AMCs lay at depths subseafloor that range from ~1 km along the fastest spreading ridges, and deepens to ~3 km or more at sliwer spreading ridges.

Axial summit trough (AST)

Depression or graben often found at the summit of fast-spreading ridges, and that is the source of most of the volcanic eruptions along these ridges, and where hydrothermal vents are common. Its width is typically a few tens of m, reaching a few hundreds of m, with depths of a few m and up to a few tens of m.

Axial volcanic ridge (AVR)

Elongated submarine volcanic construction that is elongated and likely results from eruptions along fissure systems. AVRs are common within the rift valley of slow-spreading ridges, but are also observed at fast-sreading ones. AVRs show a broad range of sizes, extending from a few to several tens of km along-axis, and raising a few tens of m to a few hundreds of m above surounding seafloor. AVRs are often emplaced parallel to the ridge axis and faults.

Black smoker

Submarine hydrothermal manifestation characterized by high-temperature fluids, typically exceeding 350°C, that form a plume of particles upon mixing with cold seawate. These particles result from the precipitation of dissolved iron and sulfur in the hydrothermal fluids as the fluid cools down and saturates, and forming a plume that is black and smoke-like.

Central volcano

Major submarine volcano or seamount, that forms at the center of mid-ocean ridge segments from slow- and ultra-slow ridges. These volcanic edifices may rise a few hundreds to a few km, and result from prolonged and sustained and focused melt supply.

Fracture zone

Fracture zones are the traces of strike-slip plate boundaries, or transform faults that link major mid-ocean ridge segments, and that are now inactive and preserved off the mid-ocean ridge axis. Transform faults often show a continuous valley that may be followed over hundreds of km,. Their trace records the changes in the direction of plate motions over time, and the difference in age of the oceanic crusts across fracture zones provide information on the lateral offset at the ridge axis when the transform fault was active.

Head scarp

Steep scarp that develops at the highest part of mass wasting of the substrate. Head scarps are commonly found along major submarine topographic scarps such as transform and rift valley walls, and often show a convex shape with very steep slopes (>45-50°).

Hydrothermal field

Zone of the seafloor that concentrates the discharge of hydrothermal fluids, and that encompasses both focused flow, typically in the form of hydrothermal vents, or as diffuse flow through the seafloor. Hydrothermal fields are found at all spreading ridges, both on- and off-axis.

Hydrothermal vent

Zone of focused discharge of hydrothermal fluids through the seafloor, often associated with a hydrothermal chimney formed by the precipitation of sulfides from the hydrothermal fluids. Hydrothermal vents and the associated chimneys may raise up to a few tens of m above surrounding seafloor, and tend to concentrate in zones of hydrothermal discharge to from hydrothermal fields

Hummock

Small volcanic mounds, typically up to a few tens of m high and up to 100-200 m in diameter, that coalesce to pave significant portions of the seafloor (hummocky terrain) particularly at slow-spreading ridges, where they also contribution to the build-up of axial volcanic ridges. These structures are likely formed by individual, focused eruptions, with the emplacement of pillow lavas.

Inside corner

Seafloor found at the corner defined by a mid-ocean ridge segment and a non-transform discontinuity or transform fault. At mid-ocean ridges with significant tectonic extension, the inside corner seafloor is elevated relative to the surrounding areas due to tectonic uplift.

Mid-ocean ridge

One of the three major types of plate boundaries found on Earth, where adjacent oceanic plates diverge, and where new oceanic lithosphere and seafloor form through a combination of volcanic and tectonic processes, that also sustain hydrothermal activity underwater. The Mid-Ocean ridge system is elevated ~2000-3000 m above surrounding seafloor, and has a total length of ~65000 km. The global mid-ocean ridge system is the most important active volcanic structure, as well as the largest geological feature on Earth.

Nodal basin

Local seafloor deep commonly found at the end of mid-ocean ridge segments, and in proximity to either transform fault or non-transform offsets. Nodal basins are often sediment-filled, and are best developed within the rift valley of slow- and ultra-slow spreading ridges.

Non-transform discontinuity

A type of mid-ocean ridge discontinuity, bounding ridge segments and laterally offsetting them between a few km and a few tens of km. Non transform offsets accommodate strike slip deformation of the adjacent plate boundaries, but lacking a well-defined zone of localization of deformation, the tectonic structure is complex so as to accommodate deformation over a broad area. Non-transform offsets may also be unstable, and may migrate along-axis, leaving traces off-axis that are oblique to the spreading direction.

Pillow lava

Lava emplaced underwater and that forms spherical, bulbous, or tubular structures. This type of lava structure results from the rapid cooling of the basalt in contact with seawater, forming a shell that is often striated. Pillow structures may have sizes of up to a few m.

Ridge segment

Mid-ocean ridge sections that are volcanically and tectonically continuous, and that do not show any lateral offset. Ridge segments are thus bound by either transform faults, non-transform offsets, or both, and develop at all types or ridges and under all spreading rates. Ridge segments have typical lengths that vary fro a few 10s of km to a few hundreds of km.

Oceanic crust

Uppermost layer of the oceanic plate that is formed magmatically, through the emplacement and cooling of magma chambers at depth, diking, and volcanic eruptions at the seafloor. The oceanic crust may be continuous when formed along mid-ocean ridge sections that are magmatically robust, and may be discontinuous or absent in ridge sections with limited melt supply, typically along soome slow- and ultra-slow spreading ridge sections.

Oceanic detachment fault

Normal fault that develops in the oceanic lithosphere with efficient accumulation of deformation over long periods of time, associated with the exposure of the detachment fault surface at the seafloor and the formation of an elevated tectonic massif. These faults may accumulate displacements of several tens of km, and when preserved at the seafloor, they display fault corrugations that are parallel to the direction of extension. Oceanic detachment faults also exhume deep-seated rocks from the deeper oceanic crust and upper mantle.

Oceanic lithosphere

Uppermost layer of an oceanic plate, and that is both elastic and deforms through dominantly brittle processes, such as localized faulting and seismogenic deformation. The oceanic lithosphere thickness on-axis corresponds to a balance between heat extraction (mainly hydrothermal activity) and heat supply (mainly melt supply from the mantle) and thickens away from the axis, as the oceanic plate cools with age. The oceanic lithosphere thus includes the oceanic crust, if formed along magmatic ridge sections, or may be composed of mantle material primarily if formed along magma-starved ridge sections. It is generally assumed that the base of the oceanic lithosphere corresponds to the ~750°C isotherm, as at temperatures above plastic deformation mechanisms may dominate over brittle ones.

Outside corner

Portion of seafloor located within the corner defined by a ridge segment, and the off-axis trace of a ridge discotninuity (fracture zone or non-transform offset), and on the conjugate side of an inside corner, across the ridge axis. At tectonically dominated ridges, such as many slow-spreading ones, the depth of the outside corner is significantly lower than that of the tecotnically uplifted inside cornier.

Rift valley

Tectonic graben formed along mid-ocean ridges that show significant tectonic activity (primarly slow- and ultra-slow spreading ridges), that is continuous along the length of individual ridge segments, and that is bound by normal faults along the rift valley walls. Rift valleys have typical widths of a ~10 and up to ~30 km, and the rift valley floor my be up to 2-3 km deeper than the adjacent seafloor outside the rift valley. The rift valley also localizes most of the volcanic and tectonic activity along these ridge sections.

Slump

Type of mass wasting commonly found at seafloor and developing over hard basement such as that found in the oceanic lithosphere near the ridge axis. Slumps often show a head scarp that indicates the initiation of the mass wasting movement of basement material, and a toe at its base, where the mass wasted material accumulates.

Transform fault

Strike-slip plate boundary, that is common at mid ocean ridges, where it offsets the ridge axis laterally. Transform faults are tectonically active, and accommodate strike-slip deformation along a well-defined deformation zone, that is stable over long periods of time. Transform faults often show a deep transform valley, with a linear tectonic ridge at its floor that indicates the position of the zone of localized deformation. Off-axis, the trace of old transform faults is visible as fracture zones,

Key words

Seafloor, submarine volcanism, submarine faulting, submarine erosion, submarine sedimentation, deep-sea hydrothermal activity, oceanic detachments, transform faults, mid-ocean ridges, ridge segmentation, non-transform offsets

Abstract

Most of the Earth's surface is paved by oceanic crust formed along mid-ocean ridges, a ~65000 km long volcanic chain, and one of the most prominent morphologic features on the planet. Seafloor morphology is thus shaped, at large spatial scales (tens to hundreds of km) by the overall ridge geometry, and in particular by both transform faults and non-transform discontinuities that dissect the ridge axis, defining ridge segments, and leave off-axis wakes in seafloor morphology. At smaller scales (tens of km and less) morphological variability is primarily controlled by the relative importance of tectonic and volcanic processes on-axis, in addition to hydrothermal activity on very local scales. While spreading rate is classically invoked as a primary control on ridge segmentation and seafloor morphology, the strongest controls are in fact melt supply to the ridge axis and on-axis lithospheric thickness. Fast-spreading ridges (>60 mm/yr) show relatively consistent and homogeneous morphologies, dominated by volcanism with limited tectonic reshaping by normal faults. With decreasing spreading rate, the variability in seafloor morphology increases, and encompasses seafloor similar to that formed at fast-spreading ridges wherever magma supply is important, and amagmatic spreading dominated by faulting, while also displaying significant variations at the scale of individual ridge segments. In all cases, tectonic deformation is pervasive, and fault-bounded abyssal hills formed on-axis are ubiquitous throughout the seafloor. Seafloor relief is also modified by mass wasting,

which is particularly active along tectonic scarps (e.g., normal faults, walls of rift and transform valleys), and by sedimentation of pelagic or continental origin. This chapter provides an overview of seascapes formed at mid-ocean ridges and interprets them as the interaction of relief-creating and relief-reworking processes on a range of scales.

1. Introduction

Mid-ocean ridges are one of Earth's most prominent geomorphic features, albeit mostly hidden from view deep below the ocean's surface, at an average depth of ~2500-2600 m. With a length of ~60,000 km, mid-ocean ridges crisscross the Earth's surface and correspond to tectonic boundaries where rigid lithospheric plates diverge. Upward motion of the underlying mantle induces partial melting through adiabatic decompression. The resulting magma ascends through the mantle, gets emplaced at shallow depths below the ridge axis, and may eventually erupt at the seafloor, forming the oceanic crust. The supply of magma to the ridge is often insufficient to fully accommodate the rate at which plates diverge relative to one another. This prompts tectonic extension, with the growth of normal faults that dissect and thin the newly formed brittle lithosphere and oceanic crust. Magmatic and tectonic processes interact within a narrow (a few km to tens of km wide), seismically and volcanically active area, the mid-ocean ridge axis.

In addition to building the crust, magmatic and tectonic activity along ridges leave a record in the relief and texture of the seafloor. Regionally, the axis of mid-ocean ridges is raised by ~2–3 km relative to the surrounding abyssal plains. The morphology of the ridge axis is extremely variable, with ridge sections featuring marked and profound tectonic rift valleys, typically 10 to 20 km wide and up to a few km in depth, hosting volcanic structures (Tapponnier and Francheteau, 1978). Other ridge sections show instead an axial high associated with abundant magmatism and volcanism at the seafloor and where faulting is less prevalent than along rift valley sections (Lonsdale, 1983; Macdonald et al., 1984). Changes in ridge axis morphology (e.g., Chen and Morgan, 1990; Buck et al., 2005) reflect different balances between magmatic and tectonic activity, which are imprinted in the seafloor topography, and provide a time record of these interactions as new oceanic crust is accreted.

In addition to faulting and volcanism, other processes contribute to shaping seafloor topography. Magmatic heat fuels hydrothermal activity, which builds edifices that can reach several tens of m in height and laterally extend over 100s of meters, while hosting deep-sea chemosynthetic ecosystems when they are active (e.g., Corliss, 1990). Pelagic sedimentation can blanket the seafloor while filling deeper areas (e.g., Mitchell, 1995; Webb and Jordan, 1997; 2001), which strongly alters the morphology of old, off-axis oceanic crust (i.e., Goff and Arbic, 2010). Erosional

processes also affect younger, tectonically active seafloor. Gravity-driven mass wasting, in particular, takes place along the locally steep relief flanks of volcanic structures, fault scarps, and sub-vertical hydrothermal edifices. This process operates at all scales, from sub-meter (e.g., hydrothermal chimney collapse) to tens of km (e.g., sculpting large tectonic massifs with reliefs of several km), and as such can profoundly alter the original tectonic, volcanic, and hydrothermal seafloor morphology formed on-axis (e.g., Tucholke, 1992; Tucholke et al., 1997; Cannat et al., 2011; Mitchell et al., 2000).

Owing to difficulties inherent to deep-sea exploration and mapping, our understanding of the geomorphology associated with mid-ocean ridges is both scattered and biased. To date, less than 50% of the global mid-ocean ridge system has been mapped using shipboard multibeam bathymetry systems, with a resolution of 50-100 m, which is appropriate for regional mapping and morphological studies at scales of 10s of km or larger. Off-axis, the data gap is much more significant, with less than 20% of the seafloor mapped to date (Wölfl et al., 2019). Finer-scale morphological studies rely on deep-sea vehicles that can acquire bathymetry at higher resolutions than from ships. These include remotely operated vehicles (ROVs) and more recently autonomous underwater vehicles (AUVs), equipped with multibeam and sonar systems (Wölfl et al., 2019). Surveying close to the seafloor, at heights that may vary from ~10–100 m, these systems provide bathymetric maps with resolutions of ~1 m, and down to a few 10s of cm (e.g., Huvenne et al., 2008; Wynn et al., 2014). Such surveys cover limited areas (typically up to a few 10s of km^2) and are available only at a handful of study areas along the global mid-ocean ridge system. Ground truthing, with visual seafloor inspection and sampling, is achieved with both ROVs and research submersibles, again available only at a few sites within the global ridge system. High-resolution bathymetry and in-situ observations thus cover a minuscule fraction of the 65,000 km of the global mid-ocean ridge system.

Direct observation of the active processes shaping the Earth's surface is a crucial step to interpreting the resulting landscapes and seascapes. While this is systematically done on land, in subaerial or in very shallow-water marine environments (e.g., coastal processes), observations of active processes at the seafloor remain extremely scarce, sparse, and localized. For the most part, geological observations are conducted at a specific point in time, with no repeated or long-term data collection to document and quantify active processes such as mass wasting,

tectonic deformation, or volcanism (among others). Existing temporal studies in the deep sea environment primarily focus on capturing volcanic eruptions along ridges, such as the East-Pacific Rise at 9ºN and the Axial Seamount section of the Juan de Fuca Ridge (e.g., Kelley et al., 2014; Fornari et al., 2015), where eruptions take place every ~5–10 years. Hydrothermal sites have also been instrumented and monitored through repeated surveys, to understand their inner dynamics and links with surrounding ecosystems (Favali et al., 2006; Juniper et al., 2007). Hence, our understanding of active deep-sea processes along mid-ocean ridges is less advanced than in subaerial environments, and quantitative constraints on rates of tectonic deformation or seafloor erosion, among others, are for the most part lacking. In a broad sense, identifying and understanding the mechanisms behind mid-ocean ridge morphology is very much a work in progress.

In this chapter, together with a short historic perspective, we seek to provide an overview of the mid-ocean ridge processes that build the crust and oceanic lithosphere, and ultimately shape the global seafloor. These processes vary continuously along the mid-ocean ridge system, resulting in a great diversity of axial morphologies. Morphological discontinuities are also imparted by transform faults, which are major tectonic structures that dissect the ridge into offset segments (e.g., Wilson, 1965), and leave permanent scars in the ocean floor called fracture zones. While mid-ocean ridges and transform faults control seafloor morphology on a global scale, volcanic, tectonic, and hydrothermal processes at the ridge axis sculpt the ocean floor on regional to local scales. This fine-scale texture is then rafted off-axis as tectonic plates diverge through the accretion of new oceanic crust. The present chapter focuses exclusively on the morphology of seafloor underlain by oceanic lithosphere, and excludes continental margins, which mark the transition from continental to oceanic tectonic plates, and whose morphology is unrelated to mid-ocean ridge processes

2. Mapping mid-ocean ridges

Shallow areas in the central north Atlantic were first identified in the mid- to late 1800s by early oceanographic and exploration campaigns which relied on line soundings to estimate the thickness of the water column (Figure 1, Top). These areas were found to lie more than 2000 m over the abyssal plains to the East and West (e.g., Maury, 1955).

Later expeditions, including that of the Meteor in the early 1920s, established the continuity of this bathymetric high, identified as the Mid-Atlantic Ridge, from the north Atlantic to the edge of the Indian ocean. This was greatly facilitated by the development of echo sounding systems that allowed continuous depth measurements along ship tracks providing single-beam bathymetric profiles. With bathymetric data being acquired worldwide, Marie Tharp and Bruce Heezen, from the Lamont-Doherty Earth Observatory, compiled countless single-beam profiles from different ocean basins (e.g., Heezen et al., 1959; 1964a; 1964b). With profound geological insight, they documented the main structural and morphological features of the oceanic crust (seamounts, mid-ocean ridges, fracture zones, and trenches, among others), and Marie Tharp drafted these elements in three dimensional representations of the ocean floor, or physiographic maps (Figure 1, Center). These maps were first compiled for individual oceans or basins, and a global map in the 1960s, clearly revealing the continuity of the global mid-ocean ridge system, straddling the world's oceans over >65,000 km, in addition to seamounts, fracture zones, trenches, and other seafloor structures (Berann et al., 1977). This physiographic map provided a global framework to interpret challenging new geological and geophysical observations. In particular, regularly spaced, symmetric magnetic anomalies (Vine and Matthews, 1963) and the banded distribution of oceanic seismicity (Sykes, 1967) were key elements to understand the role of mid-ocean ridges in the emerging theory of global plate tectonics, a scientific revolution that developed from the 1950s on, as Marie Tharp's maps shed unprecedented light on the morphology of ridges.

With the advent of submarine warfare, underwater military technology and particularly echo sounding systems evolved. Multibeam instruments sounded whole swaths of seafloor instead of providing single-beam profiles, and were first mounted on military submarines in the 1960s, as acoustic sonar technology rapidly developed. Civilian use of ship-mounted systems began in the 1970s and provided depth soundings along ship tracks over a cross-track width that increased from ~1 to ~5 times the water depth over the next few decades. These systems have proven crucial in revealing the architecture of the seafloor and the processes that shape it (Cormier et al., 2003). Shipboard systems routinely provide seafloor maps of the deep ocean with a resolution of ~100 m or better, in addition to acoustic backscatter data, which provide acoustic reflectivity maps that may be related to seafloor geology (e.g., sediment cover, exposure of rocks or hard substrates, recent volcanic units, etc.). To date, less than 20% of the ocean floor has been mapped at this ~100 m resolution, with

on-going efforts to increase this coverage in coming years (https://seabed2030.org). While the coverage is uneven, with certain regions practically uncharted (e.g., the southern Indian Ocean), the mid-ocean ridge system is relatively well mapped, particularly along the Atlantic and Pacific, as ridges host processes that have attracted numerous research projects in recent decades (volcanism, tectonism, hydrothermal activity and associated ecosystems). In this chapter we benefit from the compiled multibeam bathymetry data publicly available at http://www.gmrt.org (Ryan et al., 2009), that covers ~10% of the seafloor (release GMRT 3.9), in addition to additional data from selected cruises.

Higher-resolution data are key to establish a detailed geological context for observations, samples and measurements, and to understand how certain active processes operate at the seafloor, particularly when these processes profoundly alter seafloor relief over time. This is the case of tectonic deformation, volcanism, or hydrothermal activity, with their associated ecosystems. High-resolution maps with acoustic systems mounted on deep-sea vehicles, both remotely operated or autonomous, can produce terrain models at resolutions of a few to less than 1 m, while optical seafloor imaging provides not only photomosaics, but also 3D terrain models at much greater resolution. Such high-resolution optical and acoustic data are available at selected areas that, while they represent a minuscule fraction of the world's seafloor, have allowed scientists to study deep-sea processes and environments, and in particular to advance our understanding on how mid-ocean ridges operate, and the nature of ecosystems that develop there.

Figure 1 about here

Figure 2 about here

3. The seafloor factory

With the revolution of plate tectonics, mid-ocean ridges became the center of a new view of a dynamic Earth paved by a set of mobile tectonic plates. In the 1960s magnetic data acquired together with bathymetric surveys revealed anomalies that were parallel to, and symmetrical about the axis of all studied mid-ocean ridges (Vine and Matthews, 1963). Magnetic anomalies are the result of volcanic rocks locking in the

orientation of the ever-reversing magnetic field of the Earth at the time of their solidification at the seafloor. As such, they provide a means of dating the seafloor, and a smoking gun for the then-called "continental drift". Ageing seafloor symmetrically partitioned about ridges indeed became clear evidence of continuous plate motions over time, and even became a detailed record of the plates' direction and speed over the last ~180 million years. Based on plate divergence rates calculated from the spacing of magnetic anomalies (e.g., DeMets et al., 2010; Seton et al., 2020), ridges are often classified as ultra-slow (<20 mm/yr), slow (20-55 mm/yr), intermediate (55-75mm/yr), fast (75-180 mm/yr), and ultra-fast ridges (>180 mm/yr).

Plate separation is accommodated along mid-ocean ridges by the accretion of new oceanic lithosphere —the quasi-rigid outer layer of the Earth that can withstand large stresses before it breaks or flows— and the overlying seafloor. This is an extremely complex process, and while numerous parameters play a role, two stand out: the thickness of the brittle lithosphere under the ridge axis, and the amount of magma supplied to the ridge axis from the underlying mantle (Figure 3).

The mechanical properties of the axial lithosphere depend on composition and temperature. Brittle fracturing and faulting are the dominant deformation mechanisms at temperatures below 800-600°C in peridotitic, gabbroic and basaltic lithologies (e.g., Brace and Kohlstedt, 1980; Evans et al., 1995), while hotter temperatures activate plastic deformation. The boundary between brittle (often seismogenic) and ductile domains thus coincides with the ~650°C isotherm, which lies at a depth that reflects an equilibrium between heat supplied from below (including magmatic heat as discussed below) and heat lost to the ocean through hydrothermal activity and conductive cooling (Chen and Morgan, 1990; Lowell et al., 2013; Theissen-Krah et al., 2011). Simple thermal models that balance these two components predict thicknesses of ~2-3 km for the brittle lithosphere at the axis of fast-spreading ridges, and thicknesses in excess of ~10 km at ultra-slow ones, (e.g., Chen and Morgan, 1990; Theissen-Krah et al., 2011; Fan et al., 2021). Such lithospheric thickening with decreasing spreading rate is consistent with the observed deepening of the maximum depth of seismic deformation (e.g., Huang and Solomon, 1988; Grevemeyer et al., 2019), as well as the deepening of the axial melt lens that typically underlies the axis of fast and intermediate spreading ridges (e.g., Carbotte et al., 1998) (Figure 3A). A thick brittle lithosphere behaves as a stiff elasto-plastic plate and can support large-amplitude relief (Qin and Buck, 2005). Such mechanical properties have important

implications for the development of axis-bounding faults and the rift valley they outline (e.g., Chen and Morgan, 1990; Buck and Poliakov, 1988; Behn et al., 2002).

The availability of mantle-derived magma at the ridge axis is another key control on seafloor morphology. Plate separation drives passive mantle upwelling below the ridge axis, which results in adiabatic decompression and partial mantle melting. The amount of magma produced in the melting region varies along the mid-ocean ridge system (Keen et al., 1990; Langmuir et al., 1992; Gale et al., 2014), and this melt production determines both the amount of lava erupted at the seafloor, and the style of this submarine volcanism (Schouten et al.). Magmatic intrusions at depth beneath the ridge axis is the primary mode of oceanic crust accretion (e.g., Cann, 1970; Sinton and Detrick, 1992; Cannat et al., 2009). Thermal models typically predict a melt production flux that accounts for a ~5 to 7 km-thick oceanic crust at intermediate and fast-spreading ridges, matching seismically-inferred crustal thicknesses (see Fig. 24 in White et al., 2001 and references therein). Crustal thickness generally decreases to <4-2 km at slow to ultra-slow ridges, reflecting the colder thermal state of the underlying mantle (e.g., Bown and White, 1994; White et al., 2001; Dick et al., 2003; Lizarralde et al., 2004). Other parameters beyond spreading rate, such as mantle composition may either enhance or suppress melt production (e.g., Ito and Lin, 1995; Katz, 2010; see overview by Langmuir and Forsyth, 2015). Complex three-dimensional dynamics of magma ascent and focusing along and across-axis may also modulate the supply of melt between and within individual ridge segments (Kuo and Forsyth, 1988; Cannat, 1996; Dick et al., 2003; Gregg et al., 2012). Broadly speaking, a ridge section that receives enough melt to fully accommodate the long-term rate of plate separation through repeated magmatic intrusion will experience little tectonic thinning. By contrast, large-offset crustal-scale faults will tend to develop at ridge sections that receive comparatively little magma. Seafloor formed in these areas will thus appear more rugged and feature greater amplitude topography.

Both mantle upwelling and the emplacement of melt within the lithosphere or at the seafloor are sources of heat that can drive convection of aqueous fluids across cracks and pores throughout newly accreted crust. The most spectacular manifestation of this phenomenon is high-temperature hydrothermal venting at the seafloor, associated with unique chemosynthetic ecosystems (e.g., Cann and Strens, 1982; Elderfield and Schulz, 1986; Corliss, 1990; Alt, 2003; Fontaine and Wilcock, 2007). Hydrothermal activity along mid-ocean ridges accounts for ~10% of Earth's heat loss

(e.g., Elderfield and Schulz, 1996; Stein et al., 1995) and results in fluid-rock interactions that control the chemistry of the venting fluids at the seafloor and influence the chemistry of the global ocean (e.g., Fouquet et al., 2010). At or near the seafloor, hydrothermal fluids cool and mix with seawater, which promotes the precipitation of dissolved molecules from the venting fluids (e.g., Cu and Fe sulfides, talc), or seawater (e.g., carbonates) depending on local physicochemical conditions (e.g., Haymon, 1983; Kelley et al., 2001; Humphris and Cann, 2000; Hodkinson et al., 2015). Precipitation can build hydrothermal chimneys and mounds that can extend over large areas, rising up to several tens of m above the surrounding seafloor.

Figure 3 about here

Overall, seafloor morphology records the interaction of all aforementioned processes along the axes of mid-ocean ridges, over a wide range of spatial and temporal scales, while being continuously reworked by both erosion and sedimentation. These fine-scale volcanic, tectonic, and hydrothermal morphologies are superimposed on large-scale, regional seafloor patterns. Most importantly, the seafloor systematically deepens away from mid-ocean ridges, whose axes lie ~2500-3000 m below sea level and reaches depths in excess of 4000-5000 m at the abyssal plains. This deepening reflects an isostatic equilibrium of the oceanic crust and the denser underlying mantle, which cools down conductively as plates separate, becoming even denser away from the ridge axis as heat is lost to the overlying ocean (e.g., Parsons and Sclater, 1977; Stein and Stein, 1992). Ridge axes are also discontinuous, dissected by several types of discontinuities that often leave traces off-axis, and record a long history of ridge segmentation during plate separation.

4. Major topographic features at or near the axis of mid-ocean ridges

4.1. Axial valleys and axial highs

To first order, the morphology of mid-ocean ridge axes can be categorized between two well-recognized end-members (e.g., Macdonald, 1982; Chen and Morgan, 1990b). Slow-spreading ridges often feature a fault-bounded axial rift valley that is typically ~10-20 km wide, with variable depth that may reach up to 3-4 km (Figure 4b). By

contrast, fast-spreading ridges are often characterized by a broad axial high straddled by a narrow (<100–200 m wide) strip of seafloor where most eruptions take place (Figure 4a). In practice, a systematic examination of mid-ocean ridge bathymetry reveals more complex morphological patterns that do not solely depend on spreading rate, as illustrated in Figure 4. Axial highs are found not only at fast-spreading ridges, but also at slow ones near hot-spots (e.g., the Reykjanes Ridge near Iceland, Fig. 4d), likely reflecting an anomalously high supply of melt to the axis. Intermediate-spreading ridges (Figure 4e) can feature either type of axial morphology, and even show gradual changes from rift valley to axial high without any significant change in spreading rate (Canales et al., 1997; Shah and Sempere, 1998). Finally, ridge sections with a limited melt supply do not always feature a clearly delineated axial valley flanked by regularly-spaced normal faults. They instead develop irregularly-spaced, large-offset normal faults called detachments that shape prominent bathymetric highs (e.g., Cann et al., 2000; Tucholke et al., 2008; Cannat et al., 2006; Olive et al., 2010). These are identifiable either as exposed fault planes showing corrugations parallel to spreading (Fig. 4c), or as smooth abyssal hills that lack such striations (Fig. 4f). The latter structures form in certain sections of ultraslow ridges as a result of cross-cutting faults exhuming mantle directly at the seafloor (Cannat et al., 2006; Sauter et al., 2013).

The variability in large-scale ridge axis morphology, particularly at slow and ultra-slow spreading ridges (Figure 4), can be explained by the wide range of possible lithospheric and magmatic thickness at a given spreading rate (Figure 3). When the axial lithosphere is thicker than the magmatic thickness (and hence linked to an axial melt supply that is relatively low), mantle material is uplifted by slip on large faults and incorporated into the brittle lithosphere. Tectonic processes thereby account for the lithospheric mass imparted by plate separation (e.g., Cannat, 1996). At spreading rates >60 mm/yr, accretion is predominantly magmatic, as the lithosphere is thinner than the magmatic crustal thickness. Such systems can sustain ubiquitous magma chambers below the ridge axis (Figure 3), and do not undergo extensive faulting. At rates <60 mm/yr, accretion can be both predominantly magmatic, such as along ridges near hot-spots (e.g., Reykjanes Ridge, Fig. 4d), or tectonically dominated where the melt supply is low relative to the overall lithospheric thickness (Figs. 4c and f). These different modes of accretion are conceptualized in Figure 5 as a function of spreading rate and the variable the ratio of lithospheric thickness vs. melt supply (Olive and Dublanchet, 2020).

4.2. Abyssal hills

Off-axis seafloor is ubiquitously paved by *abyssal hills*: elongated topographic highs trending parallel to the ridge axis (e.g., Menard and mammerickx, 1967; Macdonald et al., 1996; Goff et al., 2010; Cormier and Sloan, 2018). These structures develop along the flanks of the mid-ocean ridge axis, and to first order consist of magnetically-accreted crust offset and tilted by slip on regularly-spaced normal faults (e.g., Rea, 1975; Kappel and Ryan, 1986) (Fig. 3a). Much like axial valleys and axial highs, the shape of abyssal hills reflects the balance of magmatically and tectonically accommodated plate separation (Buck et al., 2005; Behn and Ito, 2008; Ito and Behn, 2008). In particular, ridge sections that receive a large supply of magma, either because of their fast-spreading rate or proximity to a hotspot tend to develop low-relief (<100s of m), closely-spaced (~1 km) abyssal hills (Fig. 4a, d). On the other hand, slower and/or more magmatically-starved ridges form greater-amplitude (few kms), more widely-spaced (~5–10 km) hills, which are less elongated and continuous in the along-axis direction (Fig. 4c, f). This reflects the greater contribution of tectonic strain to overall plate separation, manifesting as longer-lived, larger-offset normal faults shaping taller scarps.

These variations in abyssal hill morphology are well-documented globally (e.g., Bird and Pockalny, 1994), and show greater morphological variability among slower-spreading ridges (Cormier and Sloan, 2018; see Goff et al., 2020 and references therein). This trend mimics the greater variability in magma supply and lithosphere thickness that is documented in these slow systems (Figure 3). In places where magma accommodates ~50% or less of the total plate separation rate, large-offset detachment faults may develop (Buck et al., 2005) and form dome-shaped bathymetric highs that stand out from surrounding regular, elongated abyssal hill domains (e.g., Fig. 4c vs. 4b). Figure 6 illustrates how abrupt these transitions between ridge-parallel, linear abyssal hill-bounding faults and corrugated detachment fault surfaces may be, both in the along- and across-axis directions, and thus over short periods of time, with distinct modes of accretion operating simultaneously (Figure 6b). These changes in seafloor morphology thus record the thresholds in magma supply (e.g., Tucholke et al., 2008) that suppress or activate certain modes of crustal accretion such as detachment faulting, as changes along-axis or over short time spans are expected to be gradual (e.g., Howell et al., 2019).

Figure 4 about here

Figure 5 about here

Figure 6 about here

4.3. Continuity and discontinuity of mid-ocean ridge axes, and their off-axis traces

At large scales (hundreds of km), the overall geometry of mid-ocean ridges is relatively stable over tens of millions of years, as indicated by the well-preserved shape of the initial rifting of Africa and South America (e.g., Bullard et al., 1965; Heezen and Tharp, 1965) both in the present-day ridge axis geometry and in the magnetic anomalies that cover older seafloor (e.g., Gaina et al., 2003; Perez-Diaz and Eagles, 2014). At smaller spatial scales (<100km), ridges do shift in shape and location, with lateral ridge jumps, or local changes in ridge geometry due to asymmetric spreading (e.g., Marks and Stock, 1995; Okino et al., 2004; Muller et al., 2008; Macleod et al., 2009). The discontinuous, segmented nature of the global mid-ocean ridge was evident even in early bathymetric datasets, with the identification of major transform faults and their off-axis traces as fracture zones (e.g., Heezen et al., 1964a; 1964b; Heezen and Tharp, 1965; Fox and Heezen, 1965). Transform faults were recognized early on as a new type of strike-slip plate boundary (Wilson et al., 1965) that follow small circles around Euler poles that define the relative rotation of divergent tectonic plates (Morgan, 1968).

Figure 7 about here

While transform faults bound major ridge sections, the ridge axis is also segmented by smaller-scale non-transform discontinuities (see the review by Carbotte et al., 2015, and references therein). Along ridges with a well-developed rift valley, non-transform offsets (NTOs) show a wide variety of morphologies. NTOs with offsets that are shorter than the rift valley width can be identified from systematic changes in the overall texture of the rift valley, including changes in obliquity and tectonically complex terrain (e.g., Goud and Karson, 1985; Tucholke et al., 1997; Gracia et al., 2000).

Fast-spreading ridges are dominated by diking and volcanism at the ridge axis

and display, among several kinds of small-scale ridge discontinuities (e.g., Macdonald et al., 1987), overlapping spreading centers (OSCs, Figure 7e) (Macdonald and Fox, 1986; Martinez et al., 1997). OSCs show a characteristic curvature of adjacent segment tips that overlap, outlining a topographically depressed area, and locally interact by altering the regional stress field (Sempere and Macdonald, 1986). With continued accretion at the segment tips, the intersegment area of the OSC grows through magmatic emplacement, widening the OSC over time, and leading to an unstable configuration. The OSC is thus regularly reset, a process that as in the case of NTOs (Figure 7d), leaves a wake of fossil, failed OSCs that is well preserved in off-axis seafloor morphology. These wakes also demonstrate that ridge discontinuities associated with OSCs are persistent in time, and that they may also migrate along-axis (Figure 7d).

Mid-ocean ridges often display morphological variations at the scale of individual ridge segments (Carbotte et al., 2015). "Typical" slow- and intermediate-spreading ridge segments with a well-developed rift valley (e.g., Figures 4b and e), are linear, sub-perpendicular to spreading, and feature regularly spaced, linear abyssal hills off-axis that are subparallel to the segment. They often display a systematic deepening and widening of the rift valley from the segment center, where the crust is thickest and the brittle lithosphere is thinnest, toward the segment end, where nodal basins develop (e.g., Kuo and Forsyth, 1988; Fox et al., 1992; Detrick et al., 1995; Cannat, 1996; Thibaud et al., 1998; Rabain et al., 2001). This imparts a so-called "hourglass structure" that tends to be more accentuated at slow-spreading segments (Figure 4b) than at intermediate-spreading ones (Figure 4e). These systematic segment-scale variations indicate focusing of melt towards segment centers and away from segment ends (e.g., Kuo and Forsyth, 1988; Lin et al., 1990; Gente et al., 1995), which amounts to local changes in melt supply on short (10s of km) spatial scales that drive straightforward along-axis variations in ridge morphology (e.g., Howell et al., 2016). Shorter slow-spreading ridge segments, or those developing in tectonically complex areas (e.g., oblique ridge sections, Figures 4c and f), may show no such pattern, and display significant variability instead. Segment-scale variations are also observed along ridges showing an axial high, with a deepening away from the center towards its ends that is less pronounced than at rift-valley segments (see Carbotte et al., 2015, and references therein).

Mid-ocean ridges across all spreading rates thus show systematic variations that may be linked to magmatic and tectonic gradients, which impart changes in seafloor

morphology (Carbotte et al., 2015). Ridge segments — bound by either fracture zones or non-transform offsets — can be thought of as the fundamental blocks of oceanic construction. Volcanic, tectonic and to a lesser extent hydrothermal processes interact at scales much shorter than that of segmentation to build seafloor topography, as mass wasting and sedimentation act to level and rework it.

5. Creating topography at ridges

5.1 Creating relief through volcanic processes

5.1.1 The extrusive oceanic upper crust

The global mid-ocean ridge system is also the most prominent volcanic structure on Earth, running along ~65.000 km. Volcanic processes not only build the crust, but also shape characteristic volcanic textures and landforms at the seafloor. The average amount of melt supplied to the ridge axis corresponds to an equivalent magmatic thickness of ~6-7 km (Figure 3), with significant regional variations (e.g., hotspots vs. amagmatic ultra-slow ridges). A fraction of this melt is supplied to the seafloor, building a volcanic, extrusive upper crust through successive lava eruptions, while the rest is emplaced in the lithosphere as plutonic intrusion or dikes to form the oceanic crust. Based on average extrusive thicknesses ranging from 250 to 1000 m (e.g., Blacic et al., 2004; Estep et al., 2019) and an average spreading rate of ~50 mm/yr (e.g. Cogné et al., 2006), the volume of lava erupted yearly along the ~65000 km long global mid ocean ridge system is in the range of ~0.9-3.5 km^3 per year. This volume of lava is emplaced discontinuously, as discrete volcanic eruptions. The recurrence of these eruptions depends on the overall melt supply to the axis and varies across ridge sections. Along the East Pacific Rise, several eruptions have been documented with recurrences of a few to ~10 years. Recurrence may, however, exceed hundreds or thousands of years at less volcanically active mid-ocean ridges, primarily along slow- and ultra-slow spreading centers.

A primary control on the style of lava flows is the effusion rate and erupted lava volume (e.g., Gregg and Fink, 1985; Griffiths and Fink, 1995). During low-effusion rate eruptions, seawater efficiently cools lava, freezing its surface and shaping pillows and tubes (Moore, 1975), with sizes that may exceed 1-2 m in diameter (Fox et al.,

1987). These structures are elongated downslope (e.g. flanks of seamounts, volcanic ridges, scarps, etc.) and record local emplacement conditions with limited lateral transport at the seafloor. When the lava volume and the effusion rates are sufficiently high, well-organized sheet lava flows may develop (e.g., Ballard et al., 1979; Luyendyk and Macdonald, 1985; Chadwick et al., 1999), with sheet flow structures, channels, and levees, transporting melt over distances of up to several km (Soule et al., 2005; Gini et al., Submitted). Intermediate effusion rates result in lobate lava flows, which are not well channelized and instead spread over wide areas (e.g., Clague et al., 2013). All these different lava flow types shape the seafloor at small scales (a few m up to a few tens of m, typically), with spatial distributions of different types of lava flows that vary drastically among ridges.

5.1.2. Volcanic processes and features at fast-spreading ridges

Volcanism at fast-spreading ridges and its role in building the uppermost volcanic layer of the crust is better studied and less variable than that at slow-spreading ridges, particularly along the fast-spreading East Pacific Rise. These systems are often underlain by a continuous melt lens at subseafloor depths of 1-3 km (Figure 3a), clearly imaged early on along seismic reflection profiles (Detrick et al., 1987; Hussenoeder et al., 1987; Canales et al., 2006). This melt lens, which likely collects the melt extracted from the mantle after it transits through several melt lenses both at deeper levels and sometimes offset from the axis (Marjanovic et al., 2014; Carbotte et al., 2021), supplies the lava through diking to the axial summit trough (Figure 8a), a narrow depression (graben) that varies in width from a few tens of m to ~200 m, and depths of a few tens of m (e.g., Fornari et al., 1998; Soule et al., 2009). Material erupted in the axial summit trough flows off-axis, either as lobate flows extending up to a few hundreds of m and repaving the seafloor, or as channeled lava flows, reaching distances of up to a few km (e.g., Hooft et al., 1996; Soule et al.,2005). Successive emplacement of lava flows thus builds an extrusive volcanic layer that increases from 100-300 m on-axis, to >500 m (sometimes > 1 km) off axis (Vera and Diebold, 1994; Hooft et al., 1996; Carbotte et al., 1997). Detailed, near-bottom bathymetric and side scan sonar maps of the seafloor reveal that the abundance and distribution of lava channels is both variable along the axis and over distances of a few km, and also asymmetric, probably reflecting local variations in terrain topography, in addition to uneven supply of lava along the axial summit trough. Both fast- and intermediate-

spreading ridges also show volcanic pillow mounds, which correspond to focused volcanic eruptions (e.g., White et al., 2000), and may align over eruptive fissures (e.g., Fig. 8b, Caress et al., 2012; Yeo et al., 2013).

Figure 8 about here

5.1.3 Volcanic processes and features at slow spreading ridges

Slow-spreading ridges with a limited magma supply show much more variability in volcanic styles than magmatic fast- and intermediate-spreading segments, although classically it is assumed that slow-spread volcanic seafloor is primarily paved by pillow lavas. These lavas are common and ubiquitous at the rift valley floor, and often emanate from small *axial seamounts*, *axial volcanic ridges*, and *hummocks*. Pillows often show varying degrees of fracturing, as well as sedimentation (e.g., Ballard and van Andel, 1977; Crane and Ballard, 1981; Karson et al., 1987; Brown and Karson, 1988).
Axial seamounts are ubiquitous along the rift valley floor of numerous slow-spreading segments. Their size varies from ~100 m in diameter to several km, the largest structures are often found at the center of magmatically robust ridge segments. Small- to intermediate sized axial seamounts (diameters <500 m), often pepper the rift valley floor (Figures 4b and 9a), and may show flat-topped summits, with and without summit craters (e.g., Kong et al., 1988; Smith and Cann, 1990; 1992; Smith et al., 1995). Their distribution suggests that the lava required to build these structures is delivered both along- and across the rift valley floor, and that melt supply is less focused across-axis than at fast-spreading or magma-rich ridges, where the bulk of the volcanism concentrates along the axial summit trough (Figure 8a). The distribution of these seamounts shows important variations, both locally along individual ridge segments, and regionally along ridge sections, with a strong control of the overall melt supply to the axis (e.g., Smith et. al., 1990; Mendel and Sauter, 1997; Cochran, 2008; Yeo et al., 2018). Numerous segments along ultra-slow to slow spreading ridges feature even larger volcanic edifices, with diameters in excess of 10 km, which develop at the center of segments as a result of focused and locally enhanced melt supply (e.g., Deschamps et al., 2003; Cannat et al., 2003; Escartín et al., 2014; Klischies et al. 2019; Chen et al., 2021).

Axial volcanic ridges are common along many slow-spreading ridge segments (Figure

9b). As in the case of the *axial seamounts*, axial volcanic ridges develop over a wide range of sizes. They include smaller structures, up to a few km in length, often distributed throughout the rift valley floor, and observed from ultra-slow to intermediate-spreading ridges (e.g., Luyendyk and Macdonald, 1977; Lawson et al. 1996; Grindlay et al., 1998; Chadwick et al., 2001; Michael et al., 2003; Yeo and Searle, 2013; Yeo and Clague, 2013). Larger axial volcanic ridges can extend a few tens of km along axis (e.g., Figure 9b), developing heights of a few hundreds of m, and their morphology suggests magmatic feeding through repeated dike intrusions over long periods of time (thousands of years).

Hummocks are smaller, cone- or dome-shaped edifices that are equant in plan view, and that have diameters of a few tens to ~200-300 m, rising above the surrounding seafloor by a few tens of m. (Figure 9c). They lack craters, but often show summit peaks (Figure 9c), indicating focused, short-lived volcanic eruptions (e.g., Yeo et al., 2011). They can coalesce and blanket large areas of the rift valley floor or can be found within individual patches throughout the rift valley floor, often referred to as hummocky terrain (e.g., Lawson et al., 1996; Sauter et al., 2004; Deschamps et al., 2005). These structures, which show both pillow and lobate flows, are plausibly the result of monogenetic eruptions, and may also contribute to the build-up of axial volcanic ridges.

Lava flows. Lava flows are observed at slow-spreading ridges, although they are less widespread than at fast spreading ridges (e.g., Lawson et al., 1996; Sauter and Mendel, 2004; Gini et al., submitted). The recurrence time of eruptions at slow-spreading ridges is much longer than that of fast-spreading ones, and to date no active eruption has been directly observed at the seafloor. With the seismic monitoring of mid-ocean ridges, however, potential volcanic events have been identified along the Mid-Atlantic Ridge at ~37°N, with a possible 2001 diking event with no clear evidence of seafloor eruption (Dziak et al., 2004), and along the Gakkel Ridge from acoustic and seismic events between 1999 and 2001 (Tolstoy et al., 2001; Schlindwein et al., 2005; Schlindwein and Riedel, 2010).

Figure 9 about here

Acoustic backscatter maps provide evidence of recent lava flow emplacement, owing

to the contrast in acoustic impedance of recently emplaced, unsedimented lava flows, relative to older sedimented seafloor. A section of the Reykjanes Ridge surveyed with a sonar system following a microseismic swarm in 1989 showed unfaulted, acoustically reflective lava flows suggesting a young age (Crane et al., 1997). Similar large lava flow fields have been identified as emanating from the summit of major seamounts or submarine volcanoes along the Gakkel ridge. These lava flows are unfaulted, spread over several tens of km and likely result from multiple eruption events. They are also colocated with seismic swarms that may record eruption events in the area, and with the presence of turbidity plumes in the water column (Tolstoy et al., 2001; Edwards et al., 2006; Schlindwein and Riedel, 2008). Other recent lava flows have been identified at the Lucky Strike segment of the slow-spreading Mid-Atlantic Ridge through acoustic backscatter data, showing a wide range of sizes (and hence associated eruption volumes), with flows emplaced along-axis and extending a few km (Figure 2, e.g., Yeo et al., 2016; Escartin et al., 2014; Gini et al., submitted).

5.1.4 Distribution of various volcanic structures along ridges

Ridge sections often display most if not all, of the various volcanic features described above, but in variable proportions and with different spatial distributions, again reflecting the amount of melt supplied to the ridge axis. For example, volcanic hummocky ridges are found both at fast- and slow-spreading ridges (e.g., aligned volcanic domes, Figures 8b and 9c for intermediate- and slow spreading ridges respectively). At fast ridges, they are primarily found at or near overlapping spreading centers, where melt supply may be locally reduced relative to the center of adjacent segments (White et al., 2002). Seamounts are also common at fast-spreading ridges (Figure 4a). Similarly, major volcanoes are also found at intermediate-spreading ridges, as is the case of Axial volcano along the Juan de Fuca Ridge (e.g., Applegate et al., 1990; Johnson and Embley, 1990). This particular setting resembles central volcanoes found along slow-spreading ridges, and experiences frequent eruptions (every ~5 years or so: Chadwick et al., 2010; Caress et al., 2012; Cabaniss et al., 2020). Small seamounts are also ubiquitous atop fast-spreading crust and are emplaced over the volcanic seafloor formed on-axis by eruptions flowing from the axial summit trough. The emplacement of these seamounts takes place in close proximity to the axis, e.g., ~15 km along the East Pacific Rise (Scheirer and Macdonald, 1995; White et al 1998). This distance is comparable to the width of the axial rift valley at slow spreading ridges and may thus be characteristic of volcanic upper crust

emplacement processes at magmatically well-supplied ridges. More recently, off-axis studies have also provided evidence of recent volcanism, associated with volcanic ridges and seamounts, taking place on ~20 Myr old oceanic crust (Devey et al., 2021).

5.2 Creating relief through tectonic processes

Abyssal hills, as described above, are ubiquitous and form along the axis of mid-ocean ridges at all spreading rates. Bound by normal faults, abyssal hills have a topographic relief and signature that dominate seafloor morphology at scales larger than the volcanic structures described in the previous section (see Figures 2b, 8, 9c). These abyssal hills are also disrupted or terminated by fracture zones as well as the wakes of non-transform offsets that may migrate along-axis and may be discontinuous and short-lived (Figures 4, 6, 7).

5.2.1. Tectonic relief associated with transform faults

Transform faults offset adjacent ridges laterally, with age offsets that range from a few million years (typically >40 km) to ~45 Myrs for the Romanche Fracture zone (~900 km offset) in the Equatorial Atlantic (Heezen et al., 1994). Tectonic deformation associated with these structures shapes some of the most important topographic features on the Earth's surface: narrow, extremely elongated valleys that scar the seafloor over tens to hundreds of kilometers. Another common feature associated with numerous fracture zones, and with some non-transform discontinuities along slow-spreading ridges, is the development of tectonically elevated massifs, associated with normal faults that develop larger relief at the end of the segments, and in proximity of transforms (e.g., Severinghaus and Macdonald, 1988; Allerton et al., 2000; Vogt and Yung, 2009). The inside corners of ridge-transform intersections are indeed often associated with large-offset faults (oceanic detachments) which shape prominent bathymetric highs (e.g., Cann et al., 1997; Blackman et al., 1998; Tucholke et a., 1998).

When plate motions and spreading directions change, transform faults adjust their orientation as they experience either transpression or transtension. This results in profound modifications of the transform fault morphology and structures within it. For large-offset transform faults, such as the Romanche and Vema (Figure 8a), transpression can bend the adjacent oceanic crust and tectonically uplift it, developing transverse ridges (Figure 7a), which are prominent ridges continuous over tens of km,

and sub-parallel to the fracture zone bounding the transform valley (Abrams et al., 1988; Searle et al., 1994; Bonatti et al., 2005). Within the transform valley a compressive ridge may form (Figure 8c), with significant tectonic uplift (e.g., Pockalny et al., 1997; Maia et al., 2019). Tectonic uplift, driven either by ridge-parallel normal faulting (inside corners and detachment faulting), or along transverse ridges due to transpression, generates vertical reliefs that may exceed 4-5 km, and develop over short lateral distances of ~10-20 km (Figure 7). Transform faults under transtension can show complex structures, including normal faulting and formation of oblique grabens, which can in some cases evolve into intra-transform spreading centers; as well as the emplacement of seamounts and volcanic ridges (e.g., Fornari et al., 1989, Hekinian et al., 1992; Hays and Perfit, 2004). Such intra-transform volcanism may seed the formation of rotating microplates (Bird and Naar, 1994) found along fast- and intermediate-spreading ridges (e.g., Franchetau et al., 1987; Naar and Hey, 1991; Bird et al., 1998).

At smaller scales, transform faults also reveal tectonic features within the transform valley. In addition to compression ridges described above, most transform faults show a clear and well-defined fault trace, ~100-200 m wide, and that can be continuous over 10s of km (Figures 8a-c). This structure localizes the recent shear deformation between adjacent plates across the transform fault.

5.2.2 Tectonic relief associated with non-transform offsets

The morphological signature of non-transform offsets along ridges displaying a rift valley (Figs. 4b, 4e, 6, 7d, 10b-c) is much more prominent than that formed along ridge sections with an axial high (Fig. 4a). When the lateral offset is larger than the rift valley width, and adjacent segments develop some along-axis overlap (Figures 4a, 4e, 7d, 10c), a tectonic septum develops with either tectonically uplifted massifs separating adjacent rift valleys, or highly deformed terrain showing complex faulting patterns that are oblique to the ridge axis direction (Goud and Karson, 1985; Gracia et al., 2000). These non-transform offsets leave clear wakes in seafloor bathymetry, corresponding to the termination of abyssal hills from adjacent segments along an area that lies low relative to the seafloor on either side of this tectonic discontinuity (Figures 10b, c). The traces often show a jagged structure, with short along-axis excursions over short periods of time (Figure 10c), while linear and well-defined non-transform offset traces (Figure 10g) are less frequent. The overall traces of these structures are in most cases

oblique to spreading, documenting along-axis migrations of these discontinuities due to a complex segmentation history involving expansion and shrinking of ridge segments on-axis over time (e.g., Carbotte et al., 1991; Grindlay et al., 1991; Gente et al., 1995; Tucholke et al., 1997; Spencer et al., 1997). Similar non-transform offsets, displacing the ridge axis by up to a few tens of km, also leave wakes in fast-spreading crust associated with their propagation (e.g., Searle and Hey, 1983; Naar and Hey, 1991; Bird et al., 1998), albeit with much more subdued topography associated with rotated traces of the paleo-axial high. In all cases, non-transform offsets lack long-lived strike-slip deformation along well-defined shear zones, as observed along transform faults. The relative motion of plates across the non-transform offset is accommodated instead by distributed deformation, rotation of the crust (particularly at fast-spreading ridges), and the growth of obliquely-striking faults (Figure 8d).

Figure 10 about here

5.2.3 Extensional high-angle normal faulting and abyssal hills

High-angle normal faults are ubiquitous and develop at all types of mid-ocean ridges to accommodate a portion of the plate separation that may vary from a few percent at fast magmatic spreading-centers, to ~100% along ultra-slow, amagmatic ridges (Figure 5). These faults dissect young brittle lithosphere, and manifest as steep seafloor scarps over a wide range of spatial scales. High-resolution bathymetric surveys, conducted with deep-sea vehicles, show fault scarps with heights of a few m to tens of m that are pervasive both near the axial high at fast ridges, and throughout the rift valley floor of slow- and intermediate-spreading (Figure 2, 8c, 9b, 10, bottom). Incipient faults developing on-axis are associated with widespread fissuring, both along the floor of axial rift valleys (Figures 2, 9c, 10 top), and at or near the ridge summit in more magmatic segments (Figure 4d, 8a). These faults and fissures dissect and dismember the volcanic features that were previously emplaced there (Figures 2, 9c, 10 top).

Normal faults typically lengthen along-axis and are advected off-axis as they accumulate offset and build topography. The width of the zone of active tectonic deformation near the axis can be estimated both from seismicity (maximum distance of ridge-related activity), or from the evolution of fault scarp heights / length away from the axis (distance at which these parameters cease to increase). Such estimates

are available only at a few locations, and yield zones of active deformation, and hence of active normal fault scarps, between ~20 and ~40 km (e.g., Alexander and Macdonald, 1996; Crowder and Macdonald, 2000; Bohnenstiehl and Carbotte, 2001; Smith et al., 2003; Escartin et al., 2007). Most normal faults develop at high-angles (45–60°) and accumulate limited displacements that result in both tectonic uplift and flexure of the faulted blocks. This process shapes abyssal hills with steep axis-facing slopes (fault scarp) and gentle, off-axis slopes (back-tilted block) (Figures 4 and 10 bottom). Abyssal hills typically trend parallel to the ridge axis and constitute an off-axis record of tectonic and volcanic processes active at ridges. Given the vast areas of seafloor they straddle, abyssal hills constitute the most prominent landform at the surface of the Earth, but are only visible sub-aerially in a few areas like the Afar region of Ethiopia.

Systematic variations in abyssal hill morphology have been noted across ocean basins and along the global mid-ocean ridge system. Abyssal hills formed at magmatically robust sections of slow-spreading ridges are typically spaced by ~3–10 km, while hills formed at fast spreading ridges can be as closely spaced as ~1 km (See compilation by Olive et al., 2015; Goff, 2020). Their topographic amplitude also decreases systematically from several km at slow ridges to <100 m at fast ridges. As noted earlier, hill morphology is most variable along the axis of slow and ultraslow mid-ocean ridges, in agreement with the variability in accretion modes. These characteristics can again be interpreted as reflecting the variability in mid-ocean ridge magma supply (Figure 3) and resulting modes of accretion (Figure 5). Mechanical considerations (Buck, 1993; Lavier et al., 2000; Behn and Ito, 2008) suggest that the lifespan of a normal fault is strongly modulated by the thickness of the brittle lithosphere they dissect. Because fault slip is difficult to sustain in thick off-axis lithosphere, faults that have moved off-axis are quickly abandoned in favor of newly-broken, on-axis faults. The pace at which major lithospheric faults are abandoned determines the spacing of abyssal hills. A high supply of magma to the ridge axis often results in faster off-axis advection, and thus quicker de-activation of normal faults, thereby shaping closely-spaced abyssal hills that have not had time to develop significant relief (Escartín et al., 1999; Buck et al., 2005).

Figure 11 about here

Figure 12 about here

5.2.4 Detachment faults and tectonically uplifted massifs

Slow- and ultraslow-spreading mid-ocean ridges show the greatest variability of tectonic structures, including entire areas that are shaped solely by faulting and feature virtually no volcanic construct (Figures 3-5). Among these, two kinds of seafloor features were identified early on: (1) oceanic detachment faults, with corrugated fault surfaces, also referred to as oceanic detachment faults, oceanic detachments, oceanic core complexes and megamullions, and (2) massifs with significant elevation above surrounding seafloor, often associated with the inside corner of ridge-transform intersections (see section 5.2.1) or non-transform offsets.

Oceanic detachment faults were first described in the 1990s, from both sonar and multibeam bathymetry data acquired along the Mid-Atlantic Ridge (e.g., Cann et al., 1997; Tucholke et al., 1998). These structures, which have been found at ultraslow to intermediate-spreading ridges, are recognizable in multibeam bathymetry data as massifs capped by smooth fault surfaces exposed directly at the seafloor (see Figures 4a, 6, 7b, 12). These faults often show a curvature in the extension direction (across axis), and exhibit clear corrugations in a direction parallel to spreading (e.g., Cann et al., 1997; MacLeod et al., 2002; Okino et al., 2004). Bathymetric corrugations (Figure 12) have lengths of several km, and are spaced laterally (along-axis) hundreds of m to a few km. Recent bathymetric surveys using deep-sea vehicles, together with *in-situ* observations, show that corrugations are observed down to outcrop scales, where fault surface striations also develop in the spreading direction (e.g., MacLeod et al., 2003; Parnell-Turner et al., 2018; Escartin et al., 2017; Szitkar et al., 2019). Their occurrence thus clearly disrupts the 'typical' ridge-parallel abyssal hill terrain, which is often present on the conjugate flank of the ridge, owing to the very asymmetric mode of oceanic accretion that takes place in the presence of detachments (Escartin et al., 2008; MacLeod et al., 2009; Reston & Ranero, 2011).

Slow- and ultra-slow spreading ridges also feature tectonically uplifted terrain, particularly associated with segment discontinuities (e.g. inside corners of ridge-transform intersections), that lack both the lineated abyssal hill structure associated with regular axis-parallel faulting, and the corrugated fault surfaces that are found at oceanic core complexes. Instead, these elevated massifs (~1000s of meters in relief, e.g., Severinghaus and Macdonald, 1988) often show irregular topographies, with evidence of mass-wasting along their flanks (see below). They also show outcrops of

mafic and ultramafic rocks (e.g., Tucholke and Lin, 1994), consistent with a formation linked to large-offset normal faulting but with a long and complex history of exhumation and denudation (e.g., Olive et al., 2019).

5.2.5 Amagmatic extension at ultra slow spreading ridges: smooth seafloor

Amagmatic extension is an extreme end member of oceanic accretion in the absence of melt, which has been extensively described along the ultra-slow southwest Indian ridge (Cannat et al., 2006; Sauter et al. 2013; Cannat et al., 2019). This oceanic accretion mode results in very high relief (>3 km) abyssal hills that are elongated and subparallel to the axis, but that lack high-angle fault scarps that are found elsewhere. Instead, the abyssal hills have domed or curved topography in the across axis (spreading) direction. This results in broad and wide abyssal hills with a surface that is smooth, and that lacks identifiable corrugations in bathymetric data. Figure 5 shows a schematic tectonic model associated with these structures, which are inferred to result from the cross-cutting of successive, long-lived detachment faults alternating in dip direction at the axis, resulting in the uplift of mantle material that is tectonically incorporated in the lithosphere (e.g., Sauter et al., 2013; Reston, 2018).

5.2.6 Fissuring

Fissuring is ubiquitous at the seafloor, along all ridge system types, regardless of spreading rates and magmatic supply. Fissure lengths span from a few tens of m to a few km, with openings that vary from m to tens of m. Both tectonic and magmatic fissuring along the Mid-Atlantic Ridge, has been best studied subaerially in Iceland (e.g., Acocella et al., 2000; Dauteuil et al., 2001; Sonette et al., 2010; Tentler and Temperley, 2007; Villemin et al., 2013), while submarine studies of seafloor fissuring are limited. At magmatic ridge systems, such as the fast-spreading East Pacific Rise (Wright et al., 1995; 2002) or Galapagos (e.g., White et al., 2008), fissuring is primarily of volcanic origin, and linked either to surface deformation induced by the emplacement of subseafloor dikes, or to eruptive fissures (Wright et al., 2002). Fissuring is particularly intense along the Axial Summit Trough (Figure 8a), and often dissects recent volcanic structures such as axial volcanic ridges (Figures 8b and 9c). Fissuring also develops in association with tectonic extension, particularly in the early stages of seafloor rupture and fault formation (e.g., Figures 2b, 11a, 11c). In this case,

fissures coalesce and accumulate a vertical offset in addition to purely horizontal extension, developing a fault scarp (Crider et al. 2015).

Fissuring penetrates to depths of a few hundreds of m subseafloor and modifies the physical properties of the upper oceanic crust. First, there is a likely enhancement of porosity and permeability that may facilitate water flow within the upper crust (e.g., Hearn et al., 2003), and that may be directly linked to the location of hydrothermal fields exploiting these fissure networks (e.g., Bohnenstiehl et al., 2000). Second, fissures generally develop along-axis and perpendicular to extension driving both diking and normal faulting within the rift valley floor of ridges showing significant tectonic extension (e.g., Bohnensitehl et al., 2000; Briais et al., 2000). This oriented fracture network results in a significant seismic anisotropy of the upper oceanic crust (e.g., Barclay et al., 2003).

5.3 Creating relief through hydrothermal processes

Hydrothermal activity within the oceanic crust is found along all types of ridges, and develops in a range of tectonic contexts, from the ridge axis to near- or off-axis sites associated with detachments, non-transform offsets, or major faults (e.g., German and Parson, 1998; Beaulieu et al., 2013; MacCaig et al., 2007; 2010). At the seafloor, the interaction of the venting hydrothermal fluids with seawater often results in the build-up of hydrothermal edifices and structures. The most common and best-studied hydrothermal systems are associated with magmatic heat sources at depth (Lowell et al., 2013), and result from the precipitation of the dissolved sulfides in high-temperature (>350°C) hydrothermal fluids (Figure 13a), when mixing with cold seawater (e.g., Haymon, 1983; von Damm, 1990). Hydrothermal chimneys are one of the most prominent and striking hydrothermal submarine features, and have typical heights of a few m, but can reach ~10-20 m (Figure 13b). These structures often develop on hydrothermal mounds (Figures 13a-c), which are formed by the growth and collapse of many of these chimneys over time, in addition to fallout from the hydrothermal plume itself. Hydrothermal venting typically concentrates at ridge sections to form hydrothermal fields tens to hundreds of meters wide (e.g., Lucky Strike, Figs 13b-c; TAG, Fig. 13d), while in some more magmatic systems such as the East Pacific Rise of the Juan de Fuca Ridge, vents may be distributed throughout the seafloor (e.g., Clague et al., 2020).

Hydrothermal activity can be associated with non-magmatic processes, and in

particular with low-temperature alteration of mantle rocks and their hydration (serpentinization). In these systems fluids venting at the seafloor are low-temperature (<100°C), high pH, and rich in volatiles (methane, hydrogen), and trigger the precipitation of carbonate from seawater upon mixing (Figure 13e; Kelley et al., 2005). Such systems have been identified to date along the Mid Atlantic Ridge (Lost City hydrothermal field; Kelley et al., 2005 Denny et al., 2010), and the Southwest Indian Ridge (Lecoeuvre et al., 2021).

The structures associated with both high- and low-temperature hydrothermal activity are small relative to other volcanic and tectonic features that develop along mid-ocean ridges, with diameters typically <100 m, and heights <~10-20 m. These are thus identifiable in the seafloor morphology only in high-resolution bathymetry acquired with deep-sea vehicles (AUVs and ROVs; Figure 13) and are difficult to identify morphologically off-axis if these systems are inactive. While some fields may build up over thousands of years, particularly at slow-spreading ridges (e.g., Lalou et al., 1989; 1990; 1993; Jamieson et al., 2013), these are also often obliterated by volcanic eruptions on-axis, faulting, erosion and mass wasting, or covered by sediments off axis.

Figure 13 about here

6. Modification and destruction of seafloor relief at ridges

Topography built at mid-ocean ridges by the combination of volcanic and tectonic processes, and to a lesser extent by hydrothermal activity, is modified or obliterated by two distinct processes that operate both on- and off-axis: erosion (primarily mass-wasting) and sedimentation. Mass wasting of oceanic basement is pervasive, and observed within the axial zone of ridges, particularly at slow-spreading ones where significant tectonic relief develops. In most cases, sedimentation is limited on-axis, and pelagic accumulation of sediments is only noticeable off-axis and over old seafloor. Some ridges, however, are active near continental sources of sediment, and thus experience significant on-axis sedimentation. Quantitative studies of these different processes are limited, and rates of both erosion and sedimentation are unconstrained to date, even though these significantly modify the submarine landscape, including that of abyssal hills (e.g., Goff and Tucholke, 1997).

6.1. Gravitational mass wasting

The slopes observed along mid-ocean ridges from submersible studies, which provide near-seafloor measurements that are not biased by filtering, typically show values 30°-45° (Mitchell et al., 2000; Howell et al., 2016). These slopes are also consistent with multibeam shipboard bathymetry data along the flanks of rift valleys (see www.gmrt.org), and with recent studies using high resolution bathymetry (Cannat et al. 2013). Erosion of fault scarps developing on basement initiates with the formation of gullies at small scales (Figure 14a), which may coalesce to form canyons (Tucholke et al., 1997; Goff and Tucholke, 1997), while depositing a talus of rubble at the foot of the scarp (e.g., Allerton et al., 1996; Figure 14a). This process is continuous, and efficiently erodes the tectonic fault scarp and reduces its overall slopes from a high-angle (likely >60°) to <45-30°, on-axis. At high-relief fault scarps, such as those developed by mature faults or along transform valleys, large-scale head scarps, with lengths of up to a few km, are common (e.g., Tucholke, 1992; Denny et al., 2015), and result in deep incisions (e.g., Figure 14b). High-resolution bathymetry along the walls of the Mid-Atlantic Ridge (Ferrini et al., 2013; Cannat et al., 2013) reveals mass-wasting at intermediate scales (~ 1 km), with complex slope failures, rotated blocks, elongated debris flows, and pressure ridges. The resulting overall scarp slopes range between <20° in areas that are dominating by serpentinites, and >25° for basalt dominated areas suggesting that the final fault scarp angle may be, at least in part, controlled by the frictional properties of basement lithologies (e.g., Mitchell et al., 2000; Cannat et al., 2013).

The processes of scarp erosion are efficient as they operate on-axis where fault scarps are efficiently eroded to low angles (typically ~30° or less). The observed abyssal hill morphology in older seafloor is thus shaped first by normal faulting on-axis and reshaped significantly during its formation on-axis by mass wasting erosion (e.g., Goff and Tucholke, 1997).

Figure 14 about here

6.2. Sedimentation

Sedimentation is a pervasive process that may affect oceanic lithosphere of all ages, and potentially cover basement topography, resulting in smoother seafloor textures,

and infilling of low-lying areas (e.g., Goff and Tucholke, 1997). The impact on seafloor morphology depends on the type of sedimentation.

First, pelagic sedimentation is spatially continuous although associated with extremely low sedimentation rates (typically less than a few mm/yr), and identifiable on-axis as a fine sediment dust, often used to qualitatively infer differences in the age of lava flows, particularly at fast-spreading ridges (e.g., Soule et al., 2006). While volcanic, tectonic, and hydrothermal morphologies are well-preserved on-axis, off-axis sediments efficiently infill depressions, and progressively blanket ageing seafloor (Figure 15; Collette et al., 1969; Mitchell et al., 1998; Parnell-Turner et al., 2014; see also Olson et al., 2016, and references therein), while smoothing abyssal hill scarps (e.g., Goff and Tucholke, 1997; Mithchell and Searle, 1998). At smaller scales, this infill of low-lying areas requires redistribution or diffusion of sediment (e.g., Marks, 1981; Webb and jordan, 1997), through turbidity currents and local mass wasting of unstable sediment deposits. Turbidity currents also exploit low-lying terrain corridors, such as fracture zone valleys, transport sediment over long distances, and contribute to local ponding (e.g., Jaroslow and Tucholke, 1994).

Second, sedimentation can be produced locally as a result of mass-wasting. This likely operates at the base of major topographic scarps where mass-wasting is active (see previous section, Figure 14b). Nodal basins at the end of ridge segments, primarily slow-spreading ones, are often surrounded by high-relief scarps pervasively incised by mass-wasting, and show a flat bottom (e.g., Fig. 14b). This suggests that such local sedimentation is efficient on-axis and cannot be directly associated with pelagic sediment infill. Sediment sources in these environments can be linked to local mass-wasting (e.g., Bonatti et al., 1974; Tamayo Tectonic Team, 1983; Gao, 2006). Breccias with heterogeneous basement clasts within a sediment matrix are also identified in ophiolites that are interpreted as sections of oceanic crust formed near ridge-transform intersections, or associated with significant extensional faulting and detachment formation (e.g., Bonatti and Honnorez, 1976; Moores, 1982; Portner et al., 2011).

Sediments from continents are a third source that may impact mid-ocean ridge sections (Figure 16). Detrital sedimentation can efficiently bury volcanic and tectonic features at the ridge axis, as it is the case of some back arc basins (e.g., Andaman Sea; Jourdain et al., 2016) or ridges (e.g., Gulf of California or Northern Juan de Fuca Ridge ; Lizarralde et al., 2007; Nedimovic et al., 2008), located near margins or the coast. In the Red sea, the ridge axis is also locally covered by salt glaciers or *neymars* (Augustin

et al., 2014; Feldens and Mitchell, 2015). It has been proposed that such intense syn-tectonic sedimentation may influence the very dynamics of seafloor spreading (e.g., De Sagazan and Olive, 2021).

Figure 15 about here

Figure 16 about here

7. Concluding remarks

All the volcanic, tectonic, hydrothermal, sedimentary and erosional processes briefly outlined above are active along the global mid-ocean ridge system, and their interactions shape the morphology of the seafloor over a wide range of spatial scales, from 10s to 100s of km (e.g., ridge segmentation, transform faults), to 10s of m (e.g., hydrothermal constructions). These are controlled by a wide range of factors (e.g., spreading rate, melt supply to the axis, type of sediment sources and distance to them, hydrothermal circulation, *etc*.), that vary both regionally (within and across ocean basins) and locally (along individual ridge segments). Figure 17 shows a detailed geomorphologic interpretation of a single slow-spreading ridge segment (Menez Gwenn, Northern Mid-Atlantic Ridge; Klischies et al., 2019). This segment shows a central volcano that imparts along-axis gradients in magma supply, thereby controlling the distribution of volcanic features, as well as the distribution of adjacent normal faults and the shape of the associated valley. Tectonics and volcanism also control the location, shape, and extent of sedimentary ponds, likely associated with both pelagic sedimentation and locally-derived sediment sources (e.g., mass-wasting).

Overall melt supply to the axis, rather than spreading rate, is the key parameter controlling the tectonic and volcanic accretion styles that shape the seafloor. For example, at ultra-slow spreading rates lithospheric accretion can range from almost amagmatic and avolcanic spreading, with detachment faults emplacing mantle in the lithosphere and exposing it at the seafloor, to ridge segments with major central volcanoes (e.g., South-West Indian Ridge; Cannat et al., 1996; Sauter and Cannat, 2016). Except for fast-spreading ridges, which are well-supplied magmatically and show limited variability in accretion style, spreading rate is therefore not an accurate indicator of the resulting seafloor morphology at scales of ~1-10 km, which changes

as a result of variability in the availability of melt to accommodate plate separation (Figures 3 and 5).

Figure 17 about here

While the origin and nature of different seafloor features formed along mid-ocean ridges are now relatively well established, the dynamics of these processes, such as the interactions or feedbacks between tectonic extension and mass wasting, require quantification to understand submarine landscape evolution. This is still hindered by the scarcity of data; bathymetry at a resolution of ~100 m is only available for 20% of the ocean floor, while only a few sites have been mapped with high resolution techniques (<10 to 1 m), or with optical data for geological ground truthing (both requiring surveys using deep-sea vehicles). Furthermore, understanding the dynamics of these different processes requires repeated or continuous observations. Change detection in subaerial geology has been critical not only to identify the mechanisms driving numerous processes (e.g., deformation, sedimentation, erosion, volcanism), but also to quantify the associated fluxes and rates at which they occur. As in the case of high-resolution bathymetry, temporal studies are limited to a few sites, and are representative of a very short ridge length (a few km to tens of km in each case). These temporal studies focus on active processes such as volcanic eruptions, hydrothermal activity, and faulting. To date, there are no temporal observations constraining mass wasting and sedimentation, and their links to tectonic uplift and volcanic processes along ridges. Quantifying these interactions, which span a wide range of temporal scales (<1 day to millions of yrs), as well as spatial ones (~1 m to 10s of km), will be key to understand the landscapes associated with the oceanic crust, which cover more than two thirds of the Earth's surface.

Acknowledgements: J. Escartín and J.-A. Olive are supported by CNRS and ENS, in addition to partial support by ANR SERSURF Project (ANR- 17-CE31-0020, France). We acknowledge the availability of multibeam bathymetry data through https://www.gmrt.org.

References

Abrams, L.J., Detrick, R.S., and Fox, P.J., 1988, Morphology and crustal structure of the Kane Fracture Zone transverse ridge: Journal of Geophysical Research, v. 93, no. B4, p. 3195–3210.

Acocella, V., Gudmundsson, A., Funiciello, R., 2000. Interaction and linkage of extension fractures and normal faults: examples from the rift zone of Iceland. Journal of Structural Geology 22, 1233–1246.

Alexander, R.J., Harper, G.D., and Bowman, J.R., 1993, Oceanic faulting and fault-controlled subseafloor hydrothermal alteration in the sheeted dyke complex of the Josephine Ophiolite: Journal of Geophysical Research, v. 98, no. B6, p. 9731–9759.

Allerton, S., Searle, R.C., and Murton, B.J., 1996, Bathymetric segmentation and faulting on the Mid-Atlantic Ridge, 24°00′N to 24°40′N (C. J. MacLeod, P. A. Tyler, & C. L. Walker, Eds.): Geological Society, London, Special Publications, v. 118, no. 1, p. 49–60, doi: 10.1144/GSL.SP.1996.118.01.04.

Allerton, S., Escartín, J., and Searle, R.C., 2000, Extremely asymmetric magmatic accretion of oceanic crust at the ends of slow-spreading ridge segments: Geology, v. 28, no. 2, p. 179, doi: 10.1130/0091-7613(2000)28<179:EAMAOO>2.0.CO;2.

Alt, J.C., 2003, Hydrothermal fluxes at mid-ocean ridges and on ridge flanks: Comptes Rendus Geosciences, v. 335, p. 853–864.

Antrim, L., Sempéré, J.-C., Macdonald, K.C., and Spiess, F.N., 1988, Fine scale study of a small overlapping spreading center system at 12°54′N on the East Pacific Rise: Marine Geophysical Researches, v. 9, p. 115–130.

Appelgate, B., 1990, Volcanic structural morphology of the South flank of Axial Volcano, Juan de Fuca Ridge: Result from a Sea MARC I side scan sonar survey: Journal of Geophysical Research, v. 95, no. B8, p. 12765–12783.

Augustin, N., Devey, C.W., van der Zwan, F.M., Feldens, P., Tominaga, M., Bantan, R. a., and Kwasnitschka, T., 2014, The rifting to spreading transition in the Red Sea: Earth and Planetary Science Letters, v. 395, p. 217–230, doi: 10.1016/j.epsl.2014.03.047.

Ballard, R.D., and van Andel, T.H., 1977, Morphology and tectonics of the inner rift valley at lat 36°50′N on the Mid-Atlantic Ridge: Geological Society of America Bulletin, v. 88, p. 507–530.

Ballard, R.D., Holcomb, R.T., and van Andel, T.H., 1979, The Galapagos rift at 86°W 2. Sheet flows, collapse pits, and lava lakes of the rift valley: Journal of Geophysical Research, v. 84, no. B10, p. 5407–5422.

Bandy, W.L., Michaud, F., Mortera Gutiérrez, C.A., Dyment, J., Bourgois, J., Royer, J.-Y., Calmus, T., Sosson, M., and Ortega-Ramirez, J., 2011, The Mid-Rivera-Transform Discordance: Morphology and Tectonic Development: Pure and Applied Geophysics, v. 168, no. 8–9, p. 1391–1413, doi: 10.1007/s00024-010-0208-8.

Barclay, A.H., and Toomey, D.G., 2003, Shear wave splitting and crustal anisotropy

at the Mid-Atlantic Ridge: Journal of Geophysical Research, v. 108, no. B8, p. B8, 2378, doi:10.1029/2001JB000918.

Beaulieu, S.E., Baker, E.T., German, C.R., and Maffei, A., 2013, An authoritative global database for active submarine hydrothermal vent fields: Geochemistry, Geophysics, Geosystems, v. 14, no. 11, p. 4892–4905, doi: 10.1002/2013GC004998.

Behn, M.D., Lin, J., and Zuber, M.T., 2002, Mechanisms of normal fault development at mid-ocean ridges: Journal of Geophysical Research, v. 107, no. B4, p. 10.1029/2001JB000503.

Berann, H. C., B. C. Heezen and M. Tharp, "World Ocean Floor Map", National Geographic, 1977.

Bird, R.T., and Pockalny, R.A., 1994, Late Cretaceous and Cenozoic seafloor and oceanic basement roughness: Spreading rate, crustal age and sediment thickness correlations: Earth and Planetary Science Letters, v. 123, p. 239–254.

Bird, R.T., Naar, D.F., Larson, R.L., Searle, R.C., and Scotese, C.R., 1998, Plate tectonic reconstructions of the Juan Fernandez microplate: Transformation from internal shear to rigid rotation: Journal of Geophysical Research: Solid Earth, v. 103, no. B4, p. 7049–7067, doi: 10.1029/97JB02133.

Bird, R.T., and Naar, D.F., 1994, Intratransform origin of mid-ocen ridge microplates: Geology, v. 22, p. 987–990.

Blacic, T.M., Ito, G., Canales, J.P., Detrick, R.S., and Sinton, J., 2004, Constructing the crust along the Galapagos Spreading Center 91.3°-95.5°W: Correlation of seismic layer 2A with axial magma lens and topographic characteristics: Journal of Geophysical Research, v. 109, p. B10310, doi:10.1029/2003JB003066.

Blackman, D.K., Cann, J.R., Janssen, B., and Smith, D.K., 1998, Origin of extensional core complexes: Evidence from the Mid-Atlantic Ridge at Atlantis fracture zone: Journal of Geophysical Research: Solid Earth, v. 103, no. 9, p. 21315–21333, doi: 10.1029/98jb01756.

Bohnenstiehl, D., and Carbotte, S.M., 2001, Faulting patterns near 19°30'S on the East Pacific Rise: Fault formation and growth at a superfast spreading center: Geochemistry, Geophysics, Geosystems, v. 2, p. 2001GC000156.

Bohnenstiehl, D., and Kleinrock, M.C., 2000, Evidence of spreading-rate dependence in the displacement-length ratios of abyssal hill faults at mid-ocean ridges: Geology, v. 28, no. 5, p. 395–398.

Bonatti, E., Brunelli, D., Buck, W.R., Cipriani, A., Fabretti, P., Ferrante, V., Gasperini, L., and Ligi, M., 2005, Flexural uplift of a lithospheric slab near the Vema transform (Central Atlantic): Timing and mechanisms: Earth and Planetary Science Letters, v. 240, p. 642–655.

Bonatti, E., Emiliani, C., Ferrara, G., Honnorez, G., and Rydell, H., 1974, Ultramafic-carbonate breccias from the equatorial mid-Atlantic ridge: Marine Geology, v. 16, p. 83–102.

Bonatti, E., and Honnorez, J., 1976, Sections of the Earth's crust in the Equatorial Atlantic: Journal of Geophysical Research, v. 81, no. 23, p. 4104–4116.

Bown, J.W., and White, R.S., 1994, Variation with spreading rate of oceanic crustal thickness and geochemistry: Earth and Planetary Science Letters, v. 121, p. 435–449.

Brace, W.F., and Kohlstedt, D.L., 1980, Limits on lithospheric stress imposed by laboratory experiments: Journal of Geophysical Research, v. 85, p. 6248–6252.

Brown, J.R., and Karson, J.A., 1988, Variations in axial processes on the Mid-Atlantic Ridge: The median valley of the MARK area: Marine Geophysical Researches, v. 10, p. 109–138.

Briais, A., Sloan, H., Parson, L.M., and Murton, B.J., 2000, Accretionary processes in the axial valley of the mid-Atlantic ridge 27°N-30°N from TOBI side-scan sonar images: Marine Geophysical Researches, v. 21, p. 87–119.

Bryan, W.B., 1991, From pillow lava to sheet flow: Oceanus, v. Winter, p. 43–50.

Buck, W.R., and Poliakov, A.N.B., 1998, Abyssal hills formed by stretching oceanic lithosphere: Nature, v. 392, p. 272–275.

Bullard, E., Everett, J.E., and Smith, A.G., 1965, The fit of the continents around the Atlantic: Philosophical Transactions of the Royal Society of London, v. 258, no. 1088, p. 41–51.

Cabaniss, H.E., Gregg, P.M., Nooner, S.L., and Chadwick, W.W., 2020, Triggering of eruptions at Axial Seamount, Juan de Fuca Ridge: Scientific Reports, v. 10, no. 1, p. 10219, doi: 10.1038/s41598-020-67043-0.

Canales, J.P., Dañobeitia, J.J., Detrick, R.S., Hooft, E.E.E., Bartolomé, R., and Naar, D.F., 1997, Variations in axial morphology along the Galápagos spreading center and the influence of the Galápagos hotspot: Journal of Geophysical Research, v. 102, no. B12, p. 27341–27354.

Canales, J.P., Singh, S.C., Detrick, R.S., Carbotte, S.M., Harding, A., Kent, G.M., Diebold, J.B., Babcock, J., and Nedimovic, M.R., 2006, Seismic evidence for variations in axial magma chamber properties along the southern Juan de Fuca Ridge: Earth and Planetary Science Letters, v. 246, p. 353–366.

Cann, J.R., 1970, New model for the structure of the ocean crust: Nature, v. 226, p. 928–930.

Cann, J., and Strens, M.R., 1989, Modeling periodic megaplume emission by black smoker systems: Journal of Geophysical Research, v. 94, no. B9, p. 12227–12237.

Cann, J.R., Blackman, D.K., Smith, D.K., McAllister, E., Janssen, B., Mello, S., Avgerinos, E., Pascoe, A.R., and Escartín, J., 1997, Corrugated slip surfaces formed at North Atlantic ridge-transform intersections: Nature, v. 385, p. 329–332.

Cannat, M., 1996, How thick is the magmatic crust at slow spreading oceanic ridges? Journal of Geophysical Research: Solid Earth, v. 101, no. B2, p. 2847–2857, doi: 10.1029/95JB03116.

Cannat, M., Sauter, D., Mendel, V., Ruellan, E., Okino, K., Escartin, J., Combier, V., and Baala, M., 2006, Modes of seafloor generation at a melt-poor ultraslow-spreading ridge: Geology, v. 34, no. 7, p. 605–608.

Cannat, M., Briais, A., Deplus, C., Escartín, J., Georgen, J., Lin, J., Mercouriev, S., Meyzen, C., Muller, M., Pouliquen, G., Rabain, A., and da Silva, P., 1999, Mid-Atlantic Ridge–Azores hotspot interactions: along-axis migration of a hotspot-derived event of enhanced magmatism 10 to 4 Ma ago: Earth and Planetary Science Letters, v. 173, no. 3, p. 257–269, doi: 10.1016/S0012-821X(99)00234-4.

Cannat, M., Rommeveaux-Jestin, C., and Fujimoto, H., 2003, Melt supply variations to a magma-poor ultra-slow spreading ridge (Southwest Indian Ridge 61° to 69°E): Geochemistry, Geophysics, Geosystems, v. 4, no. 8, p. 9104, doi:10.1029/2002GC000480, doi: 10.1029/2002GC000480.

Cannat, M., Mangeney, A., Ondreas, H., Fouquet, Y., and Normand, A., 2013, High-resolution bathymetry reveals contrasting landslide activity shaping the walls of the Mid-Atlantic Ridge axial valley: GEOCHEMISTRY GEOPHYSICS GEOSYSTEMS, v. 14, no. 4, p. 996–1011, doi: 10.1002/ggge.20056.

Cannat, M., Sauter, D., Escartin, J., Lavier, L., and Picazo, S., 2009, Oceanic corrugated surfaces and the strength of the axial lithosphere at slow spreading ridges: Earth and Planetary Science Letters, v. 288, p. 174–183.

Cannat, M., Mangeney, A., Ondreas, H., Fouquet, Y., and Normand, A., 2013, High-resolution bathymetry reveals contrasting landslide activity shaping the walls of the Mid-Atlantic Ridge axial valley: GEOCHEMISTRY GEOPHYSICS GEOSYSTEMS, v. 14, no. 4, p. 996–1011, doi: 10.1002/ggge.20056.

Cannat, M., Sauter, D., Lavier, L., Bickert, M., Momoh, E., and Leroy, S., 2019, On spreading modes and magma supply at slow and ultraslow mid-ocean ridges: Earth Planet. Sci. Let.., v. 519, p. 223--233.

Carbotte, S.M., Smith, D.K., Cannat, M., and Klein, E.M., 2015, Tectonic and magmatic segmentation of the Global Ocean Ridge System: a synthesis of observations: Geological Society, London, Special Publications, p. 10.1144/SP420.5, doi: 10.1144/SP420.5.

Carbotte, S., J. Mutter and G. Ponce-Correa, 1998, Influence of magma supply and spreading rate on crustal magma bodies and emplacement of the extrusive layer: Insights from the East Pacific Rise at lat 16°N, Geology, v. 26, no. 5, 455–458.

Carbotte, S.M., Mutter, J.C., and Xu, L., 1997, Contribution of volcanism and tectonism to axial and flank morphology of the southern East Pacific Rise, 17°10'-17°40'S, from a study of layer 2A geometry: Journal of Geophysical Research, v. 102, no. B5, p. 10,110-165,184.

Carbotte, S.M., Marjanović, M., Arnulf, A.F., Nedimović, M.R., Canales, J.P., and Arnoux, G.M., 2021, Stacked Magma Lenses Beneath Mid-Ocean Ridges: Insights From New Seismic Observations and Synthesis With Prior Geophysical and Geologic Findings: Journal of Geophysical Research: Solid Earth, v. 126, no. 4, p. 1–19, doi: 10.1029/2020JB021434.

Carbotte, S.M., Smith, D.K., Cannat, M., and Klein, E.M., 2015, Tectonic and magmatic segmentation of the Global Ocean Ridge System: a synthesis of observations: Geological Society, London, Special Publications, p. 10.1144/SP420.5, doi: 10.1144/SP420.5.

Caress, D.W., Clague, D. a., Paduan, J.B., Martin, J.F., Dreyer, B.M., Chadwick, W.W., Denny, A., and Kelley, D.S., 2012, Repeat bathymetric surveys at 1-metre resolution of lava flows erupted at Axial Seamount in April 2011: Nature Geoscience, v. 5, no. 7, p. 483–488, doi: 10.1038/ngeo1496.

Caress, D.W., Clague, D. a., Paduan, J.B., Martin, J.F., Dreyer, B.M., Chadwick, W.W., Denny, A., and Kelley, D.S., 2012, Repeat bathymetric surveys at 1-metre resolution of lava flows erupted at Axial Seamount in April 2011: Nature Geoscience, v. 5, no. 7, p. 483–488, doi: 10.1038/ngeo1496.

Chadwick, W.W., Gregg, K.T.P., and Embley, R.W., 1999, Submarine lineated sheet flows: a unique lava morphology formed on subsiding lava ponds: Bulletin of Volcanology, v. 61, p. 194–206.

Chadwick, W.W., Scheirer, D.S., Embley, R.W., and Johnson, H.P., 2001, High-resolution bathymetric surveys using scanning sonar: Lava flow morphology, hydrothermal vents, and geologic structure at recent eruption sites on the Juan de Fuca Ridge: Journal of Geophysical Research, v. 106, no. B8, p. 16075–16099.

Chadwick, W.W., Nooner, S.L., Butterfield, D. a., and Lilley, M.D., 2012, Seafloor deformation and forecasts of the April 2011 eruption at Axial Seamount: Nature Geoscience, v. 5, no. 7, p. 474–477, doi: 10.1038/ngeo1464.

Chen, Y., and Morgan, W.J., 1990a, A nonlinear rheology for mid-ocean ridge axis topography: Journal of Geophysical Research, v. 95, p. 17583–17604.

Chen, Y., and Morgan, W.J., 1990b, Rift valley/no rift valley transition at mid-ocean ridges: Journal of Geophysical Research, v. 95, p. 17571–17581.

Christeson, G.L., Goff, J.A., and Reece, R.S., 2019, Synthesis of Oceanic Crustal Structure From Two-Dimensional Seismic Profiles: Reviews of Geophysics, v. 57, no. 2, p. 504–529, doi: 10.1029/2019RG000641.

Clague, D.A., Dreyer, B.M., Paduan, J.B., Martin, J.F., Chadwick, W.W., Caress, D.W., Portner, R.A., Guilderson, T.P., McGann, M.L., Thomas, H., Butterfield, D.A., and Embley, R.W., 2013, Geologic history of the summit of Axial Seamount, Juan de Fuca Ridge: Geochemistry, Geophysics, Geosystems, v. 14, no. 10, p. 4403–4443, doi: 10.1002/ggge.20240.

Clague, D.A., Dreyer, B.M., Paduan, J.B., Martin, J.F., Caress, D.W., Gill, J.B., Kelley, D.S., Thomas, H., Portner, R.A., Delaney, J.R., Guilderson, T.P., and McGann, M.L., 2014, Eruptive and tectonic history of the Endeavour Segment, Juan de Fuca Ridge, based on AUV mapping data and lava flow ages: Geochemistry, Geophysics, Geosystems, v. 15, no. 8, p. 3364–3391, doi: 10.1002/2014GC005415.

Clague, D.A., Martin, J.F., Paduan, J.B., Butterfield, D.A., Jamieson, J.W., Le Saout, M., Caress, D.W., Thomas, H., Holden, J.F., and Kelley, D.S., 2020, Hydrothermal Chimney Distribution on the Endeavour Segment, Juan de Fuca Ridge:

Geochemistry, Geophysics, Geosystems, v. 21, no. 6, p. 1–12, doi: 10.1029/2020GC008917.

Cochran, J.R., 2008, Seamount volcanism along the Gakkel Ridge, Arctic Ocean: Geophysical Journal International, v. 174, no. 3, p. 1153–1173, doi: 10.1111/j.1365-246X.2008.03860.x.

Cogné, J.-P., and Humler, E., 2006, Trends and rhythms in global seafloor generation rate: Geochemistry, Geophysics, Geosystems, v. 7, no. 3, p. n/a-n/a, doi: 10.1029/2005GC001148.

Collette, B.J., Ewing, J.I., Lagaay, R.A., and Truchan, M., 1969, Sediment distribution in the oceans; The Atlantic between 10 degrees and 19 degrees N: Marine Geology, v. 7, no. 4, p. 279–345

Conder, J.A., and Forsyth, D.W., 2001, Seafloor spreading on the Southeast Indian Ridge over the last one million years: a test of the Capricorn plate hypothesis: Earth and Planetary Science Letters, v. 188, p. 91–105.

Corliss, J.B., 1990, Hot springs and the origin of life: Nature, v. 347, p. 624.

Cormier, M.,Contribution of multibeam bathymetry to understanding the processes that shape mid-ocean ridges, GEBCO Centenary Conference, Monaco, 2003. https:https://www.gebco.net/about_us/presentations_and_publications

Cormier, M.H., and Sloan, H., 2018, Abyssal Hills and Abyssal Plains, in Micallef, A., Krastel, S., and Savini, A. eds., Springer Geology, Springer Geology, Springer International Publishing, Cham, p. 389–408.

Crane, K., and Ballard, R.D., 1981, Volcanics and structure of the FAMOUS narrowgate rift: evidence for cyclic evolution: AMAR 1: Journal of Geophysical Research, v. 86, no. B6, p. 5112–5124.

Crane, K., Johnson, L., Appelgate, B., Nishimura, C., Buck, R., Jones, C., Vogt, P., and Kos'yan, R., 1997, Volcanic and Seismic Swarm Events on the Reykjanes Ridge and Their Similarities to Events on Iceland: Results of a Rapid Response Mission: Marine Geophysical Research, v. 19, no. 4, p. 319–338, doi: 10.1023/A:1004298425881.

Crawford, W.C., Singh, S.C., Seher, T., Combier, V., Dusunur, D., Cannat, M., Rona, P., Devey, C.W., Dyment, J., and Murton, B., 2010, Crustal structure, magma chamber and faulting beneath the Lucky Strike hydrothermal fields, in Diversity of Hydrothermal Sytems on Slow Spreading Ocean Ridges, AGU, Washington DC, p. 113–132.

Crider, J., 2015, The initiation of brittle faults in crystalline rock: J. Struct. Geol., v. 77, pp. 159-174.

Crowder, L.K., and Macdonald, K.C., 2000, New constraints on the width of the zone of active faulting on the East Pacific Rise 8°30'N - 10°00'N from SeaBeam bathymetry and SeaMARC II side-scan sonar: Marine Geophysical Researches, v. 21, p. 513–527.

Dauteuil, O., Angelier, J., Bergerat, F., Verrier, S., and Villemin, T., 2001, Deformation partitioning inside a fissure swarm of the northern Icelandic rift:

Journal of Structural Geology, v. 23, p. 1359–1372.

Davis, E.E., and Villinger, H., 1992, Tectonic and Thermal Structure of the Middle Valley Sedimented Rift, Northern Juan de Fuca Ridge, in Davis, E.E., Mottl, M.J., and Fisher, A.T. eds., Proceedings of the Ocean Drilling Program, 139 Initial Reports, Ocean Drilling Program, p. 9–41.

de Martin, B.J., Sohn, R.A., Canales, J.P., and Humphris, S.E., 2007, Kinematics and geometry of active detachment faulting beneath the Trans-Atlantic Geotraverse (TAG) hydrothermal field on the Mid-Atlantic Ridge: Geology, v. 35, no. 8, p. 711–714.

Demets, C., Gordon, R.G., and Argus, D.F., 2010, Geologically current plate motions: Geophysical Journal International, v. 182, p. 1–80, doi: 10.1111/j.1365-246X.2009.04491.x.

Denny, A.R., Kelley, D.S., and Früh-Green, G.L., 2016, Geologic evolution of the Lost City Hydrothermal Field: Geochemistry, Geophysics, Geosystems, v. 17, no. 2, p. 375–394, doi: 10.1002/2015GC005869.

De Sagazan, C., and Olive, J.-A., 2021, Assessing the impact of sedimentation on fault spacing at the Andaman Sea spreading center: Geology, v. 49.

Deschamps, A., Fujiwara, T., Asada, M., Montesi, L., and Gente, P., 2005, Faulting and volcanism in the axial valley of the slow-spreading center of the Mariana back-arc basin from Wadatsumi side-scan sonar images: Geochemistry, Geophysics, Geosystems, v. 6, no. 5, p. Q05006, doi:10.1029/2004GC000881.

Detrick, R.S., Needham, H.D., and Renard, V., 1995, Gravity anomalies and crustal thickness variations along the Mid-Atlantic Ridge between 33°N and 40°N: Journal of Geophysical Research: Solid Earth, v. 100, no. B3, p. 3767–3787, doi: 10.1029/94JB02649.

Detrick, R.S., Harding, A.J., Kent, G.M., Orcutt, J.A., Mutter, J.C., and Buhl, P., 1993, Seismic Structure of the Southern East Pacific Rise: Science, v. 259, no. 5094, p. 499–503, doi: 10.1126/science.259.5094.499.

Devey, C.W., Greinert, J., Boetius, A., Augustin, N., and Yeo, I., 2021, How volcanically active is an abyssal plain? Evidence for recent volcanism on 20 Ma Nazca Plate seafloor: Marine Geology, p. 106548, doi: 10.1016/j.margeo.2021.106548.

Dick, H.J.B., Tivey, M.A., and Tucholke, B.E., 2008, Plutonic foundation of a slow-spreading ridge segment: Oceanic core complex at Kane Megamullion, 23° 30′N, 45 °20′W: Geochemistry, Geophysics, Geosystems, v. 9, p. Q05014, doi:10.1029/2007GC001645.

Dick, H.J.B., Lissenberg, C.J., and Warren, J.M., 2010, Mantle Melting, Melt Transport, and Delivery Beneath a Slow-Spreading Ridge: The Paleo-MAR from 23°15′N to 23°45′N: Journal of Petrology, v. 51, no. 1 & 2, p. 425–467, doi:10.1093/petrology/egp088.

Dziak, R.P., Smith, D.K., Bohnenstiehl, D.R., Fox, C.G., Desbruyères, D., Matsumoto, H., Tolstoy, M., and Fornari, D.J., 2004, Evidence of a recent magma dike intrusion at

the slow spreading Lucky Strike segment, Mid-Atlantic Ridge: Journal of Geophysical Research, v. 109, p. B12102, doi: 10.1029/2004JB003141.

Elderfield, H., and Schulz, A., 1996, Mid-Ocean ridge hydrothermal fluxes and the chemical composition of the ocean: Annual Reviews of Earth and Planetary Sciences, v. 24, p. 191–224.

Escartín, J., Soule, S.A., Cannat, M., Fornari, D.J., Düşünür, D., and Garcia, R., 2014, Lucky Strike seamount: Implications for the emplacement and rifting of segment-centered volcanoes at slow spreading mid-ocean ridges: Geochemistry, Geophysics, Geosystems, v. 15, no. 11, p. 4157–4179, doi: 10.1002/2014GC005477.

Escartin, J., Barreyre, T., Cannat, M., Garcia, R., Gracias, N., Deschamps, A., Salocchi, A., Sarradin, P.-M., and Ballu, V., 2015, Hydrothermal activity along the slow-spreading Lucky Strike ridge segment (Mid-Atlantic Ridge): Distribution, heatflux, and geological controls: Earth and Planetary Science Letters, v. 431, p. 173–185, doi: 10.1016/j.epsl.2015.09.025.

Escartín, J., Soule, S.A., Fornari, D.J., Tivey, M.A., Schouten, H., and Perfit, M.R., 2007, Interplay between faults and lava flows in construction of the upper oceanic crust: The East Pacific Rise crest 9°25′-9°58′N: Geochemistry, Geophysics, Geosystems, v. 8, no. 6, p. n/a-n/a, doi: 10.1029/2006GC001399.

Escartín, J., Mével, C., Petersen, S., Bonnemains, D., Cannat, M., Andreani, M., Augustin, N., Bezos, A., Chavagnac, V., Choi, Y., Godard, M., Haaga, K., Hamelin, C., Ildefonse, B., et al., 2017, Tectonic structure, evolution, and the nature of oceanic core complexes and their detachment fault zones (13°20′N and 13°30′N, Mid Atlantic Ridge): Geochemistry, Geophysics, Geosystems, v. 18, no. 4, p. 1451–1482, doi: 10.1002/2016GC006775.

Estep, J., Reece, R., Kardell, D.A., Christeson, G.L., and Carlson, R.L., 2019, Seismic Layer 2A: Evolution and Thickness From 0- to 70-Ma Crust in the Slow-Intermediate Spreading South Atlantic: Journal of Geophysical Research: Solid Earth, v. 124, no. 8, p. 7633–7651, doi: 10.1029/2019JB017302.

Evans, B., Fredrich, J.T., and Wong, T.-F., 1990, The brittle-ductile transition in rocks: Recent experimental and theoretical progress: Geophysical Monograph, v. 56, p. 1–20.

Favali, P., and Beranzoli, L., 2006, Seafloor Observatory Science: a review: Annals of Geophysics, v. 49, no. 2/3, p. 515–567.

Feldens, P., and Mitchell, N.C., 2015, Salt Flows in the Central Red Sea, in Rasul, N.M.A. and Stewart, I.C.F. eds., Berlin Heidelberg, p. 205–218.

Ferrini, V.L., Shillington, D.J., Gillis, K., MacLeod, C.J., Teagle, D. a. H., Morris, A., Cazenave, P.W., Hurst, S., and Tominaga, M., 2013, Evidence of mass failure in the Hess Deep Rift from multi-resolutional bathymetry data: Marine Geology, v. 339, p. 13–21, doi: 10.1016/j.margeo.2013.03.006.

Fornari, D., Von Damm, K., Bryce, J., Cowen, J., Ferrini, V., Fundis, A., Lilley, M., Luther, G., Mullineaux, L., Perfit, M., Meana-Prado, M.F., Rubin, K., Seyfried, W., Shank, T., et al., 2012, The East Pacific Rise Between 9°N and 10°N: Twenty-Five

Years of Integrated, Multidisciplinary Oceanic Spreading Center Studies: Oceanography, v. 25, no. 1, p. 18–43, doi: 10.5670/oceanog.2012.02.

Fornari, D.J., Gallo, D.G., Edwards, M.H., Madsen, J.A., Perfit, M.R., and Shor, A.N., 1989, Structure and topography of the Siqueiros transform fault system: Evidence for the development of intra-transform spreading centers: Marine Geophysical Researches, v. 11, no. 4, p. 263–299, doi: 10.1007/BF00282579.

Fornari, D.J., Haymon, R.M., Perfit, M.R., Gregg, K.T.P., and Edwards, M.H., 1998, Axial summith through of the East Pacific Rise 9°-10°N: Geological characteristics and evolution of the axial zone on fast-spreading ridges: Journal of Geophysical Research, v. 102, no. B5, p. 9827–9855.

Fouquet, Y., Cambon, P., Etoubleau, J., Charlou, J.L., OndréAs, H., Barriga, F.J.A.S., Cherkashov, G., Semkova, T., Poroshina, I., Bohn, M., Donval, J.P., Henry, K., Murphy, P., and Rouxel, O., 2010, Geodiversity of Hydrothermal Processes Along the Mid-Atlantic Ridge and Ultramafic-Hosted Mineralization: a New Type Of Oceanic Cu-Zn-Co-Au Volcanogenic Massive Sulfide Deposit, in Diversity Of Hydrothermal Systems On Slow Spreading Ocean Ridges, American Geophysical Union, p. 321–367.

Fox, P.J., Lowrie, A., and Heezen, B.C., 1969, Oceanographer Fracture Zone: Deep-Sea Research, v. 16, p. 59–66.

Fox, C.G., Murphy, K.M., and Embley, R.W., 1988, Automated display and statistical analysis of interpreted deep-sea bottom photographs: Marine Geology, v. 78, no. 3–4, p. 199–216, doi: 10.1016/0025-3227(88)90109-0.

Fox, P.J., Grindlay, N.R., and Macdonald, K.C., 1991, The Mid-Atlantic Ridge (31°S-34°30′S): Temporal and spatial variations in accretionary processes: Marine Geophysical Researches, v. 13, p. 1–20.

Fouquet, Y., Cambon, P., Etoubleau, J., Charlou, J.L., OndréAs, H., Barriga, F.J.A.S., Cherkashov, G., Semkova, T., Poroshina, I., Bohn, M., Donval, J.P., Henry, K., Murphy, P., and Rouxel, O., 2010, Geodiversity of Hydrothermal Processes Along the Mid-Atlantic Ridge and Ultramafic-Hosted Mineralization: a New Type Of Oceanic Cu-Zn-Co-Au Volcanogenic Massive Sulfide Deposit, in Diversity Of Hydrothermal Systems On Slow Spreading Ocean Ridges, American Geophysical Union, p. 321–367.

Francheteau, J., Yelles-Chaouche, A., and Craig, H., 1987, The Juan Fernandez microplate north of the Pacific-Nazca-Antarctic plate junction at 35°S: Earth and Planetary Science Letters, v. 86, p. 253–268.

Fundis, A.T., Soule, A.S., Fornari, D.J., and Perfit, M.R., 2010, Paving the seafloor: Volcanic emplacement processes during the 2005–2006 eruptions at the fast spreading East Pacific Rise, 9°50′N: Geochemistry, Geophysics, Geosystems, v. 11, no. 8, p. Q08024, doi:10.1029/2010GC003058.

Gaina, C., Gernigon, L., and Ball, P., 2009, Palaeocene–Recent plate boundaries in the NE Atlantic and the formation of the Jan Mayen microcontinent: Journal of the Geological Society, v. 166, no. 4, p. 601–616, doi: 10.1144/0016-76492008-112.

Gao, D., 2006, Gravitational sliding on the Mid-Atlantic Ridge at the Kane Transform: Implications for submarine basin-slope degradation and deformation: AAPG Bulletin, v. 90, no. 2, p. 159–176, doi: 10.1306/08190504133.

Gale, A., Langmuir, C.H., and Dalton, C.A., 2014, The Global Systematics of Ocean Ridge Basalts and their Origin: Journal of Petrology, v. 55, no. 6, p. 1051–1082, doi: 10.1093/petrology/egu017.

Gente, P., Pockalny, R.A., Durand, C., Deplus, C., Maia, M., Ceuleneer, G., Mevel, C., Cannat, M., and Laverne, C., 1995, Characteristics and evolution of the segmentation of the Mid-Atlantic Reidge between 20°N and 24°N during the last 10 million years: Earth and Planetary Science Letters, v. 129, p. 55–71.

German, C.R., and Parson, L.M., 1998, Distributions of hydrothermal activity along the Mid-Atlantic Ridge: interplay of magmatic and tectonic controls: Earth and Planetary Science Letters, v. 160, p. 327–341.

Gini, C., J. Escartín, M. Cannat, T. Barreyre, Extrusive upper crust formation at slow-spreading ridges: fault steering of lava flows and magma supply gradients, Submitted to Earth and Planetary Sciences.

Goff, J.A., and Arbic, B.K., 2010, Global prediction of abyssal hill roughness statistics for use in ocean models from digital maps of paleo-spreading rate, paleo-ridge orientation, and sediment thickness: Ocean Modelling, v. 32, p. 36–43.

Goff, J.A., and Tucholke, B.E., 1997, Multiscale spectral analysis of bathymetry on the flank of the Mid-Atlantic Ridge: Modification of the seafloor by mass wasting and sedimentation: Journal of Geophysical Research, v. 102, no. B7, p. 15447–15462.

Goud, M.R., and Karson, J.A., 1985, Tectonics of short-offset, slow-slipping transform zones in the FAMOUS area, Mid-Atlantic Ridge: Marine Geophysical Researches, v. 7, p. 489–512.

Grevemeyer, I., Reston, T.J., and Moeller, S., 2013, Microseismicity of the Mid-Atlantic Ridge at 7°S-8°15′S and at the Logatchev Massif oceanic core complex at 14°40′N-14°50′N: Geochemistry, Geophysics, Geosystems, v. 14, no. 9, p. 3532–3554, doi: 10.1002/ggge.20197.

Grevemeyer, I., Hayman, N.W., Lange, D., Peirce, C., Papenberg, C., Van Avendonk, H.J.A., Schmid, F., de La Peña, L.G., and Dannowski, A., 2019, Constraining the maximum depth of brittle deformation at slow- and ultraslow-spreading ridges using microseismicity: Geology, v. 47, no. 11, p. 1069–1073, doi: 10.1130/G46577.1.

Gràcia, E., Charlou, J.L., Radford-Knoery, J., and Parson, L.M., 2000, Non-transform offsets along the Mid-Atlantic Ridge south of the Azores (38°N–34°N): ultramafic exposures and hosting of hydrothermal vents: Earth and Planetary Science Letters, v. 177, no. 1–2, p. 89–103, doi: 10.1016/S0012-821X(00)00034-0.

Grindlay, N.R., and Fox, P.J., 1993, Lithospheric stresses associated with non-transform offsets of the Mid-Atlantic Ridge: implications for a finite element analysis: Tectonics, v. 12, no. 4, p. 982–1003.

Grindlay, N.R., Madsen, J.A., Rommevaux-Jestin, C., and Sclater, J., 1998, A different

pattern of ridge segmentation and mantle Bouguer gravity anomalies along the ultra-slow spreading Southwest Indian Ridge (15°30'E to 25°E): Earth and Planetary Science Letters, v. 161, no. 1–4, p. 243–253, doi: 10.1016/S0012-821X(98)00154-X.

Griffiths, R.W., and Fink, J.H., 1992, Solidification and morphology of submarine lavas: A dependence on extrusion rate: Journal of Geophysical Research, v. 97, no. B13, p. 19729, doi: 10.1029/92JB01594.

Grindlay, N.R., Fox, P.J., and MacDonald, K.C., 1991, Second-order ridge axis discontinuities in the south Atlantic: Morphology, structure, and evolution: Marine Geophysical Researches, v. 13, no. 1, p. 21–49, doi: 10.1007/BF02428194.

Haymon, R.M., 1983, Growth history of hydrothermal black smoker chimneys: Nature, v. 301, p. 695–698.

Hays, M.R., and Perfit, M., 2004, INTRA-TRANSFORM VOLCANISM ALONG THE SIQUEIROS FRACTURE ZONE 8°20′ N – 8°30′ N, EAST PACIFIC RISE: University of Florida, 264 p.

Hearn, C.K., Homola, K.L., and Johnson, H.P., 2013, Surficial permeability of the axial valley seafloor: Endeavour Segment, Juan de Fuca Ridge: Geochemistry, Geophysics, Geosystems, v. 14, no. 9, p. 3409–3424, doi: 10.1002/ggge.20209.

Heezen B., Tharp M, Ewing M (1959) The floors of the oceans. I. The North Atlantic. Text to accompany the physiographic diagram of the North Atlantic. Special paper 65. The Geological Society of America, New York

Heezen, B.C., Gerard, R.D., and Tharp, M., 1964b, Physiography of the Indian Ocean: Journal of Geophysical Research, v. 69, no. 4, p. 733–739.

Heezen, B.C., Gerard, R.D., and Tharp, M., 1964a, The Vema Fracture Zone in the Equatorial Atlantic: Journal of Geophysical Research, v. 69, no. 4, p. 733–739.

Heezen, B.., Bunce, E., Hersey, J., and Tharp, M., 1964c, Chain and romanche fracture zones: Deep Sea Research and Oceanographic Abstracts, v. 11, no. 1, p. 11–33, doi: 10.1016/0011-7471(64)91079-4.

Heezen B, Tharp M, Ewing M (1959) The floors of the oceans. I. The North Atlantic. Text to accompany the physiographic diagram of the North Atlantic. Special paper 65. The Geological Society of America, New York.

Heezen, B.C., and Tharp, M., 1965, Tectonic fabric of the Atlantic and Indian oceans and continental drift: Philosophical Transactions of the Royal Society of London. Series A, Mathematical and Physical Sciences, v. 258, no. 1088, p. 90–106, doi: 10.1098/rsta.1965.0024.

Hekinian, R., Bideau, D., Cannat, M., Francheteau, J., and Hébert, R., 1992, Volcanic activity and crust-mantle exposure in the ultrafast Garrett transform fault near 13°28'S in the Pacific: Earth and Planetary Science Letters, v. 108, no. 259–275.

Hodgkinson, M.R.S., Webber, A.P., Roberts, S., Mills, R.A., Connelly, D.P., and Murton, B.J., 2015, Talc-dominated seafloor deposits reveal a new class of hydrothermal system: Nature Communications, v. 6, p. 10150, doi:

10.1038/ncomms10150.

Hooft, E.E.E., Schouten, H., and Detrick, R.S., 1996, Constraining crustal emplacement processes from the variation in Layer 2A thickness at the East Pacific Rise: Earth and Planetary Science Letters, v. 142, p. 289–309.

Horning, G., Sohn, R.A., Canales, J.P., and Dunn, R.A., 2018, Local Seismicity of the Rainbow Massif on the Mid-Atlantic Ridge: Journal of Geophysical Research: Solid Earth, v. 123, no. 2, p. 1615–1630, doi: 10.1002/2017JB015288.

Howell, S., Ito, G., Behn, M. D., Martinez, F., Olive, J.-A., and J. Escartín, 2016, Magmatic and tectonic extension at the Chile Ridge: Evidence for mantle controls on ridge segmentation: Geochem. Geophys. Geosyst., v. 17.

Howell, S.M., Olive, J.A., Ito, G., Behn, M.D., Escartín, J., and Kaus, B., 2019, Seafloor expression of oceanic detachment faulting reflects gradients in mid-ocean ridge magma supply: Earth and Planetary Science Letters, v. 516, p. 176–189, doi: 10.1016/j.epsl.2019.04.001.

Hussenoeder, S.A., Collins, J.A., Kent, G.M., and Detrick, R.S., 1996, Seismic analysis of the axial magma chamber reflector along the southern East Pacific Rise from conventional reflection profiling: Journal of Geophysical Research: Solid Earth, v. 101, no. B10, p. 22087–22105, doi: 10.1029/96JB01907.

Huvenne, V. A. I., K. Robert, L. Marsh, C. Lo Iacono, T. Le Bas, T. B. Wynn, 2008, ROVs and AUVs, in Submarine Geomorphology (Eds. A. Micallef, S. Krastel. A. Savini), p. 93-108.

Ito, G., and Lin, J., 1995, Oceanic spreading center–hotspot interactions: Constraints from along-isochron bathymetric and gravity anomalies: Geology, v. 23, no. 7, p. 657, doi: 10.1130/0091-7613(1995)023<0657:OSCHIC>2.3.CO;2.

Jamieson, J.W., Hannington, M.D., Clague, D. a., Kelley, D.S., Delaney, J.R., Holden, J.F., Tivey, M.K., and Kimpe, L.E., 2013, Sulfide geochronology along the Endeavour Segment of the Juan de Fuca Ridge: Geochemistry, Geophysics, Geosystems, v. 14, no. 7, p. 2084–2099, doi: 10.1002/ggge.20133.

Jaroslow, G.E., and Tucholke, B.E., 1994, Mesozoic-Cenozoic sedimentation in the Kane Fracture Zone, western North Atlantic, and uplift history of the Bermuda Rise: Geological Society of America Bulletin, v. 106, p. 317–319.

Johnson, H.P., and Embley, R.W., 1990, Axial seamount: An active ridge axis volcano on the central Juan de Fuca Ridge: Journal of Geophysical Research, v. 95, no. B8, p. 12689–12696.

Jourdain, A., Singh, S.C., Escartin, J., Klinger, Y., Raju, K.A.K., and McArdle, J., 2016, Crustal accretion at a sedimented spreading center in the Andaman Sea: Geology, v. 44, no. 5, p. 351–354, doi: 10.1130/G37537.1.

Juniper, S.K., Escartin, J., and Cannat, M., 2007, Monitoring and Observatories: Multidisciplinary, Time-Series Observations at Mid-Ocean Ridges: Oceanography, v. 20, no. 1, p. 128–137, doi: 10.5670/oceanog.2007.86.

Kamesh Raju, K.A., Ramprasad, T., Rao, P.S., Rao, B.R., and Varghese, J., 2004, New insights into the tectonic evolution of the Andaman basin, northeast Indian Ocean: Earth and Planetary Science Letters, v. 17, p. 145- 162,doi:10.1016/S0012.

Kappel, E.S., and Ryan, W.B.F., 1986, Volcanic episodicity and a non-steady-state rift valley along northeast Pacific spreading centers: Evidence from SeaMARC I: Journal of Geophysical Research, v. 91, p. 13925–13940.

Karson, J.A., Thompson, G., Humphris, S.E., Edmon, J.M., Bryan, W.B., Brown, J.B., Winters, A.T., Pockalny, R.A., Casey, J.F., Campbell, A.C., Klinkhammer, G.P., Palmer, M.R., Kinzler, R.J., and Sulanowska, M.M., 1987, Along-axis variations in seafloor spreading in the MARK Area: Nature, v. 328, p. 681–685.

Katsumata, K., Sato, T., Kasahara, J., Hirata, N., Hino, R., Takahashi, N., Sekine, M., Miura, S., Koresawa, S., and Wada, N., 2001, Microearthquake seismicity and focal mechanisms at the Rodriguez Triple Junction in the Indian Ocean using ocean bottom seismometers: Journal of Geophysical Research, v. 106, no. B12, p. 30689–30699.

Katz, R.F., 2010, Porosity-driven convection and asymmetry beneath mid-ocean ridges: Geochemistry, Geophysics, Geosystems, v. 11, p. Q0AC07, doi:10.1029/2010GC003282.

Keen, M.J., Klein, E.M., and Melson, W.G., 1990, Ocean-ridge basalt compositions correlated with paleobathymetry: Nature, v. 345, p. 423–426.

Kelley, D.S., Karson, J.A., Blackman, D.K., Früh-Green, G.L., Butterfield, D.A., Lilley, M.D., Olson, E.J., Schrenk, M.O., Roe, K.K., Lebon, G.T., and Rivizzigno, P., 2001, An off-axis hydrothermal vent field near the Mid-Atlantic Ridge at 30° N: Nature, v. 412, no. 6843, p. 145–149, doi: 10.1038/35084000.

Kelley, D.S., Karson, J.A., Früh-Green, G.L., Yoerger, D.R., Shank, T.M., Butterfield, D.A., Hayes, J.M., Schrenk, M.O., Olson, E.J., Proskurowski, G., Jakuba, M., Bradley, A., Larson, B., Ludwig, K., et al., 2005, A Serpentinite-Hosted Ecosystem: The Lost City Hydrothermal Field: Science, v. 307, p. 1428–1434.

Kelley, D.S., Delaney, J.R., and Juniper, S.K., 2014, Establishing a new era of submarine volcanic observatories: Cabling Axial Seamount and the Endeavour Segment of the Juan de Fuca Ridge: Marine Geology, v. 352, p. 426–450, doi: 10.1016/j.margeo.2014.03.010.

Klischies, M., Petersen, S., and Devey, C.W., 2019, Geological mapping of the Menez Gwen segment at 37°50′N on the Mid-Atlantic Ridge: Implications for accretion mechanisms and associated hydrothermal activity at slow-spreading mid-ocean ridges: Marine Geology, v. 412, no. January, p. 107–122, doi: 10.1016/j.margeo.2019.03.012.

Kong, L.S.L., Detrick, R.S., Fox, P.J., Mayer, L.A., and Ryan, W.B.F., 1988, The morphology and tectonics of the Mark area from Sea Beam and Sea MARC I observations (Mid-Atlantic Ridge 23° N): Marine Geophysical Researches, v. 10, no. 1–2, p. 59–90, doi: 10.1007/BF02424661.

Kuo, B.-Y., and Forsyth, D.W., 1988, Gravity anomalies of the ridge-transform

system in the South Atlantic between 31 and 34.5°S: Upwelling centers and variations in crustal thickness: Marine Geophysical Researches, v. 10, no. 3–4, p. 205–232, doi: 10.1007/BF00310065.

Lawson, K., Searle, R.C., Pearce, J.A., Browning, P., and Kempton, P., 1996, Detailed volcanic geology of the MARNOK area, Mid-Atlantic Ridge north of Kane transform, in MacLeod, C.J., Tyler, P.A., and Walker, C.L. eds., Tectonic, magmatic, hydrothermal and biological segmentation of mid-ocean ridges, Geological Society, London, p. 61–102.

Lalou, C., Thompson, G., Arnold, M., Brichet, E., Druffel, E., and Rona, P.A., 1990, Geochronology of TAG and Snakepit hydrothermal fields, Mid-Atlantic Ridge: witness to a long and complex hydrothermal history: Earth and Planetary Science Letters, v. 97, p. 113–128.

Lalou, C., Reyss, J.L., Brichet, E., Arnold, M., Thompson, G., Fouquet, Y., and Rona, P.A., 1993, New age data for Mid-Atlantic ridge hydrothermal sites: TAG and Snakepit chronology revisited: Journal of Geophysical Research, v. 98, no. B6, p. 9705–9713.

Langmuir, C., and Forsyth, D., 2007, Mantle Melting Beneath Mid-Ocean Ridges: Oceanography, v. 20, no. 1, p. 78–89, doi: 10.5670/oceanog.2007.82.

Langmuir, C.H., Klein, E.M., and Plank, T., 1992, Petrological systematics of mid-ocean ridge basalts: constraints on melt generation beneath mid-ocean ridges, in Phipps Morgan, J., Blackman, D.K., and Sinton, J.M. eds., Mantle flow and melt generation at mid-ocean ridges, American Geophysical Union, Washington DC, p. 183–280.

Lowell, R. P., Farough, A., Hoover, J., and Cummings, K., 2013, Characteristics of magma-driven hydrothermal systems at oceanic spreading centers: Geochem. Geophys. Geosyst., v. 14, p. 1756– 1770, doi:10.1002/ggge.20109.

Morton, J.L., Holmes, M. L., and Kolski, R. A., 1987, Volcanism and massive sulfide formation at a sedimented spreading center, Escanaba Trough, Gorda Ridge, northeast Pacific Ocean: Geophys. Res. Lett., v. 14, no 7, pp 769—772.

Mutter, J.C., Carbotte, S.M., Su, W., Xu, L., Buhl, P., Detrick, R.S., Kent, G.M., Orcutt, J.A., and Harding, A.J., 1995, Seismic images of active magma systems beneath the East Pacific Rise between 17°05′ and 17°35′S: Science, v. 268, p. 391–395.

Lecoeuvre, A., Ménez, B., Cannat, M., Chavagnac, V., and Gérard, E., 2021, Microbial ecology of the newly discovered serpentinite-hosted Old City hydrothermal field (southwest Indian ridge): ISME Journal, v. 15, no. 3, p. 818–832, doi: 10.1038/s41396-020-00816-7.

Ligi, M., Bonatti, E., Bosworth, W., Cai, Y., Cipriani, A., Palmiotto, C., Ronca, S., and Seyler, M., 2018, Birth of an ocean in the Red Sea: Oceanic-type basaltic melt intrusions precede continental rupture: Gondwana Research, v. 54, p. 150–160, doi: 10.1016/j.gr.2017.11.002.

Lizarralde, D., Gaherty, J.B., Collins, J.A., Hirth, G., and Kim, S.D., 2004, Spreading-

rate dependence of melt extraction at mid-ocean ridges from mantle seismic refraction data: Nature, v. 432, p. 744–747.

Lizarralde, D., Axen, G.J., Brown, H.E., Fletcher, J.M., Gonzalez-Fernandez, A., Harding, A.J., Holbrook, W.S., Kent, G.M., Paramo, P., Sutherland, F., and Umhoefer, P.J., 2007, Variation in styles of rifting in the Gulf of California: Nature, v. 448, p. doi:10.1038/nature06035.

Luyendyk, B.P., and Macdonald, K.C., 1985, A GEOLOGICAL TRANSECT ACROSS THE CREST OF THE EAST PACIFIC RISE AT 21°N LATITUDE MADE FROM THE DEEP SUBMERSIBLE ALVIN: Marine Geophysical Researches, v. 7, p. 467–488.

Macdonald, K.C., 1982, Mid-Ocean Ridges: Fine Scale Tectonic, Volcanic and Hydrothermal Processes Within the Plate Boundary Zone: Annual Review of Earth and Planetary Sciences, v. 10, no. 1, p. 155–190, doi: 10.1146/annurev.ea.10.050182.001103.

Macdonald, K.C., Fox, P.J ., Alexander, R.T., Pockalny, R., and Gente, P., 1996, Volcanic growth faults and the origin of Pacific abyssal hills: Nature, v. 380, p. 125–129.

Macdonald, K.C., and Fox, P.J., 1983, Overlapping spreading centres: New accretion geometry on the East Pacific Rise: Nature, v. 302, p. 55–58.

Macdonald, K.C., Sempere, J.C., Fox, P.J., and Tyce, R., 1987, Tectonic evolution of ridge-axis discontinuities by the meeting, linking, or self-decapitation of neighboring ridge segments: Geology, v. 15, p. 993–997.

MacLeod, C.J., Searle, R.C., Casey, J.F., Mallows, C., Unsworth, M., Achenbach, K., and Harris, M., 2009, Life cycle of oceanic core complexes: Earth and Planetary Science Letters, v. 287, p. 333–344.

Maia, M., Sichel, S., Briais, A., Brunelli, D., Ligi, M., Ferreira, N., Campos, T., Mougel, B., Brehme, I., Hémond, C., Motoki, A., Moura, D., Scalabrin, C., Pessanha, I., et al., 2016, Extreme mantle uplift and exhumation along a transpressive transform fault: Nature Geoscience, v. 9, no. 8, p. 619–623, doi: 10.1038/ngeo2759.

MacLeod, C.J., Searle, R.C., Casey, J.F., Mallows, C., Unsworth, M., Achenbach, K., and Harris, M., 2009, Life cycle of oceanic core complexes: Earth and Planetary Science Letters, v. 287, p. 333–344.

Marjanović, M., Carbotte, S.M., Carton, H., Nedimović, M.R., Mutter, J.C., and Canales, J.P., 2014, A multi-sill magma plumbing system beneath the axis of the East Pacific Rise: Nature Geoscience, v. 7, no. 11, p. 825–829, doi: 10.1038/ngeo2272.

Marks, N.S., 1981, Sedimentation on new ocean crust: The Mid-Atlantic Ridge at 37°N: Marine Geology, v. 43, no. 1–2, p. 65–82, doi: 10.1016/0025-3227(81)90129-8.

Marks, K.M., and Stock, J.M., 1995, Asymmetric seafloor spreading and short ridge jumps in the Australian-Antarctic discordance: Marine Geophysical Researches, v. 17, p. 361–373.

Martínez, F., Hey, R.N., and Johnson, P.D., 1997, The East ridge system 28.5-32°S

East Pacific rise: Implications for overlapping spreading center development: Earth and Planetary Science Letters, v. 151, p. 13–31.

Maury, M. F., Physical Geography of the Sea, New York, 1855. On these developments see H.M. Rozwadowski, Technology and ocean-scape: defining the deep sea in mid-nineteenth century, History of Technology 17 (2001) 217e247, esp. 222, 224e225, 232, 242e243; H.M. Rozwadowski, Fathoming the Ocean: The Discovery and Explo- ration of the Deep Sea, Cambridge, MA, 2005, 69e95.

McCaig, A.M., Delacour, A., Fallick, A.E., Castelain, T., and Früh-Green, G.L., 2010, Detachment fault control on hydrothermal circulation systems: Interpreting the subsurface beneath the TAG hydrothermal field using the isotopic and geological evolution of oceanic core complexes in the Atlantic: Geophysical Monograph Series, v. 188, p. 207–239, doi: 10.1029/2008GM000729.

McCaig, A., Cliff, R.A., Escartin, J., Fallick, A.E., and MacLeod, C.J., 2007, Oceanic deachment faults focus very large volumes of black smoker fluids: Geology, v. 35, p. 935–938, doi:10.1130/G23657A.1.

Menard, H.W., and Mammerickx, J., 1967, Abyssal hills, magnetic anomalies, and the East Pacific Rise: Earth and Planetary Science Letters, v. 2, p. 465–472.

Mendel, V., and Sauter, D., 1997, Seamount volcanism at the super-slow spreading Southwest Indian Ridge between 57°E and 70°E: Geology, v. 25, no. 2, p. 99–102.

Michael, P.J., Langmuir, C.H., Dick, H.J.B., Snow, J.E., Goldstein, S.L., Graham, D.W., Lehnert, K., Kurras, G.J., Jokat, W., Mühe, R., and Edmonds, H.N., 2003, Magmatic and amagmatic seafloor generation at the utraslow-spreading Gakkel ridge, Arctic Ocean: Nature, v. 423, no. 26, p. 956–962.

Mitchell, N.C., 1995, Diffusion transport model for pelagic sediments on the Mid-Atlantic Ridge: Journal of Geophysical Research, v. 100, no. B10, p. 19991–20009.

Mitchell, N.C., Tivey, M.A., and Gente, P., 2000, Seafloor slopes at mid-ocean ridges from submersible observations and implications for interpreting geology from seafloor topography: Earth and Planetary Science Letters, v. 183, p. 543–555.

Mitchell, N.C., Allerton, S.A., and Escartín, J., 1998a, Sedimentation on young oceanic floor at the Mid-Atlantic Ridge, 29°N: Earth and Planetary Science Letters, v. 148, p. 1–8.

Mitchell, N.C., and Searle, R.C., 1998b, Fault scarp statistics at the Galapagos spreading centre from deep tow data: Marine Geophysical Researches, v. 20, p. 183–193.

Moore, J.G., 1975, Mechanism of Formation of Pillow Lava: American Scientist, v. 63, no. 3, p. 269–277.

Morgan, W.J., 1968, Rises, trenches, great faults, and crustal blocks: Journal of Geophysical Research, v. 73, no. 6, p. 1959–1982.

Moore, J.G., 1975, Mechanism of Formation of Pillow Lava: American Scientist, v. 63, no. 3, p. 269–277.

Moores, E.M., 1982, Origin and emplacement of ophiolites: Journal of Geophysical Research, v. 20, no. 4, p. 735–760.

Müller, R.D., Sdrolias, M., Gaina, C., and Roest, W.R., 2008, Age, spreading rates, and spreading asymmetry of the world's ocean crust: Geochemistry, Geophysics, Geosystems, v. 9, no. 4, p. n/a-n/a, doi: 10.1029/2007GC001743.

Naar, D.F., and Hey, R.N., 1991, Tectonic evolution of the Easter microplate: Journal of Geophysical Research, v. 98, no. B5, p. 7961–7993.

Nedimović, M.R., Carbotte, S.M., Diebold, J.B., Harding, A.J., Canales, J.P., and Kent, G.M., 2008, Upper crustal evolution across the Juan de Fuca ridge flanks: Geochemistry, Geophysics, Geosystems, v. 9, no. 9, p. n/a-n/a, doi: 10.1029/2008GC002085.

Okino, K., Matsuda, K., Christie, D.M., Nogi, Y., and Koizumi, K., 2004, Development of oceanic detachment and asymmetric spreading at the Australian-Antarctic Discordance: Geochemistry, Geophysics, Geosystems, v. 5, no. 12, p. Q12012, doi:10.1029/2004GC000793.

Olive, J.-A., Behn, M. D., Ito, G., Buck, W. R., Escartín, J., and S. Howell, 2015, Sensitivity of seafloor bathymetry to climate-driven fluctuations in mid-ocean ridge magma supply: Science, v. 350(6258).

Olive, J.A., Parnell-Turner, R., Escartín, J., Smith, D.K., and Petersen, S., 2019, Controls on the seafloor exposure of detachment fault surfaces: Earth and Planetary Science Letters, v. 506, p. 381–387, doi: 10.1016/j.epsl.2018.11.001.

Olive, J.-A., and Dublanchet, P., 2020, Controls on the magmatic fraction of extension at mid-ocean ridges: Earth Planet. Sci. Lett., v. 549.

Parnell-Turner, R., Escartín, J., Olive, J.-A., Smith, D.K., and Petersen, S., 2018, Genesis of corrugated fault surfaces by strain localization recorded at oceanic detachments: Earth and Planetary Science Letters, v. 498, p. 116–128, doi: 10.1016/j.epsl.2018.06.034.

Parnell-Turner, R., Cann, J.R., Smith, D.K., Schouten, H., Yoerger, D., Palmiotto, C., Zheleznov, A., and Bai, H., 2014, Sedimentation rates test models of oceanic detachment faulting: Geophysical Research Letters, v. 41, no. 20, p. 7080–7088, doi: 10.1002/2014GL061555.

Parnell-Turner, R., White, N., Henstock, T.J., Jones, S.M., Maclennan, J., and Murton, B.J., 2017, Causes and Consequences of Diachronous V-Shaped Ridges in the North Atlantic Ocean: Journal of Geophysical Research: Solid Earth, v. 122, no. 11, p. 8675–8708, doi: 10.1002/2017JB014225.

Parsons, B., and Sclater, J.G., 1977, An analysis of the variation of ocean floor bathymetry and heat flow with age: Journal of Geophysical Research, v. 82, p. 803–827.

Pérez-Díaz, L., and Eagles, G., 2014, Constraining South Atlantic growth with seafloor spreading data: Tectonics, v. 33, no. 9, p. 1848–1873, doi: 10.1002/2014TC003644.

Perfit, M., Fornari, D.J., Smith, M.C., Bender, J.F., Langmuir, C.H., and Haymon, R.M., 1994, Small scale spatial and temporal variations in mid-ocean ridge crest magmatic processes: Geology, v. 22, p. 375–379.

Portner, R.A., Murphy, M.J., and Daczko, N.R., 2011, A detrital record of lower oceanic crust exhumation within a Miocene slow-spreading ridge: Macquarie Island, Southern Ocean: Geological Society of America Bulletin, v. 123, no. 1/2, p. 255–273; doi: 10.1130/B30082.1.

Qin, R., and Buck, W.R., 2005, Effect of lithospheric geometry on rift valley relief: Journal of Geophysical Research, v. 110, p. B03404, doi:10.1029/2004JB003411.

Rabain, A., Cannat, M., Lin, J., and Bergman, E.A., 1990, Rift grabens, seismicity and volcanic segmentation of the Mid-Atlantic Ridge: Kane to Atlantis Fracture Zones: EOS Trans. AGU, v. 71, no. 43, p. 1572.

Reston, T., and Ranero, C.R., 2011, The 3-D geometry of detachment faulting at mid-ocean ridges: Geochemistry, Geophysics, Geosystems, v. 12, no. 7, p. Q0AG05, doi:10.1029/2011GC003666.

Reston, T., 2018, Flipping detachments: The kinematics of ultraslow spreading ridges: Earth and Planetary Science Letters, v. 503, p. 144–157, doi: 10.1016/j.epsl.2018.09.032.

Ryan, W.B.F., Carbotte, S.M., Coplan, J.O., O'Hara, S., Melkonian, A., Arko, R., Weissel, R.A., Ferrini, V., Goodwillie, A., Nitsche, F., Bonczkowski, J., and Zemsky, R., 2009, Global Multi-Resolution Topography synthesis: Geochemistry, Geophysics, Geosystems, v. 10, no. 3, p. n/a-n/a, doi: 10.1029/2008GC002332.

Sauter, D., Cannat, M., Rouméjon, S. *et al.*, 2013, Continuous exhumation of mantle-derived rocks at the Southwest Indian Ridge for 11 million years: Nature Geosci v. 6, p. 314–320, doi.org/10.1038/ngeo1771.

Sauter, D., Mendel, V., Rommevaux-Jestin, C., Parson, L.M., Fujimoto, H., Mével, C., Cannat, M., and Tamaki, K., 2004, Focused magmatism versus amagmatic spreading along the ultra-slow spreading Southwest Indian Ridge: Evidence from TOBI side scan sonar imagery: Geochemistry, Geophysics, Geosystems, v. 5, no. 10, p. Q10K09, doi:10.1029/2004GC000738.

Scheirer, D.S., and Macdonald, K.C., 1995, Near-axis seamounts on the flanks of the East Pacific Rise, 8°N to 17°N: Journal of Geophysical Research, v. 100, no. B2, p. 2239–2259.

Schlindwein, V., Müller, C., and Jokat, W., 2005, Seismoacoustic evidence for volcanic activity on the ultraslow spreading Gakkel Ridge, Arctic Ocean: Geophysical Research Letters, v. 32, p. L18306, doi:10.1029/2005GL023767.

Schlindwein, V., and Riedel, C., 2010, Location and source mechanism of sound signals at Gakkel ridge, Arctic Ocean: Submarine Strombolian activity in the 1999-2001 volcanic episode: Geochemistry, Geophysics, Geosystems, v. 11, no. 1, p. n/a-n/a, doi: 10.1029/2009GC002706.

Schmid, F., Cremanns, M., Augustin, N., Lange, D., Petersen, F., and Kopp, H., 2021,

Microseismicity and Lava Flows Hint at Magmato-Tectonic Processes Near the Southern Tip of the Fonualei Rift and Spreading Center in the Lau Basin: Journal of Geophysical Research: Solid Earth, v. 126, no. 4, p. 1–20, doi: 10.1029/2020JB021340.

Searle, R.C., and Hey, R.N., 1983, Gloria observations of the propagating rift at 95.5°W on the Cocos-Nazca spreading center: Journal of Geophysical Research, v. 88, no. B8, p. 6433–6447.

Searle, R.C., Thomas, M. V, and Jones, E.J.W., 1994, Morphology and tectonics of the Romanche Transform and its evolution: Marine Geophysical Researches, v. 16, p. 427–453.

Searle, R.C., Cowie, P.A., Mitchell, N.C., Allerton, S., MacLeod, C.J., Escartin, J., Russell, S.M., Slootweg, P.A., and Tanaka, T., 1998, Fault structure and detailed evolution of a slow spreading ridge segment: The Mid-Atlantic Ridge at 29°N: Earth and Planetary Science Letters, v. 154, no. 1–4.

Sempéré, J.C., and Macdonald, K.C., 1986, Overlapping spreading centers: implications from crack growth simulation by the displacement discontinuity method: Tectonics, v. 5, no. 1, p. 151–163.

Sempéré, J.-C., Blondel, P., Briais, P., Fujiwara, T., Géli, L., Isezaki, N., Pariso, J.E., Parson, L., Patriat, P., and Rommevaux, C., 1995, The Mid-Atlantic Ridge between 29°N and 31°30'N in the last 10 Ma: Earth and Planetary Science Letters, v. 130, p. 45–55.

Seton, M., Müller, R.D., Zahirovic, S., Williams, S., Wright, N.M., Cannon, J., Whittaker, J.M., Matthews, K.J., and McGirr, R., 2020, A Global Data Set of Present-Day Oceanic Crustal Age and Seafloor Spreading Parameters: Geochemistry, Geophysics, Geosystems, v. 21, no. 10, p. 1–15, doi: 10.1029/2020GC009214.

Seton, M., Müller, R.D., Zahirovic, S., Williams, S., Wright, N.M., Cannon, J., Whittaker, J.M., Matthews, K.J., and McGirr, R., 2020, A Global Data Set of Present-Day Oceanic Crustal Age and Seafloor Spreading Parameters: Geochemistry, Geophysics, Geosystems, v. 21, no. 10, p. 1–15, doi: 10.1029/2020GC009214.

Severinghaus, J.P., and MacDonald, K.C., 1988, High inside corners at ridge-transform intersections: Marine Geophysical Researches, v. 9, p. 353–367.

Shah, A.K., and Sempéré, J.-C., 1998, Morphology of the transition from an axial high to a rift valley at the Southeast Indian Ridge and the relation to variations in mantle temperature: Journal of Geophysical Research, v. 103, no. B3, p. 5203–5223.

Singh, S.C., Crawford, W.C., Carton, H., Seher, T., Combier, V., Cannat, M., Canales, J.P., Düsünür, D., Escartin, J., and Miranda, J.M., 2006, Discovery of a magma chamber and faults beneath a Mid-Atlantic Ridge hydrothermal field: Nature, v. 442, no. 7106, doi: 10.1038/nature05105.

Sinha, M.C., Navin, D.A., MacGregor, L.M., Constable, S., Pierce, C., White, A., Heinson, G., and Inglis, M.A., 1997, Evidence for melt beneath the slow-spreading Mid-Atlantic Ridge: Philosophical Transactions of Royal Society of London, v. 355, p. 233–253.

Sinton, J.M., and Dietrick, R.S., 1992, Mid-ocean Ridge magma chambers: Journal of Geophysical Research, v. 97, no. B1, p. 197–216.

Smith, D.K., and Cann, J.R., 1992, The role of seamount volcanism in crustal construction at the Mid-Atlantic Riddge (24°N-30°N): Journal of Geophysical Research, v. 97, p. 1645–1658.

Smith, D.K., and Cann, J.R., 1990, Hundreds of small volcanoes on the median valley floor of the Mid-Atlantic Ridge: Nature, v. 344, p. 427–431.

Smith, D.K., Escartin, J., Cannat, M., Tolstoy, M., Fox, C.G., Bohnenstiehl, D.R., and Bazin, S., 2003, Spatial and temporal distribution of seismicity along the northern Mid-Atlantic Ridge (15°-35°N): Journal of Geophysical Research B: Solid Earth, v. 108, no. 3.

Sonnette, L., Angelier, J., Villemin, T., and Bergerat, F., 2010, Faulting and fissuring in active oceanic rift: Surface expression, distribution and tectonic-volcanic interaction in the Thingvellir Fissure Swarm, Iceland: Journal of Structural Geology, v. 32, p. 407–422, doi: 10.1016/j.jsg.2010.01.003.

Soule, S.A., Fornari, D.J., Perfit, M.R., Tivey, M.A., Ridley, W.I., and Schouten, H., 2005, Channelized lava flows at the East Pacific Rise crest 9°-10°N: The importance of off-axis lava transport in developing the achitecture of young oceanic crust: Geochemistry, Geophysics, Geosystems, v. 6, no. 8, p. Q08005, doi:10.1029/2005GC000912.

Soule, S.A., Escartín, J., and Fornari, D.J., 2009, A record of eruption and intrusion at a fast spreading ridge axis: Axial summit trough of the East Pacific Rise at 9-10°N: Geochemistry, Geophysics, Geosystems, v. 10, no. 10, doi: 10.1029/2008GC002354.

Soule, S.A., Fornari, D.J., Perfit, M.R., and Rubin, K.H., 2007, New insights into mid-ocean ridge volcanic processes from the 2005-2006 eruption of the East Pacific Rise, 9°46'N-9°56'N: Geology, v. 35, no. 12, p. 1079–1082; doi: 10.1130/G23924A.1.

Spencer, S., Smith, D.K., Cann, J.R., Lin, J., and McAllister, E., 1997, Structure and stability of non-transform discontinuities on the Mid-Atlantic Ridge between 24°N and 30°N: Marine Geophysical Researches, v. 19, p. 339–362.

Stein, C.A., and Stein, S., 1992, A model for the global variation in oceanic depth and heatflow with lithospheric age: Nature, v. 359, p. 123–128.

Stein, C.A., Stein, S., and Pelayo, A.M., 1995, Heat Flow and Hydrothermal Circulation, in Geophysical Monograph Series, p. 425–445, doi: 10.1029/GM091p0425.

Sykes, L.R., 1967, Mechanism of earthquakes and nature of faulting on the mid-oceanic ridges: Journal of Geophysical Research, v. 72, no. 8, p. 2131–2153, doi: 10.1029/JZ072i008p02131.

Szitkar, F., Dyment, J., Petersen, S., Bialas, J., Klischies, M., Graber, S., Klaeschen, D., Yeo, I., and Murton, B.J., 2019, Detachment tectonics at Mid-Atlantic Ridge 26°N: Scientific Reports, v. 9, no. 1, p. 11830, doi: 10.1038/s41598-019-47974-z.

Tamayo, T.G., 1984, Tectonics at the intersection of the East Pacific Rise with Tamayo Transform fault: Marine Geophysical Researches, v. 6, p. 159–185.

Tapponnier, P., and Francheteau, J., 1978, Necking of the lithosphere and the mechanics of slowly acreting plate boundaries: Journal of Geophysical Research, v. 83, p. 3955–3970.

Tentler, T., and Temperley, S., 2007, Magmatic fissures and their systems in Iceland: A tectonomagmatic model: Tectonics, v. 26, p. TC5019, doi:10.1029/2006TC002037.

Thibaud, R., Gente, P., and Maia, M., 1998, A systematic analysis of the Mid-Atlantic Ridge morphology between 15°N and 40°N: Constraints of the thermal structure: Journal of Geophysical Research, v. 103, no. B10, p. 24233–24243.

Tilmann, F., Flueh, E.R., Planert, L., Reston, T., and Weinrebe, W., 2004, Microearthquake seismicity of the Mid-Atlantic Ridge at 5°S: a view of tectonic extension: Journal of Geophysical Research, v. 109, p. B06102, doi:10.1029/2003JB002827.

Tolstoy, M., Waldhauser, F., Bohnenstiehl, D.R., Weekly, R.T., and Kim, W.-Y., 2008, Seismic identification of along-axis hydrothermal flow on the East Pacific Rise: Nature, v. 451, p. 181–185, doi:10.1038/nature06424.

Tucholke, B.E., 1992, Massive submarine rockslide in the rift-valley wall of the Mid-Atlantic Ridge: Geology, v. 20, p. 129–132.

Tucholke, B.E., and Lin, J., 1994, A geological model for the structure of ridge segments in slow-spreading ocean crust: Journal of Geophysical Research, v. 99, no. B6, p. 11937–11958.

Tucholke, B.E., Stewart, W.K., and Kleinrock, M.C., 1997, Long-term denudation of ocean crust in the central North-Atlantic Ocean: Geology, v. 25, no. 2, p. 171–174.

Tucholke, B.E., Lin, J., Kleinrock, M.C., Tivey, M., Reed, T.B., Goff, J., and Jaroslow, G.E., 1997, Segmentation and crustal structure of the western Mid-Atlantic Ridge flank, 25°25'-27°10'N and 0-29 m.y.: Journal of Geophysical Research, v. 102, no. B5, p. 10203–10223.

Tucholke, B.E., Lin, J., and Kleinrock, M.C., 1998, Megamullions and mullion structure defining oceanic metamorphic core complexes on the Mid-Atlantic Ridge: Journal of Geophysical Research, v. 103, no. B5, p. 9857–9866.

Turner, I.M., Peirce, C., and Sinha, M.C., 1999, Seismic imaging of the axial region of the Valu Fa Ridge, Lau Basin-- the accretionary processes of an intermediate back-arc spreading ridge: Geophysical Journal International, v. 138, p. 495–519.

Umhoefer, P.J., Darin, M.H., Bennett, S.E.K., Skinner, L.A., Dorsey, R.J., and Oskin, M.E., 2018, Breaching of strike-slip faults and successive flooding of pull-apart basins to form the Gulf of California seaway from ca. 8–6 Ma: Geology, v. 46, no. 8, p. 695–698, doi: 10.1130/G40242.1.

Vera, E.E., and Diebold, J.B., 1994, Seismic imaging of oceanic layer 2A between 9°30'N and 10°N on the East Pacific Rise from two-ship wide-aperture profiles:

Journal of Geophysical Research, v. 99, no. B2, p. 3031–3041.

Vera, E.E., Mutter, C.J., Buhl, P., Orcutt, J.A., Harding, A.J., Kappus, M.E., Detrick, R.S., and Brocher, T.M., 1990, The structure from 0- to 0.2-m.y.-old oceanic crust at 9°N on the East Pacific Rise from expanded spread profiles: Journal of Geophysical Research, v. 95, no. B10, p. 15529–15556.

Villemin, T., and Bergerat, F., 2013, From surface fault traces to a fault growth model: The Vogar Fissure Swarm of the Reykjanes Peninsula, Southwest Iceland: Journal of Structural Geology, v. 51, p. 38–51, doi: 10.1016/j.jsg.2013.03.010.

Vine, F.J., and Matthews, D.H., 1963, Magnetic anomalies over oceanic ridges: Nature, v. 199, p. 947–949.

Vogt, P., and Jung, W.Y., 2009, Treitel Ridge: A unique inside corner hogback on the west flank of extinct Aegir spreading ridge, Norway basin: Marine Geology, v. 267, p. 86–100.

Von Damm, K.L., 1990, Seafloor hydrothermal activity: black smokers and chimneys: Annual Reviews of Earth and Planetary Sciences, v. 18, p. 173–204.

Webb, H.F., and Jordan, T.H., 1997, Quantifying the distribution and transport of pelagic sediments on young abyssal hills: Geophysical Research Letters, v. 20, no. 20, p. 2203–2206.

Webb, H.F., and Jordan, T.H., 2001, Pelagic sedimentation on rough seafloor topography 1. Forward Model: Journal of Geophysical Research: Solid Earth, v. 106, no. B12, p. 30433–30449, doi: 10.1029/2000JB900275.

White, R.S., Minshull, T.A., Bickle, M.J., and Ronbinson, C.J., 2001, Melt generation at very slow-spreading oceanic ridges: Constraints from geochemical and geophysical data: Journal of Petrology, v. 42, no. 6, p. 1171–1196.

White, S.M., Macdonald, K.C., Scheirer, D.S., and Cormier, M.-H., 1998, Distribution of isolated volcanoes on the flanks of the East Pacific Rise, 15.3°S-20°S: Journal of Geophysical Research, v. 105, no. B12, p. 30371–30384.

White, S.M., Macdonald, K.C., and Sinton, J.M., 2002, Volcanic mound fields on the East Pacific Rise, 16°-19°S: Low effusion rate at overlapping spreading centers for the past 1 Myr: Journal of Geophysical Research, v. 107, no. B10, p. 2240, doi:10.1029/2001JB000483.

White, S.M., Macdonald, K.C., Scheirer, D.S., and Cormier, M.-H., 1998, Distribution of isolated volcanoes on the of the East Pacific Rise, 15.3°S-20°S: Journal of Geophysical Research, v. 105, no. B12, p. 30371–30384.

White, S.M., Meyer, J.D., Haymon, R.M., Macdonald, K.C., Baker, E.T., and Resing, J.A., 2008, High-resolution surveys along the hot spot-affected galápagos spreading center: 2. Influence of magma supply on volcanic morphology: Geochemistry, Geophysics, Geosystems, v. 9, no. 9, p. n/a-n/a, doi: 10.1029/2008GC002036.

Wilcock, W.S.D., Archer, S.D., and Purdy, G.M., 2002, Microearthquakes on the Endeavour segment of the Juan de Fuca Ridge: Journal of Geophysical Research:

Solid Earth, v. 107, no. B12, p. EPM 4-1-EPM 4-21, doi: 10.1029/2001JB000505.

Wilson, J.T., 1965, A new class of faults and their bearing on continental drift: Nature, v. 207, p. 343–347.

Wolfe, C., Purdy, G.M., Toomey, D.R., and Solomon, S.C., 1995, Microearthquake characteristics and crustal velocity structure at 29°N of the Mid-Atlantic Ridge: The architecture of a slow-spreading serment: Journal of Geophysical Research, v. 100, no. B12, p. 24449–24472.

Wölfl, A.-C., Snaith, H., Amirebrahimi, S., Devey, C.W., Dorschel, B., Ferrini, V., Huvenne, V.A.I., Jakobsson, M., Jencks, J., Johnston, G., Lamarche, G., Mayer, L., Millar, D., Pedersen, T.H., et al., 2019, Seafloor Mapping – The Challenge of a Truly Global Ocean Bathymetry: Frontiers in Marine Science, v. 6, no. JUN, p. 1–16, doi: 10.3389/fmars.2019.00283.

Wright, D.J., Haymon, R.M., and Fornari, D.J., 1995, Crustal fissuring and its relationship to magmatic and hydrothermal processes on the East Pacific Rise crest (9°12′ to 54°N): Journal of Geophysical Research, v. 100, no. B4, p. 6097–6120.

Bohnenstiehl, D., and Kleinrock, M.C., 2000, Fissuring near the TAG active hydrothermal mound, 26°N on the Mid-Atlantic Ridge: Journal of Volcanology and Geothermal Research, v. 98, p. 33–48.

Wright, D.J., Haymon, R.M., White, S.M., and Macdonald, K.C., 2002, Crustal fissuring on the crest of the East Pacific Rise crest at 17°15′-40′S: Journal of Geophysical Research, v. 107, no. B5, p. 10.1029/2001JB000544.

Wright, D.J., Haymon, R.M., and Fornari, D.J., 1995, Crustal fissuring and its relationship to magmatic and hydrothermal processes on the East Pacific Rise crest (9°12′ to 54°N): Journal of Geophysical Research, v. 100, no. B4, p. 6097–6120.

Wynn, R.B., Huvenne, V. a I., Le Bas, T.P., Murton, B.J., Connelly, D.P., Bett, B.J., Ruhl, H. a., Morris, K.J., Peakall, J., Parsons, D.R., Sumner, E.J., Darby, S.E., Dorrell, R.M., and Hunt, J.E., 2014, Autonomous Underwater Vehicles (AUVs): Their past, present and future contributions to the advancement of marine geoscience: Marine Geology, v. 352, p. 451–468, doi: 10.1016/j.margeo.2014.03.012.

Yeo, I.A., Clague, D.A., Martin, J.F., Paduan, J.B., and Caress, D.W., 2013, Preeruptive flow focussing in dikes feeding historical pillow ridges on the Juan de Fuca and Gorda Ridges: Geochemistry, Geophysics, Geosystems, v. 14, no. 9, p. 3586–3599, doi: 10.1002/ggge.20210.

Yeo, I.A., and Searle, R.C., 2013, High-resolution Remotely Operated Vehicle (ROV) mapping of a slow-spreading ridge: Mid-Atlantic Ridge 45°N: Geochemistry, Geophysics, Geosystems, v. 14, no. 6, p. 1693–1702, doi: 10.1002/ggge.20082.

Yeo, I.A., Devey, C.., LeBas, T.P., Augustin, N., and Steinführer, A., 2016, Segment-scale volcanic episodicity: Evidence from the North Kolbeinsey Ridge, Atlantic: Earth and Planetary Science Letters, v. 439, p. 81–87, doi: 10.1016/j.epsl.2016.01.029.

Yu, Z., Singh, S.C., Gregory, E.P.M., Maia, M., Wang, Z., and Brunelli, D., 2021, Semibrittle seismic deformation in high-temperature mantle mylonite shear zone

along the Romanche transform fault: Science Advances, v. 7, no. 15, p. eabf3388, doi: 10.1126/sciadv.abf3388.

Figure captions

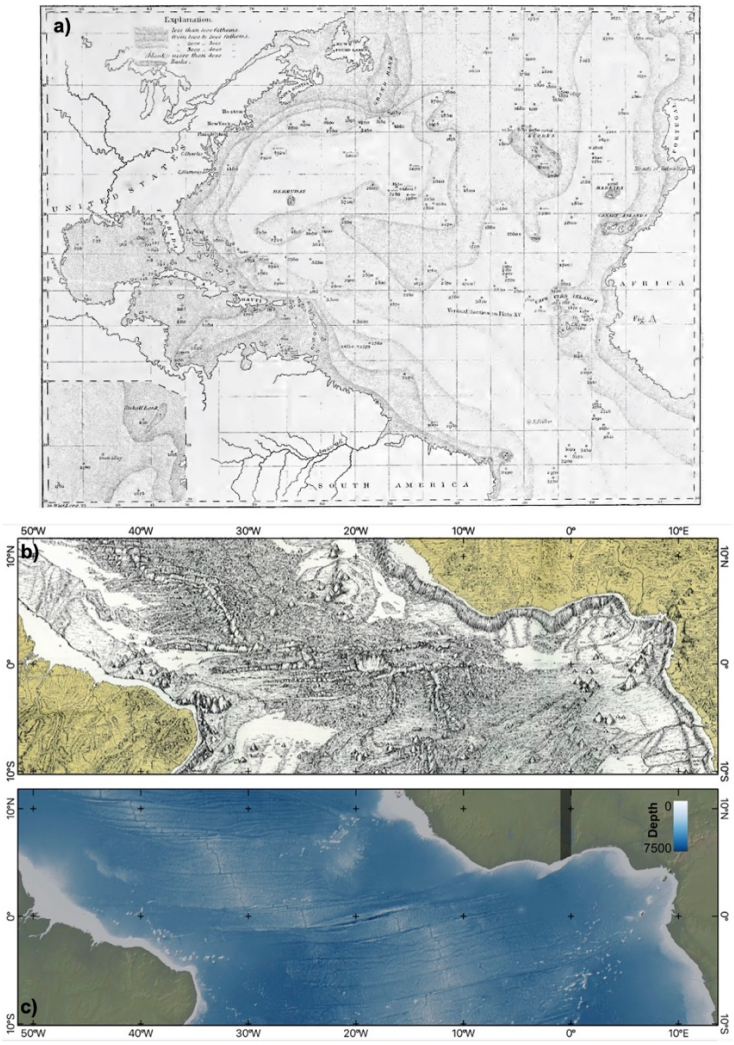

Figure 1. *a) Bathymetric map of the Northern Atlantic from line soundings compiled by Maury (1955) and revealing the rise at the center of the basin. Center: Section of the Physiographic map drafted by M. Tharp of the central Atlantic based on along-track bathymetric profiles. This map is a portion of the 1957 physiographic map published as an inset to Heezen and Tharp (1959). Bottom: Combined multibeam and satellite-derived bathymetry for the same area as in the Center Panel, showing the accurate depiction of major seafloor structures identified by Tharp and Heezen (data from http://www.gmrt.org).*

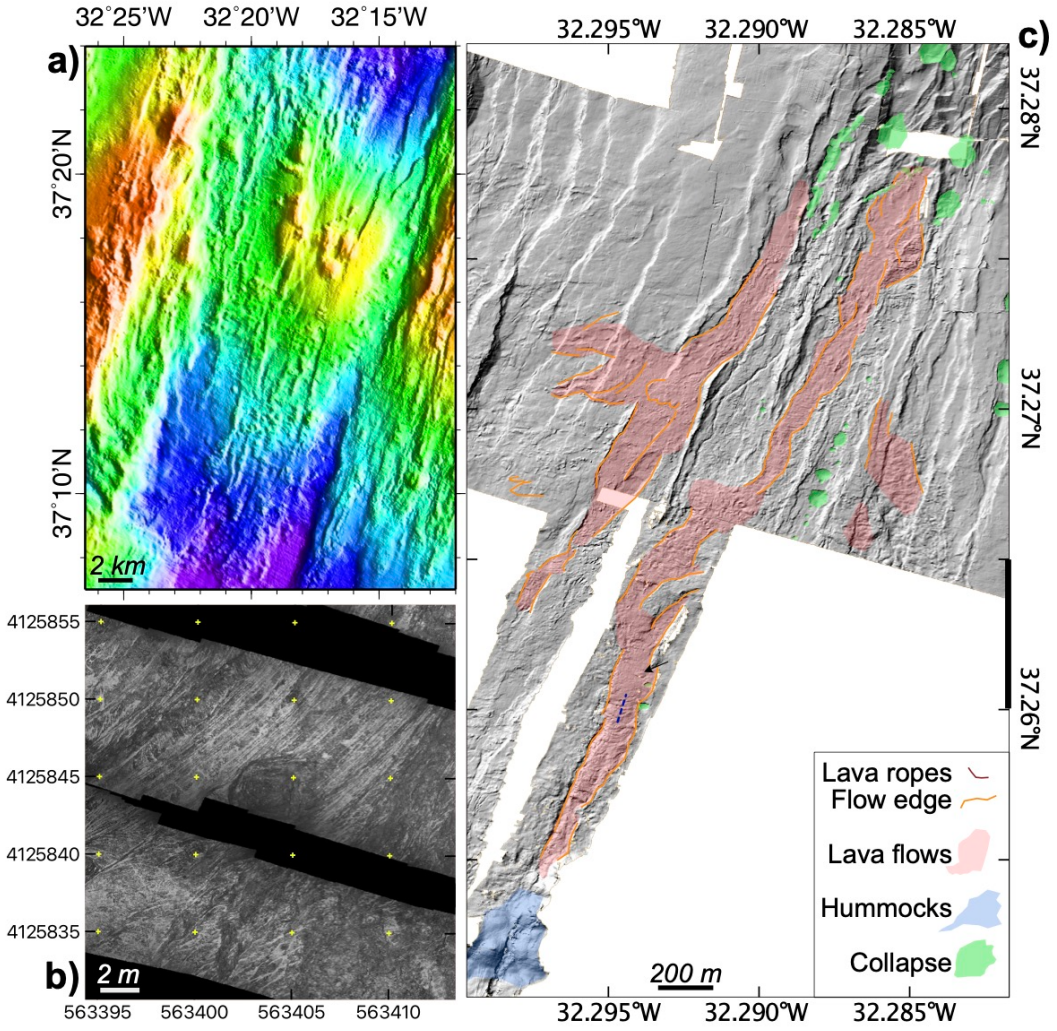

Figure 2. a) *Shipboard bathymetry of the slow-spreading Lucky Strike ridge segment, showing the central volcano within the marked rift valley, and the axis-parallel faults and volcanic structures within. b) Shaded relief map of high-resolution bathymetry acquired with an autonomous underwater vehicle (see location in a), showing lava flows along-axis volcanic hummocks, collapses along dikes, and numerous fault scarps. c) Seafloor photomosaic of a recent lava flow along the axis of the Lucky Strike segment, showing a flat, lineated surface with lava coils that form shearing within the flow during emplacement. Data: Shipboard bathymetry from the Sudaçores cruise (Cannat et al., 1999; https://doi.org/10.17600/98010080); AUV microbathymetry (https://doi.org/10.17882/80574) from the MOMAR'08 and Bathyluck'09 cruises (https://doi.org/10.17600/8010110 & https://doi.org/10.17600/9030040); Seafloor photomosaic (https://doi.org/10.17882/80447) acquired with ROV during the Bathyluck'09 cruise. Modified Gini et al. (submitted).*

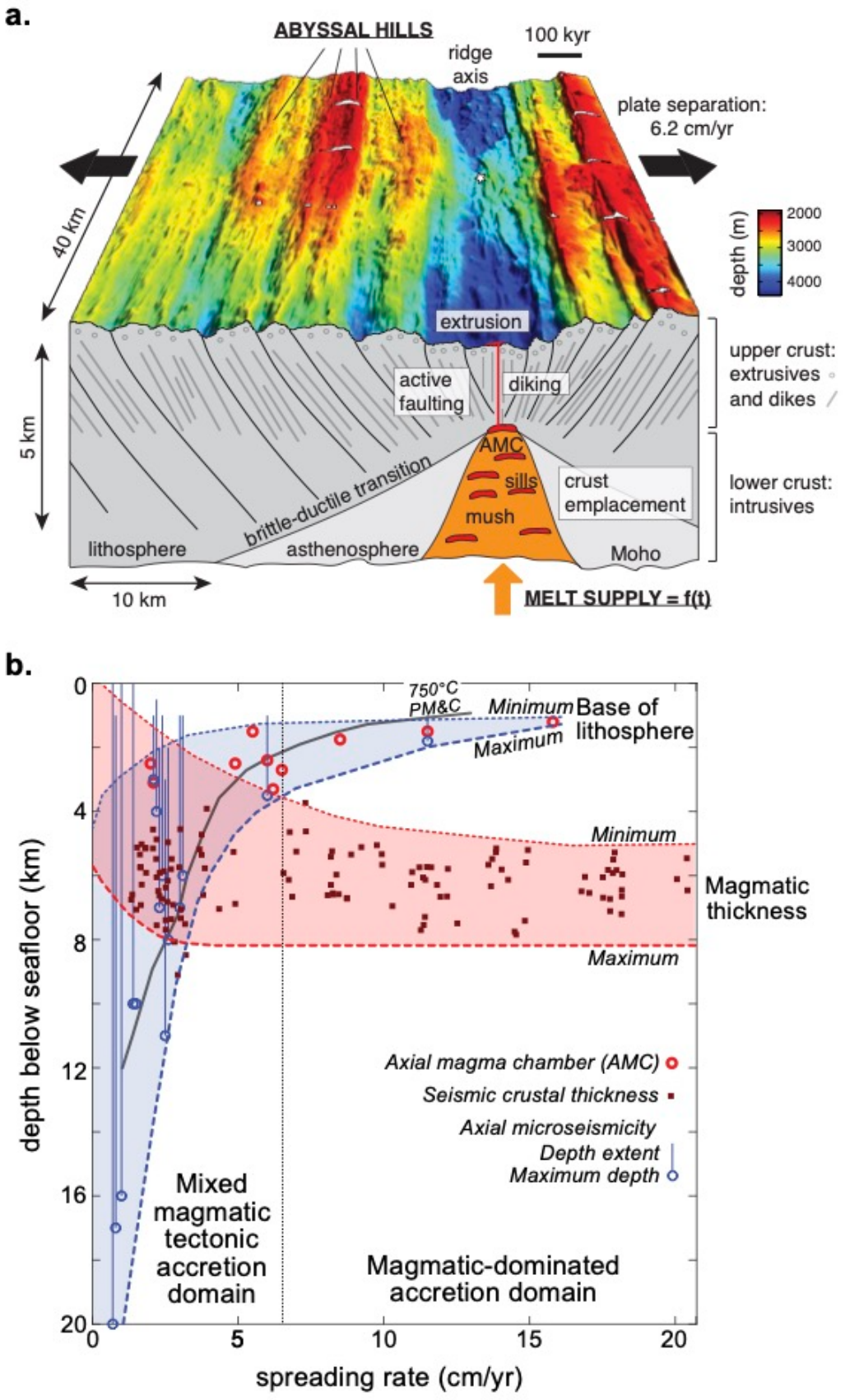

***Figure 3**. a) Schematic of key processes shaping the axis of the intermediate-spreading Chile Ridge (6 cm/yr), modified from Olive et al. (2015). b) Diagram showing the plausible range of*

both lithospheric thickness and magma supply to the ridge axis, expressed as melt thickness, as a function of spreading rate. Microseismicity at the ridge axis shows variable depth distributions, and its maximum depth is a proxy for the depth of the base of the lithosphere. Similarly, axial magma chambers (>1000°C), which feed volcanic eruptions at the seafloor by diking through the overlying brittle lithosphere. The depth range of the lithosphere base (blue shaded area) is ~2 km for very fast-spreading ridges (>12 cm/yr), but this depth range increases with decreasing spreading rate. Magma supply to the ridge axis is also variable, with an equivalent magmatic thickness ranges of 5-8 km at fast spreading-ridges, and show both an overall decrease, and at the same time an increase in the variability towards slow- and ultra-slow ridges (red shaded area). Seismic crustal thickness data corresponds to the compilation by Christeson et al. (2019). Depth of the brittle lithosphere is constrained by the depth of microseismicity (Wolfe et al., 1995; Katsumata et al., 2001; Wilcock et al., 2002; Tilmann et al., 2004; de Martin et al., 2007; Tolstoy et al., 2008; Crawford et al., 2010; Grevemeyer et al., 2013; Parnell-Turner et al., 2017; Horning et al., 2018; Schmid et al., 2021; Yu et al., 2021), and from the depth of axial magma chambers or AMC (Morton et al., 1987; Vera et al., 1990; Detrick et al., 1993; Mutter et al., 1995; Carbotte et al., 1996; Sinha et al., 1997; Turner et al., 1999; Blacic et al., 2004; Singh et al., 2006)

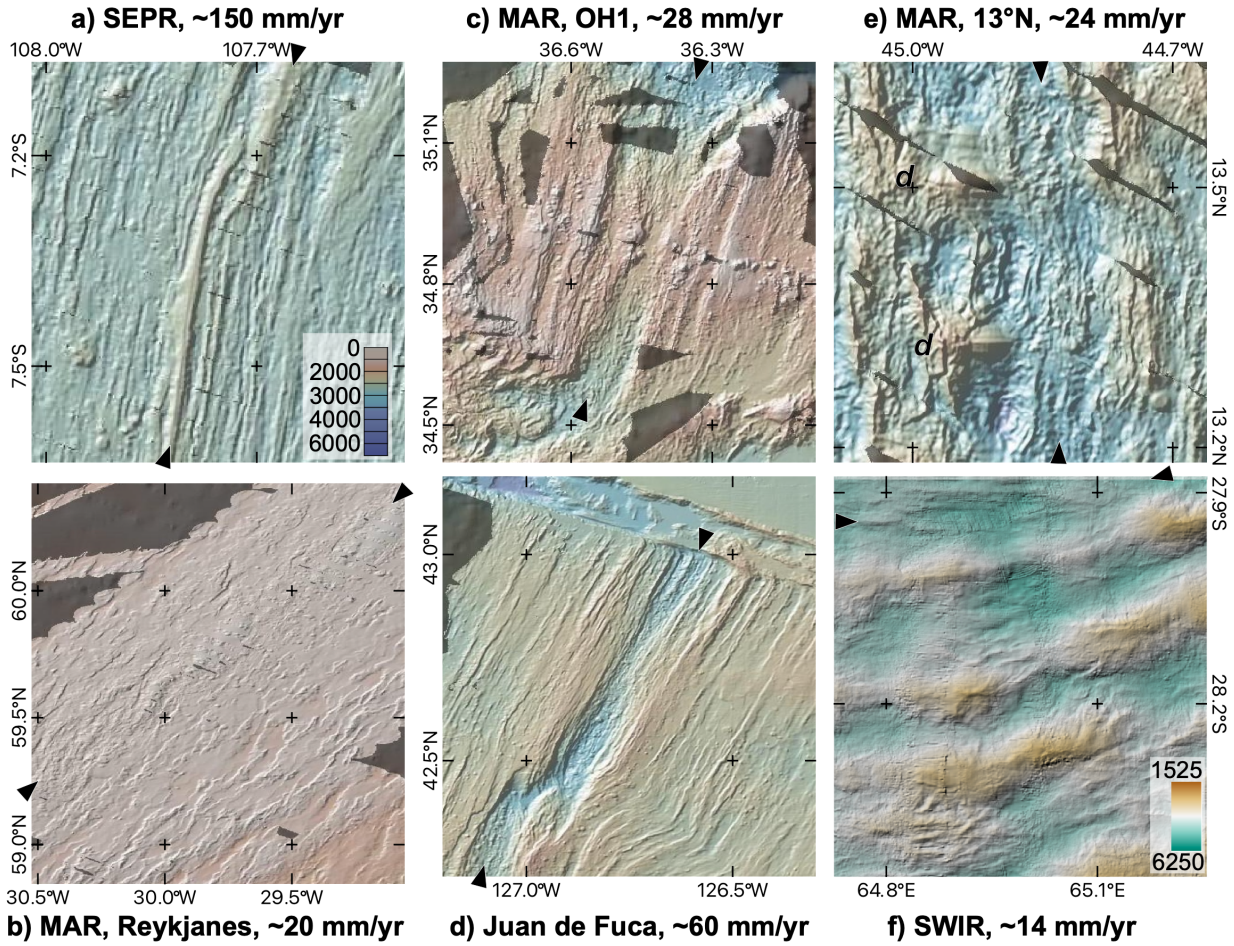

Figure 4. *Bathymetry maps of different mid-ocean ridge sections and their corresponding full spreading rate. Axial highs (right, a and b) are found both at fast and slow spreading ridges that are magmatically robust (e.g., near hot-spots), while well-developed rift valleys (center), considered to be 'typical' of slow-spreading ridges (c) also develop at intermediate spreading rates (d). Tectonic deformation with development of long-lived normal faults develops at slow (e) and ultra-slow spreading ridges (f). Bathymetry in a through e is from www.gmrt.org, and in f) from Cannat et al. (2006), acquired during the SMOOTHSEAFLOOR cruise (https://doi.org/10.17600/10200050).*

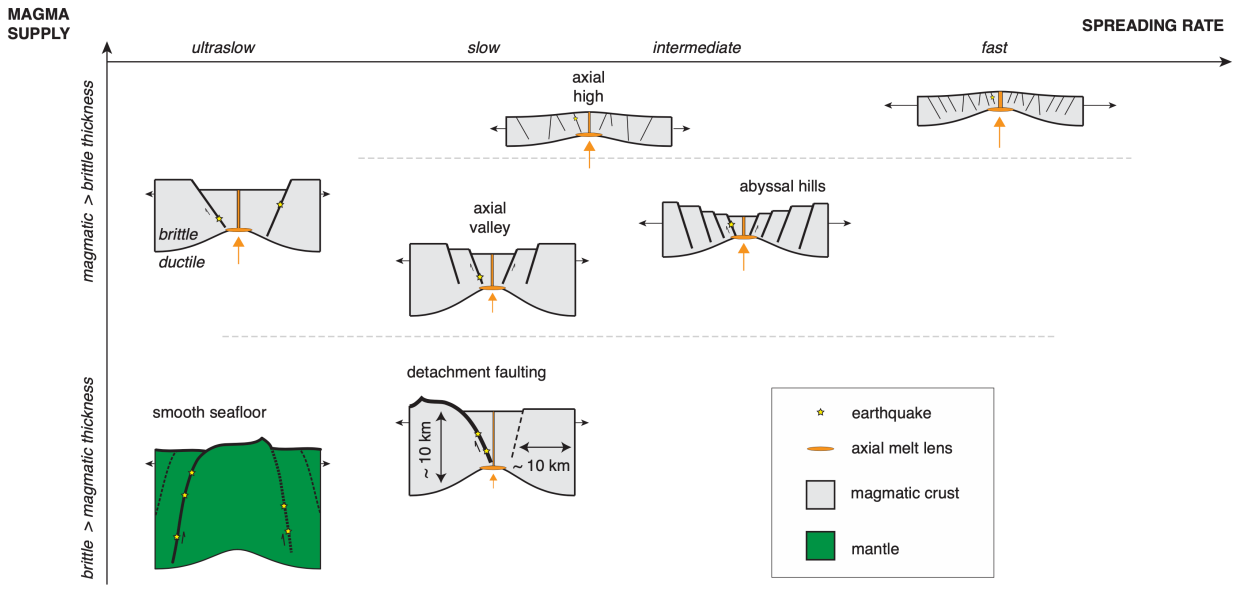

Figure 5. *Diagram showing the different modes of oceanic accretion and seafloor formation, which reflect the balance between magma supply and brittle lithospheric thickness at the ridge axis (see Fig. 3). The variability in modes of accretion increases with decreasing spreading rate, and as a result of numerous factors impacting melt supply (mantle temperature and composition, presence of volatiles, ridge geometry and obliquity) and lithospheric thickness (hydrothermal circulation, fracturation). Modified from Olive and Dublanchet (2020).*

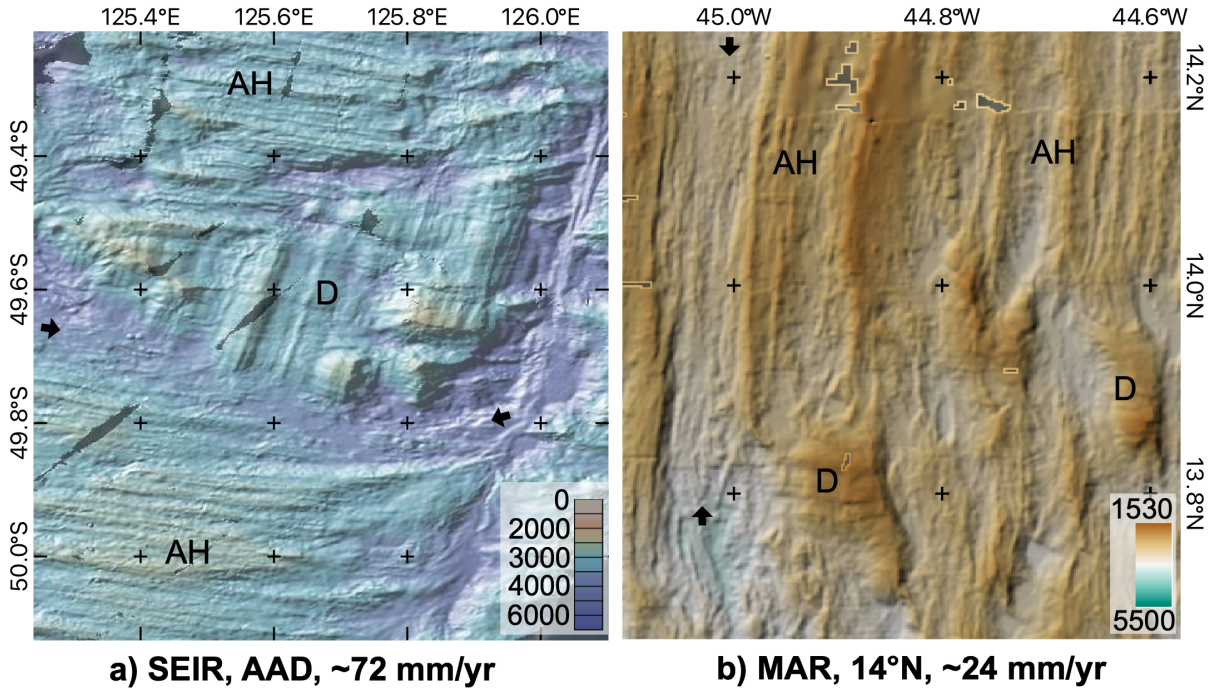

Figure 6. *Bathymetry showing abrupt transitions from regular faulting defining linear abyssal hills (AH) to oceanic detachment with extension-parallel corrugations (D), observed at*

intermediate to ultra-slow spreading ridges, in addition to an asymmetry in seafloor structure across the axis. Bathymetry in a) is from www.gmrt.org, and in b) from Smith et al. (2006), acquired during cruise KN210-05. Black arrows indicate the position of the ridge axis.

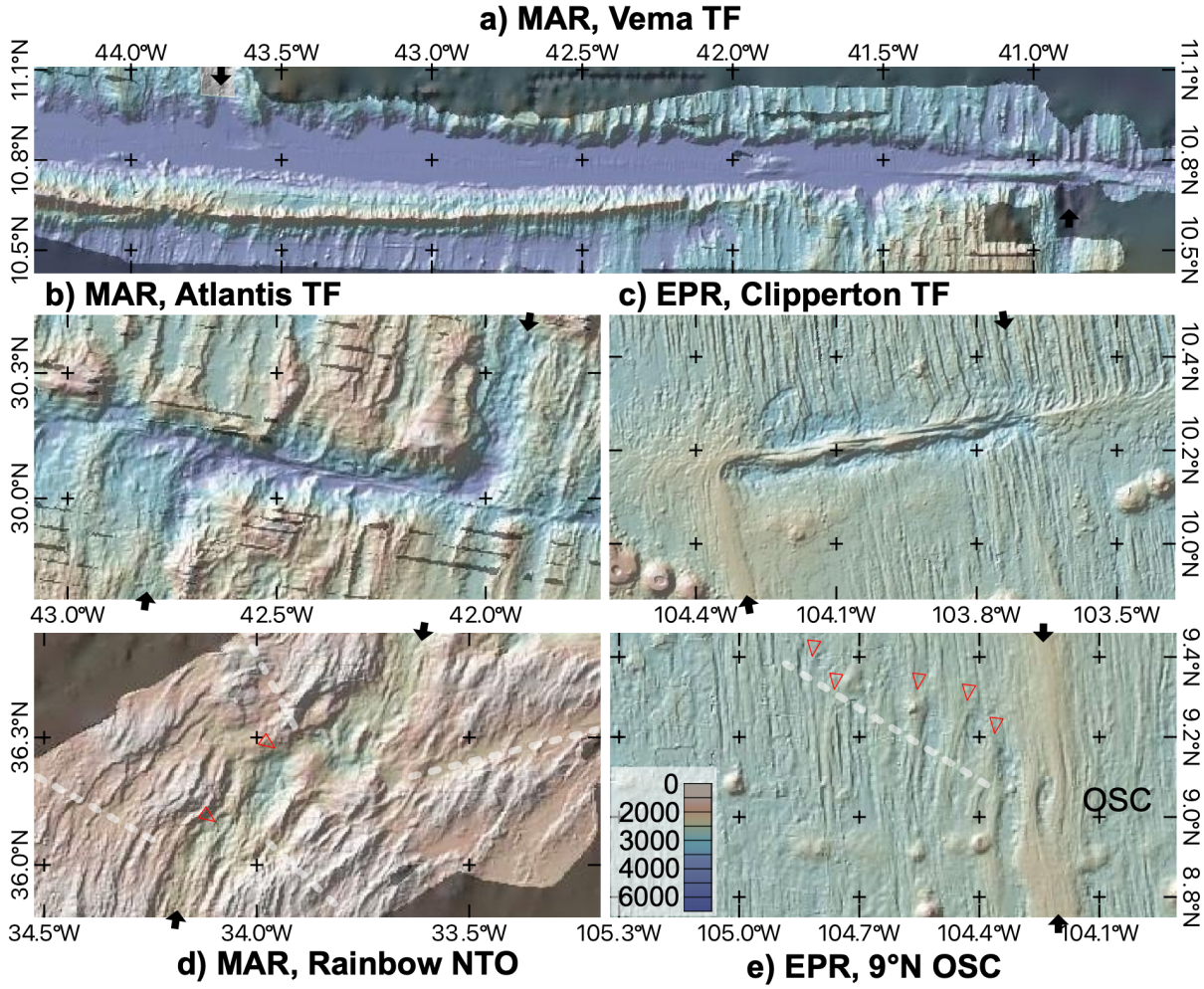

Figure 7*. The global mid ocean ridge system is discontinuous, with both major transform faults that are stable over time (a-c), and that laterally offset the ridge tens to a few hundreds of km. The ridge system also shows segments bound by either d) non-transform offsets (NTOs, indicated by red triangles), that develop primarily at slow-spreading ridges, and e) overlapping spreading centers (OSCs), with characteristic hooked ridges showing the interaction of adjacent segments, and that are preserved off-axis (red triangles). Both NTOs and OSC are unstable and leave wakes in the seafloor bathymetry showing along-axis propagation (dashed white translucent lines). Bathymetry from www.gmrt.org.*

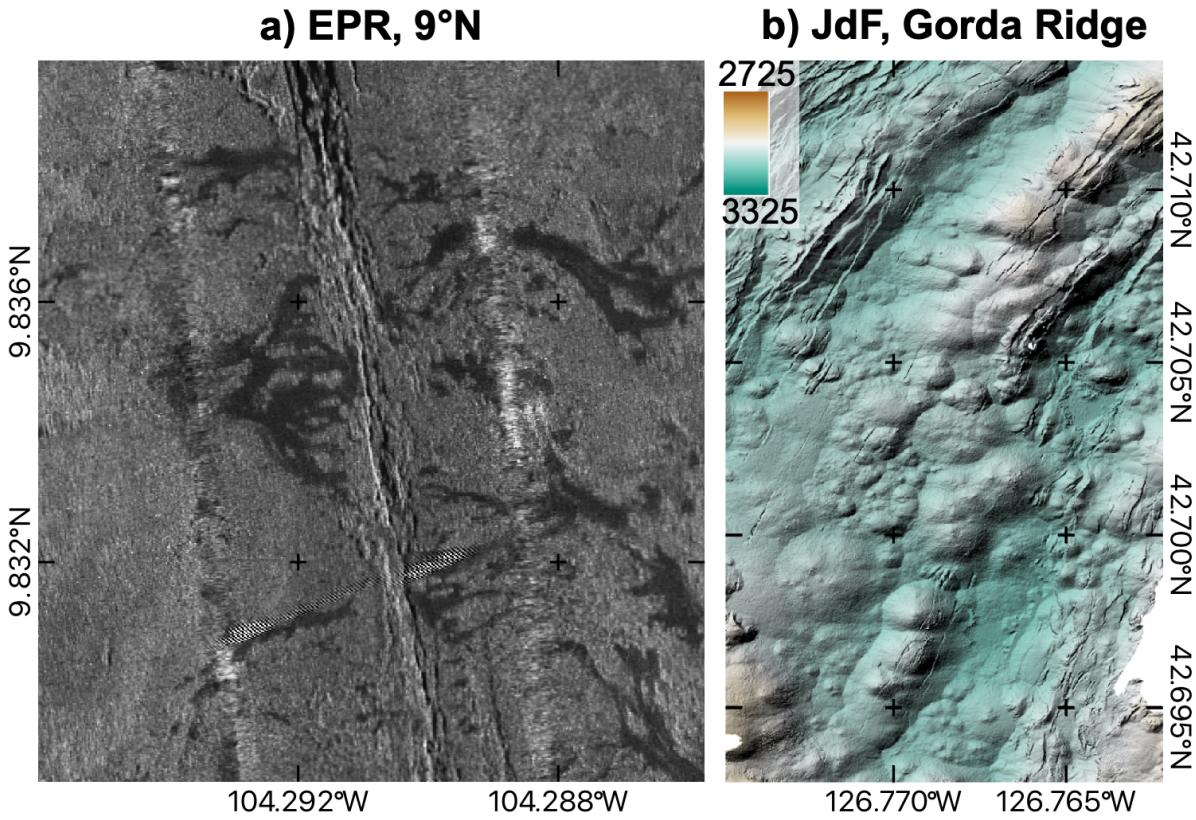

***Figure 8**. a) Side scan sonar image at the summit of the East Pacific Rise at ~9.8°N , showing faulted and fissured axial summit trough, from which lava flows emanate and extend off-axis (e.g., Fornari et al., 2004; Soule et al., 2005; 2007), indicated by the darker terrain (low acoustic reflectivity). The grey background (higher acoustic reflectivity) corresponds to lobate lavas flows. b) Hummocky pillow ridges along the Gorda segment of the Juan de Fuca Ridge. These mounds correspond to aligned, focused volcanic eruptions, and have a relief of a few tens of m (Caress et al., 2012; Yeo et al., 2013). Sonar data in a) was acquired during 2001 cruise AT07-04 (Fornari et al., 2004), and high-resolution bathymetry in b) was acquired with an AUV during cruise TN183 (Clague et al., 2014).*

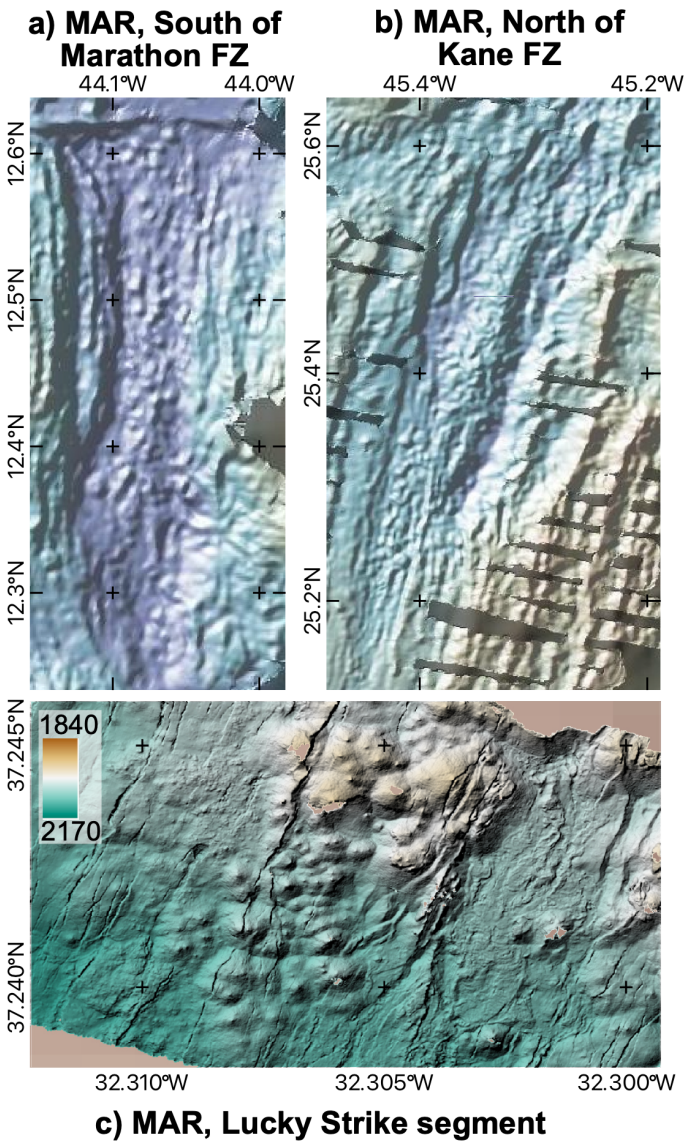

Figure 9. *Volcanic structures within the rift valley along segments from the Mid-Atlantic Ridge. a) Rift valley of a segment south of the Marathon Fracture Zone showing numerous seamounts peppering the floor of a well-developed rift valley. b) Large axial volcanic ridge within the rift valley, emplaced at the end of a magmatic segment, and a discontinuity characterized by an oblique rift valley and complex abyssal hills off-axis. c) High-resolution bathymetry of a volcanic ridge formed by a series of coalescing hummocks along the Lucky Strike segment. a) and b) Bathymetry from www.gmrt.org (and and b) and c) near-seafloor, high-resolution bathymetry acquired with deep-sea vehicles (https://doi.org/10.17882/80574) along the Lucky Strike segment (Escartin et al., 2015; Gini et al., submitted).*

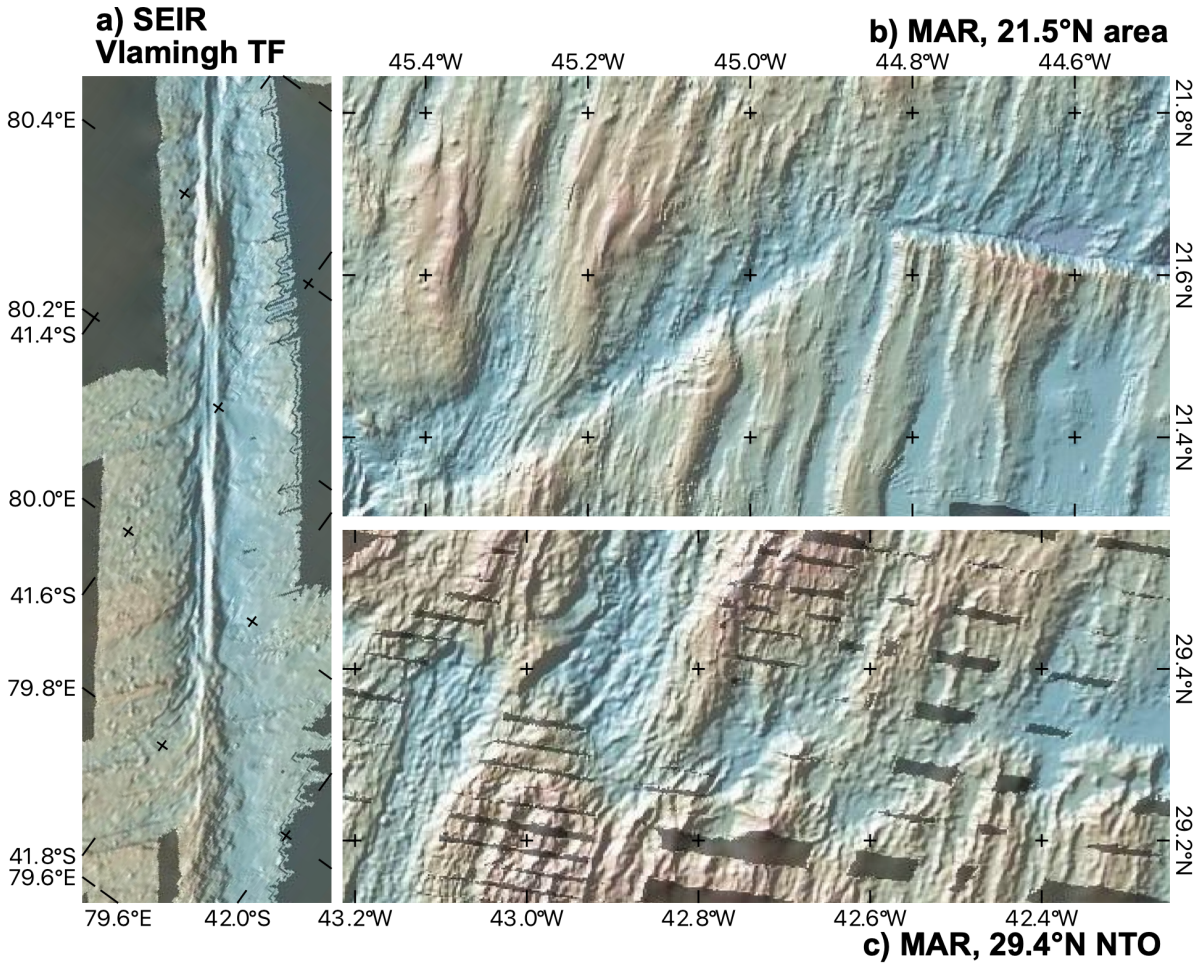

Figure 10*. a) Detail of the ridge along the southwestern end of the Vlahming transform fault (Conder and Forsyth, 2001), showing the trace of the recent shear zone running along the transform ridge, and seamounts emplaced at the vicinity of the segment end to the northwest of the fault. b) Disruption of abyssal hills at a fracture zone that transitions to a linear and well-defined non-transform offset that propagates southwards along the axis, associated with the growth and waning of segments on-axis (Gente et al., 1995). c) Jagged trace of the non-transform offset trace bounding the 29°N segment to the north (Sempere et al., 1995). This complex geometry of the non-transform offset records a persistent ridge discontinuity that is unstable, with short along-axis excursions, and that displays a rotation of the seafloor structure associated with the end of abyssal hills and associated normal faults. Bathymetry from www.gmrt.org.*

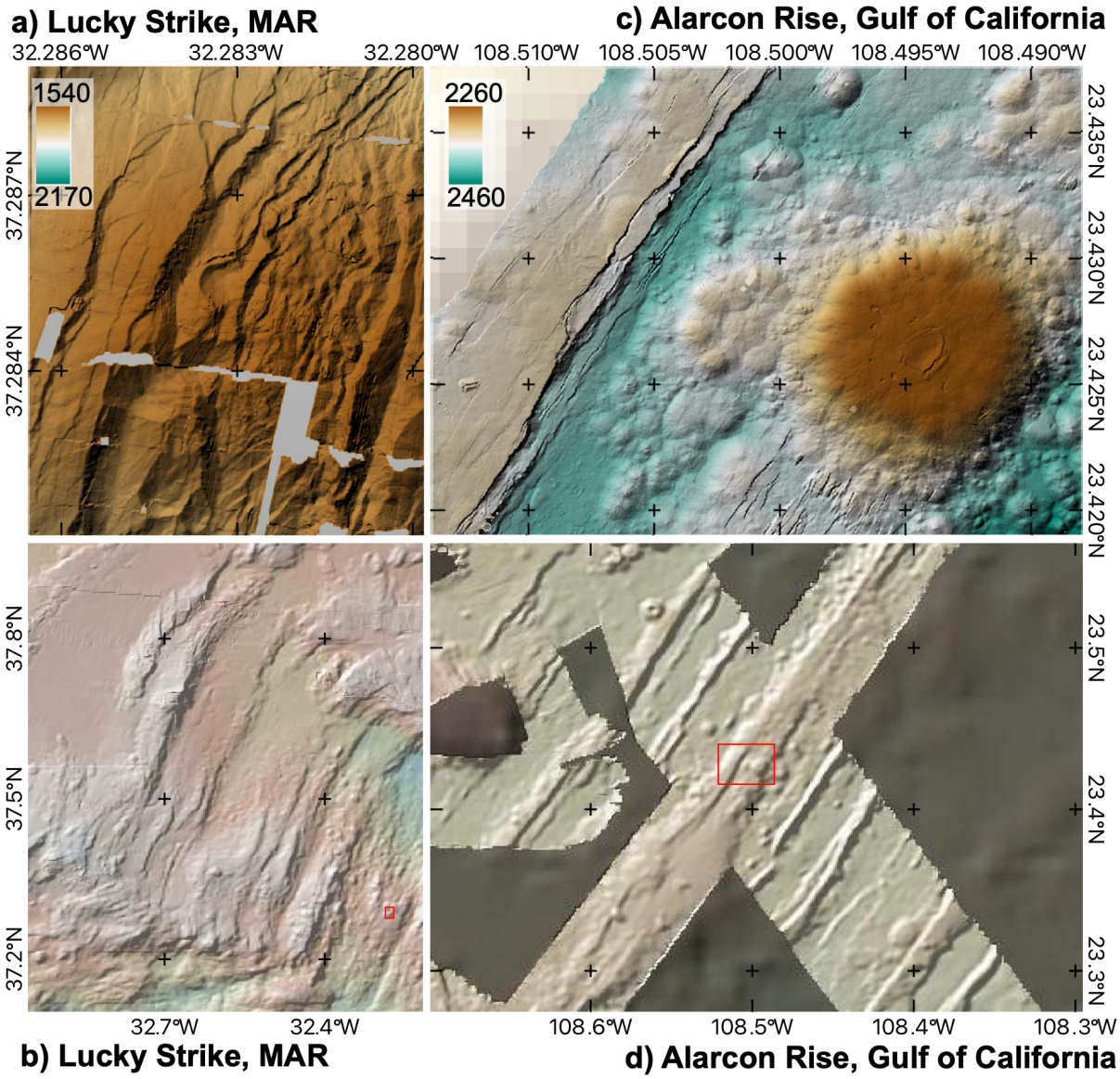

Figure 11*. Fault scarps form at the ridge axis and at small scales (top), that develop and grow both in height and along axis, forming ridge-parallel abyssal hills (bottom) and both at the slow-spreading Lucky Strike ridge segment along the MAR (a and b, right) and the intermediate spreading Alarcon Rise along the Gulf of California (c and d; Clague et al., 2018). Red boxes in bottom figures b) and d) indicate the position of high-resolution maps shown on top. High resolution bathymetry acquired with deep-sea vehicles at Lucky Strike in a) (https://doi.org/10.17882/80574; Escartin et al., 2015; Gini et al., submitted) and Alarcon Rise in c) (Clague et al., 2018), and shipboard bathymetry (bottom) from www.gmrt.org.*

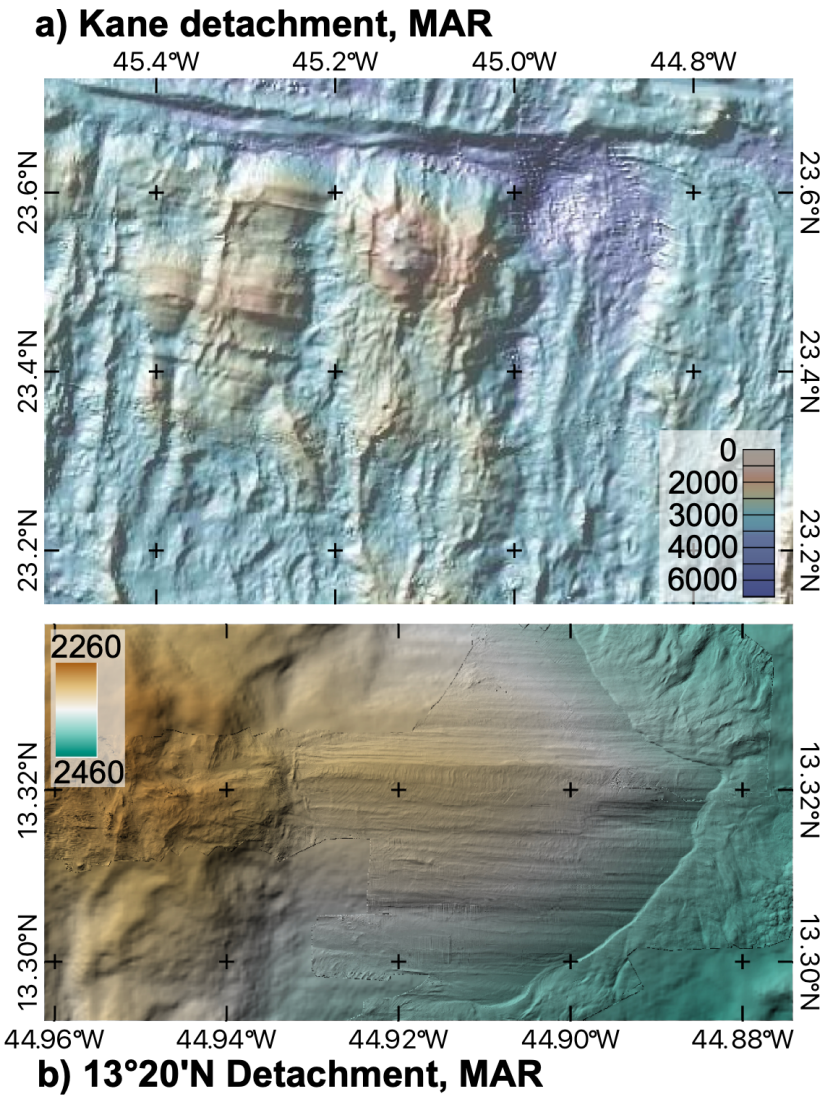

Figure 12*. a) Oceanic detachment fault system and inside corner high south of the Kane fracture zone (Mid-Atlantic Ridge). This detachment is long-lived, as shown by continuous striations off-axis and over several faulted sections of the oceanic core complex. Towards the axis two prominent inside corner highs develop adjacent to the fracture zone (e.g., Dick et al., 2008; 2010). b) High resolution bathymetry map from the 13°20'N detachment along the Mid-Atlantic Ridge, showing the fine-scale corrugations along the domed fault surface, as well as its emergence from the rift valley floor, corresponding to the hanging wall cutoff (Escartín et al., 2017; Parnell-Turner et al., 2018). Shipboard bathymetry in a) is from www.gmrt.org. Bathymetry in b) is from Escartin et al. (2017) and available at https://doi.org/10.17882/48335.*

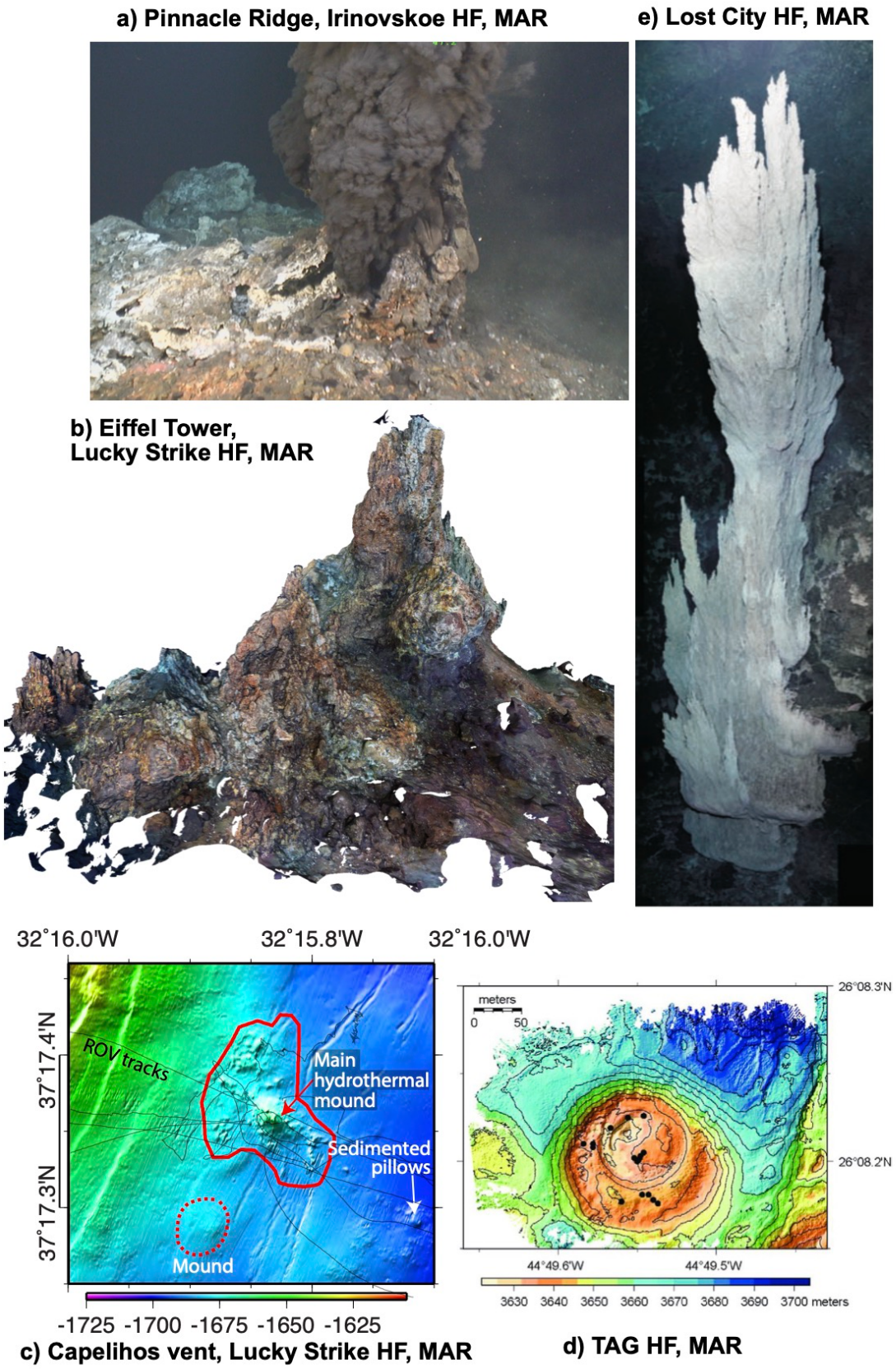

Figure 13*. Hydrothermal edifices, mounds, and fields: a) the active Pinnacle Ridge vent (~1.5 m wide) is located at the summit of a hydrothermal mound that rises a few m above the*

surrounding seafloor. This vent is one of two active vents from the Irinovskoe Hydrothermal Field (HF) emplaced on the 13°20'N detachment fault surface (see Figure 12b; Escartín et al., 2017). ROV image acquired during the 2013 ODEMAR cruise. b) The active Eiffel Tower hydrothermal chimney at the Lucky Strike hydrothermal field rises ~20 m above the seafloor and is built over a broad hydrothermal mound. c) Microbathymetry of the Capelinhos vent (lucky Strike Hydrothermal field), developing over a network of fissures and faults (see Escartin et al., 2015). d) Bathymetry of the TAG hydrothermal field (Mid-Atlantic Ridge), showing a circular platform with various phases of development (data courtesy of R. Sohn, WHOI). e) Active carbonate hydrothermal spire, approximately ~10 m high, from the low-temperature, serpentinite-hosted, Lost City hydrothermal site, located at the Atlantis Massif detachment and adjacent to the Atlantis transform fault (Figure 7b). Modified from Kelley et al. (2005).

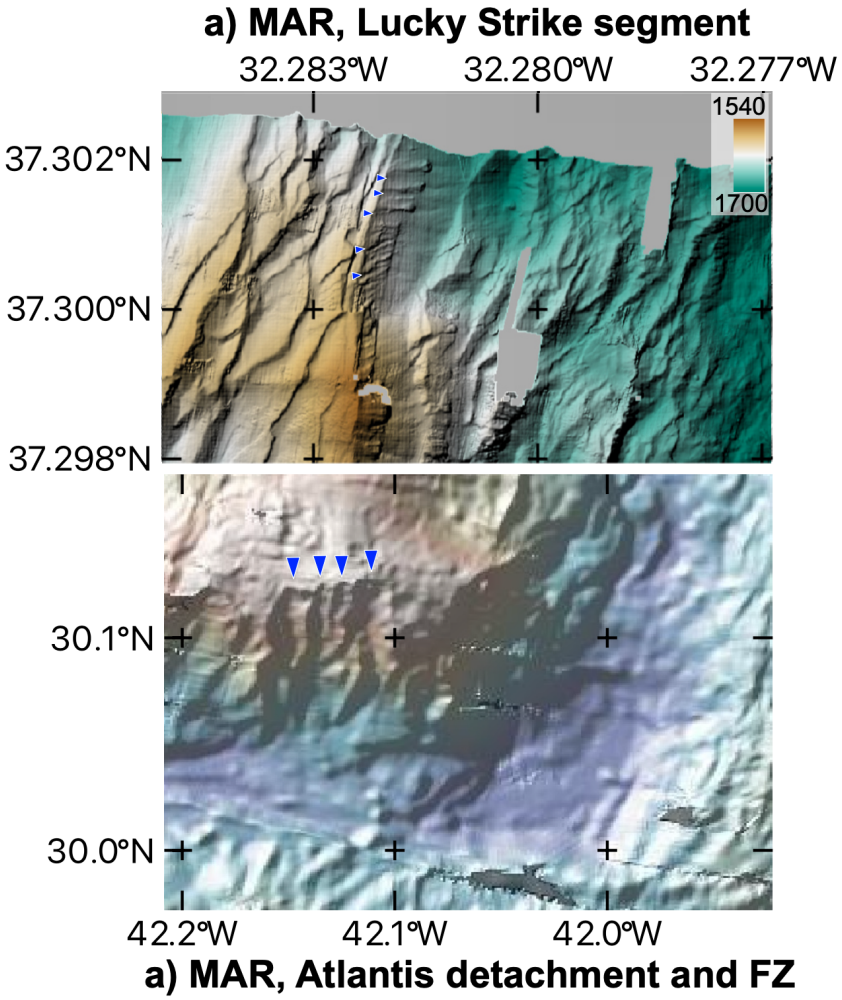

Figure 14*. a) High-resolution bathymetry from the Lucky Strike segment center, showing incipient fault forming within the rift valley and at the summit of the Lucky Strike volcano.*

The fault scarps develop small-scale gullies in the upper scarp and accumulate talus with smooth surfaces at the scarp bottom. b) Multibeam bathymetry of the SE corner of the Atlantis Massif, North of the Atlantis Transform Fault. The rift valley wall shows slopes of <30° with mass wasting features, and clear mass wasting scarps develop along the transform wall to the South. High resolution bathymetry in a) acquired with deep-sea vehicles at Lucky Strike (https://doi.org/10.17882/80574; Escartin et al., 2015; Gini et al., submitted). Multibeam bathymetry in b) from www.gmrt.org.

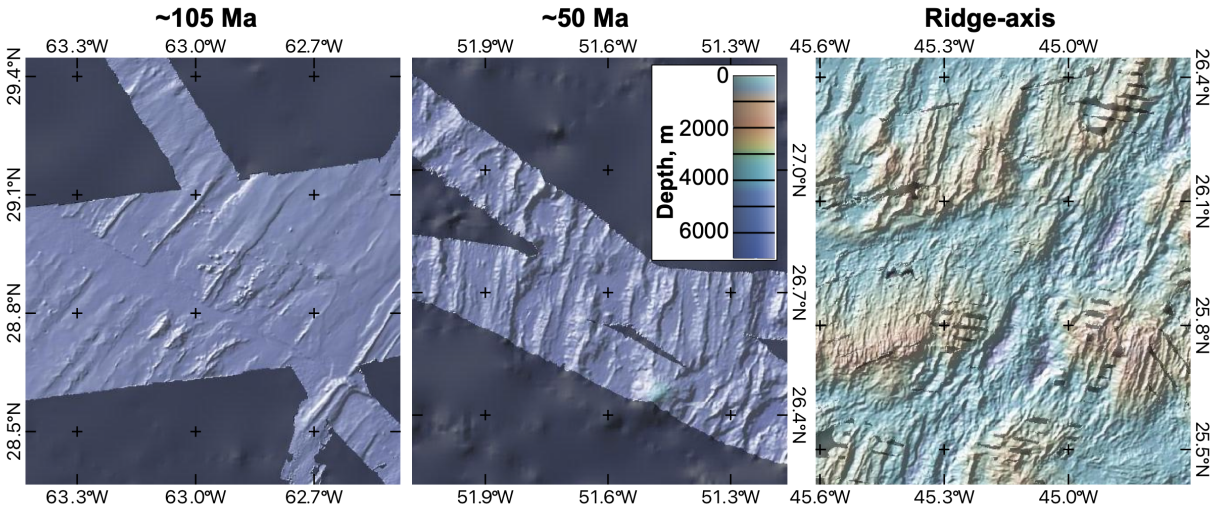

***Figure 15**. Effects of pelagic sedimentation on the seafloor morphology from multibeam bathymetry at the northern Atlantic oceanic crust, from the axis (right), over crust ~ 50 Ma (center) and older crust of ~105 Ma (left). Pelagic sedimentation is minimal at the ridge axis (right), and tends to infill low-lying areas, either between abyssal hills or along fracture zones (center) and non-transform offsets. At older seafloor sediment thickness may be sufficient to cover most of the basement topography, and only the summit of abyssal hills are visible (left). Data from https://www.gmrt.org.*

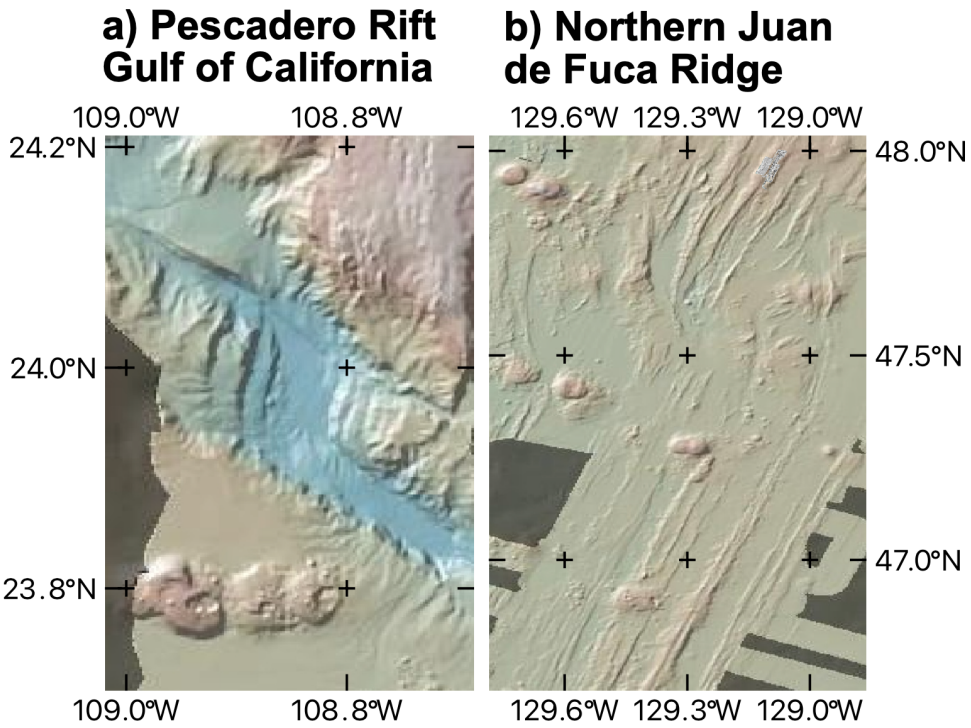

Figure 16. *Sedimented ridge segments. a) Pescadero rift, in the Gulf of California, where the rift valley is fully sedimented and all volcanic and tectonic features are covered (e.g., Lizarralde et al., 2007). b) Northern Juan de Fuca Ridge, near the western North American Coast, showing sediments ponding between abyssal hills and seamounts emplaced off-axis, covering them partially. Data from https://www.gmrt.org.*

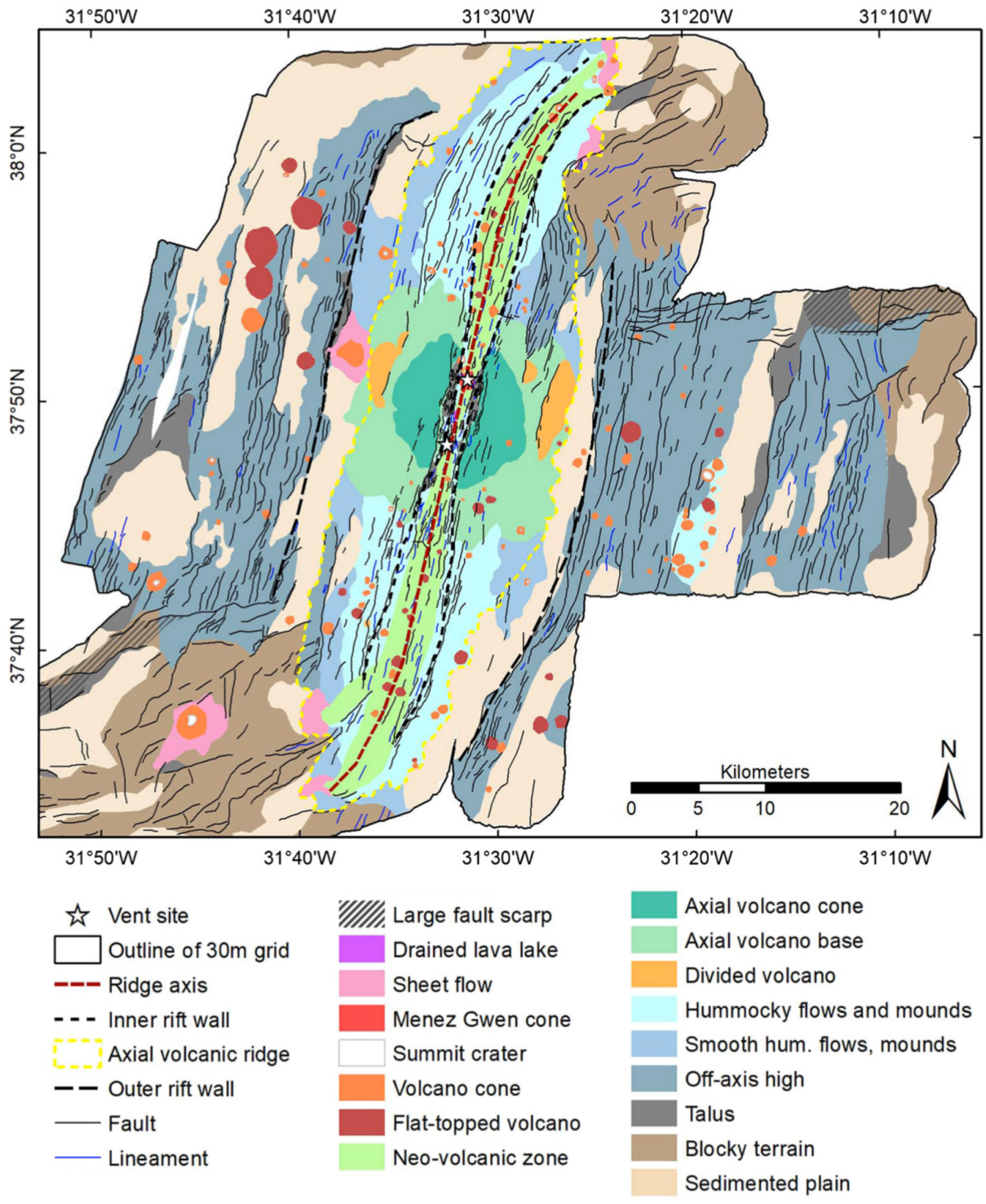

Figure 17*. Geomorphologic interpretation of the Menez Gwen segment along the Northern Mid-Altantic Ridge. This map shows the along-axis variations of volcanic, tectonic and sedimentary features, with an imbrication at different scales reflecting the interaction of the different processes. Modified from Klischies et al. (2019).*